Chemical Process Alternatives for Radioactive Waste

Principal Investigator:

Leonel E. Lagos, Ph.D., PMP®

Florida International University Collaborators:

Dwayne McDaniel, Ph.D., P.E. (Project Manager)
Amer Awwad, M.S., P.E.
Anthony Abrahao, M.S.
Ahmadreza Abbasi Baharanchi, Ph.D.
Aparna Aravelli, Ph.D.
William Tan, Ph.D.
DOE Fellows

FIU | **Applied Research Center**
FLORIDA INTERNATIONAL UNIVERSITY

This document represents one (1) of four (4) reports that comprise the Year End Reports for the period of September 29, 2017 to September 28, 2018 prepared by the Applied Research Center at Florida International University for the U.S. Department of Energy Office of Environmental Management (DOE-EM) under Cooperative Agreement No. DE-EM0000598.

The complete set of FIU's Year End Reports for this reporting period includes the following documents:

Project 1: Chemical Process Alternatives for Radioactive Waste
        Document number: FIU-ARC-2018-800006470-04b-262

Project 2: Environmental Remediation Science and Technology
        Document number: FIU-ARC-2018-800006471-04b-261

Project 3: Waste and D&D Engineering and Technology Development
        Document number: FIU-ARC-2018-800006472-04b-251

Project 4: DOE-FIU Science & Technology Workforce Development Initiative
        Document number: FIU-ARC-2018-800006473-04b-281

Each document will be submitted to OSTI separately under the respective project title and document number as shown above. In addition, the documents are available at the DOE Research website for the Cooperative Agreement between the U.S. Department of Energy Office of Environmental Management and the Applied Research Center at Florida International University: http://doeresearch.fiu.edu

TABLE OF CONTENTS

LIST OF FIGURES

LIST OF TABLES

PROJECT 1 OVERVIEW

The Department of Energy's (DOE's) Office of Environmental Management (EM) has a mission to clean up the contaminated soils, groundwater, buildings and wastes generated over the past 60 years by the R&D and production of nuclear weapons. The nation's nuclear weapons complex generated complex radioactive and chemical wastes. This project is focused on tasks to support the safe and effective storage, retrieval and treatment of high-level waste (HLW) from tanks at Hanford and Savannah River sites. The objective of this project is to provide the sites with modeling, pilot-scale studies on simulated wastes, technology assessment and testing, and technology development to support critical issues related to HLW retrieval and processing. Florida International University (FIU) engineers work directly with site engineers to plan, execute and analyze results of applied research and development.

Although a number of tasks have been initiated and completed over the course of the cooperative agreement, at the end of this past year, there were 4 active tasks. These tasks are listed below and this report contains a detailed summary of the work accomplished for FIU's Performance Year 8.

Subtask 17.3 – Evaluation of pipeline flushing requirements for HLW at Hanford and Savannah River: The objective of this task is to develop a test loop that can bridge technical gaps associated with the flushing of HLW within the transfer and processing lines at Hanford and Savannah River. This loop will aid in implementing optimal flush operations with minimized water usage and the possibility of water hammer and plug formations. These practices will aim to develop a correlation for flush parameters based on characteristics of the system at the start of flushing. The data and correlations will be useful for improving existing guidelines. Characterization of post-flush pipeline cleanliness is an additional objective of the task which will be implemented using various elements of the loop. With discussions between FIU and engineers from Hanford and SRNL, these evaluations will help to establish criterion for flushing operations.

Task 18.2 – Development of Inspection Tools for DST Primary Tanks: The objective of this task is to develop inspection tools that will assist engineers in evaluating the structural integrity of the primary and secondary tank floors in the double shell tanks (DSTs) at the Hanford Site. This effort has led to the development of multiple inspection tools that are able to provide live visual feedback These include a magnetic wheeled miniature motorized rover that can travel through the refractory cooling channels under the primary tank and a pneumatic pipe crawler that can inspect tank ventilation pipes and its central plenum. In addition, FIU is developing a marsupial robotic system that can navigate through the drain lines and inspect the secondary liner via the drain slots.

Task 19.1 – Pipeline Erosion and Corrosion Evaluation: The objective of this task is to provide the sites with a means to evaluate the structural integrity of waste transfer pipeline components. This has involved the evaluation of potential sensors and the viability of utilizing them to provide real time data for long durations of time. The sensors can be installed and provide thickness measurements of pipeline components and fittings found in jumper pits, evaporators, and valve boxes.

Task 19.2 – Evaluation of Non-metallic Components in the Waste Transfer System: The objective of this task is to provide the Hanford Site with data obtained from experimental testing of the hose-in-hose transfer lines, Teflon® gaskets, EPDM O-rings, and other nonmetallic components used in their tank farm waste transfer system under simultaneous stressor exposures. The experiments will be limited to various combinations of simultaneous stressor exposure to caustic solutions, high temperatures and high pressure. Evaluation of baseline materials will be conducted for comparison to materials that have been conditioned with the various simultaneous stressors.

TASK 17.3
Evaluation of Pipeline Flushing Requirements for HLW at Hanford and Savannah River

EXECUTIVE SUMMARY

Study of waste processes at Hanford and Savannah River Sites (SRS) require extensive experimental and/or computational investigations with a number of complexities. Processes such as in-tank mixing and retrieval, pipe transfer, and flushing operations deal with numerous parameters that need to be included in tests or simulations. The pretreatment facility design strategy requires that each slurry transfer in process lines be followed by a flush with water in order to minimize the likelihood of plugging. Investigation of the flushing operations required a comprehensive literature review of the processes involved, existing guidelines, and related experimental work and simulants. Current guidelines establish the minimum flush volume and velocity requirements which were proven to be adequate for several test cases (WTP-RPT-175 Rev. 0 and WTP-RPT-178 Rev. 0). In these test cases the compressed air that was used to pressurize water for flushing purposes and the velocity profiles during flushing exceeded recommended values to avoid pipeline erosion (RPP-RPT-59600, Rev. 0). Efforts during this performance period focused on the design and construction of an experimental pipe loop for study of non-Newtonian slurry flushing. The test bed was designed to investigate parameters that effect the efficiency of flushing operation with the objective of finding flush velocity values/modes leading to satisfactory cleaning of transport lines with a minimum amount of water usage.

A test matrix containing parameters such as pipeline length, flow rate, and simulant composition (solid concentration, rheology, particle size and density) was also developed. In the initial phase of testing, material composition and loop length will be fixed to a mixture of 17 wt% kaolin in water (to attain density, viscosity, and yield stress in the applicable range to operations at Savannah River and Hanford sites) and 165 feet, respectively. This matrix provides a parametric study on the flush velocity. Prescribed velocities in this test matrix comply with the maximum and minimum recommended flush velocity values by the flushing guidelines for Hanford waste (RPP-RPT-59600, Rev. 0, SRNL-STI-2015-00014, TFC-ENG-STD-26, REV C-1).

Efforts will focus on creating repeatable sediment beds inside the pipeline in both fully-flooded and gravity-drained systems. Bed characterization (i.e., measurement of sediment height, solids concentration, and rheology) will be conducted to ensure consistency of the initial conditions between tests. A combination of PulseEcho techniques, a Coriolis meter, and optical inspections will be used to accomplish initial bed characterization (ensuring consistency between tests), control/monitor density variations (initial bed creation, flush velocity control, and post-flush evaluations), and serve as a reference (validation of PulseEcho and pipe surface cleanness evaluation), respectively. This report presents the details of the development of the test loop and the test matrix.

INTRODUCTION

Pipelines which transport high-level waste at DOE sites should be operated above the critical velocity to avoid formation of stationary or moving beds of solid sediments inside the pipes. These formations can result in partial line plugging (which may lead to excessive pumping load and erosion) or full line plugging (which may lead to pump burst or pipeline failure). The pretreatment facility design strategy requires that each slurry transfer in the process lines be followed by a flush with water in order to minimize the likelihood of plugging. Recently, the Defense Nuclear Facilities Safety Board (DNFSB/TECH-40, 2016) has indicated a need for vigorous investigations on the technical basis for prescribing the flush velocity in pipelines.

Previous reports related to pipeline flushing of several simulants (WTP-RPT-175 Rev. 0 and WTP-RPT-178 Rev. 0) were noted. This study revealed that, in a number of tests, the minimum required flush volumes were more than the minimum required values provided by the design guidelines in 24590-WTP-GPG-M-0058, Rev. 0 (Hall 2006). In addition, flush velocities in the pipelines exceeded the maximum velocity stated in the flushing guidelines (RPP-RPT-59600, Rev. 0) and post-flush pipeline cleanness assessments were not reported.

This effort is intended to determine effective flushing operations using a minimal amount of water and provide additional guidelines in support of recently developed flushing standards (TFC-ENG-STD-26). Successful execution requires the creation and characterization of sediment beds, flushing in different modes, and evaluation of operation effectiveness through measurement of post-flush pipeline residues. To extend previous flushing studies, FIU's strategy will be to create different case studies to target different materials and pipe lengths. In addition, existing ultrasonic and visualization methods inspired by the work conducted at PNNL (PNNL-20350 FINAL and PNNL-19441 Rev. 0) will be used in the collection and assessment of data. In each round of testing, the focus will be on influential parameters set for one simulant in a fixed pipe length. These parameters include flush velocity mode (continuous one-step, continuous two-step, and pulsing) and initial conditions (gravity drained versus fully flooded systems). These initial conditions can be created before the start of flushing operations by using two ball valves. To achieve the objectives of this pipeline-flushing task, efforts have so far focused on construction of a 165-ft test loop made of 3-inch schedule 40 carbon steel pipes and fittings. This loop will be equipped with elements and instruments to perform different functions such as system loading, flushing, post-flush evaluations and inline monitoring of flush stream properties.

EXPERIMENTAL LOOP DESIGN AND CONSTRUCTION

An experimental loop with the capability of operating in different operational modes has been designed (Figure 1). Operational modes include slurry circulation (to load the system), draining, flushing, and post-flush circulation and are shown in Figure 2. A detailed schematic design of the pipe loop is shown in Figure 3 and the different initial conditions considered (gravity drained versus fully flooded systems) are shown in Figure 4.
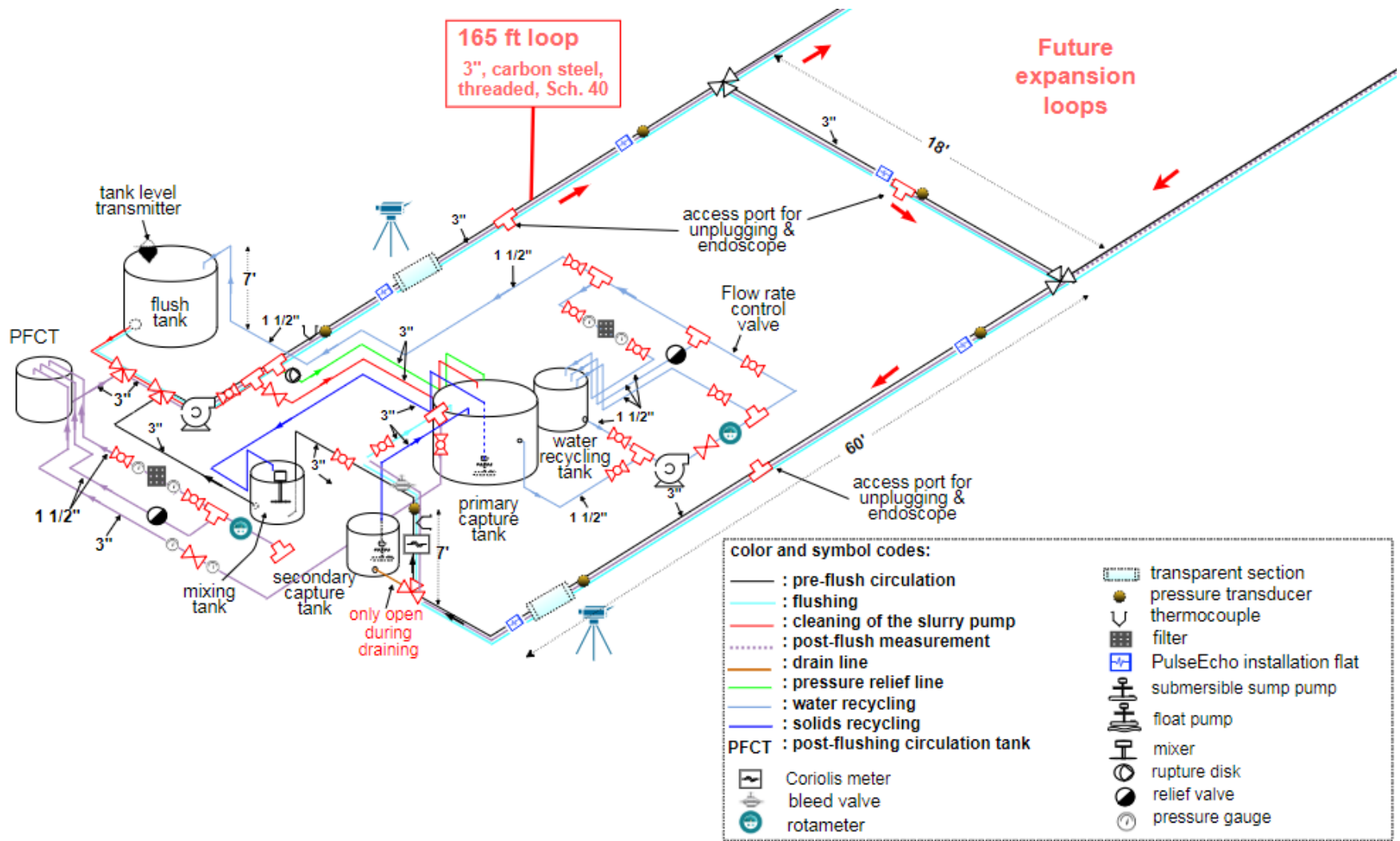
Figure 1. Conceptual design of the flushing test loop.
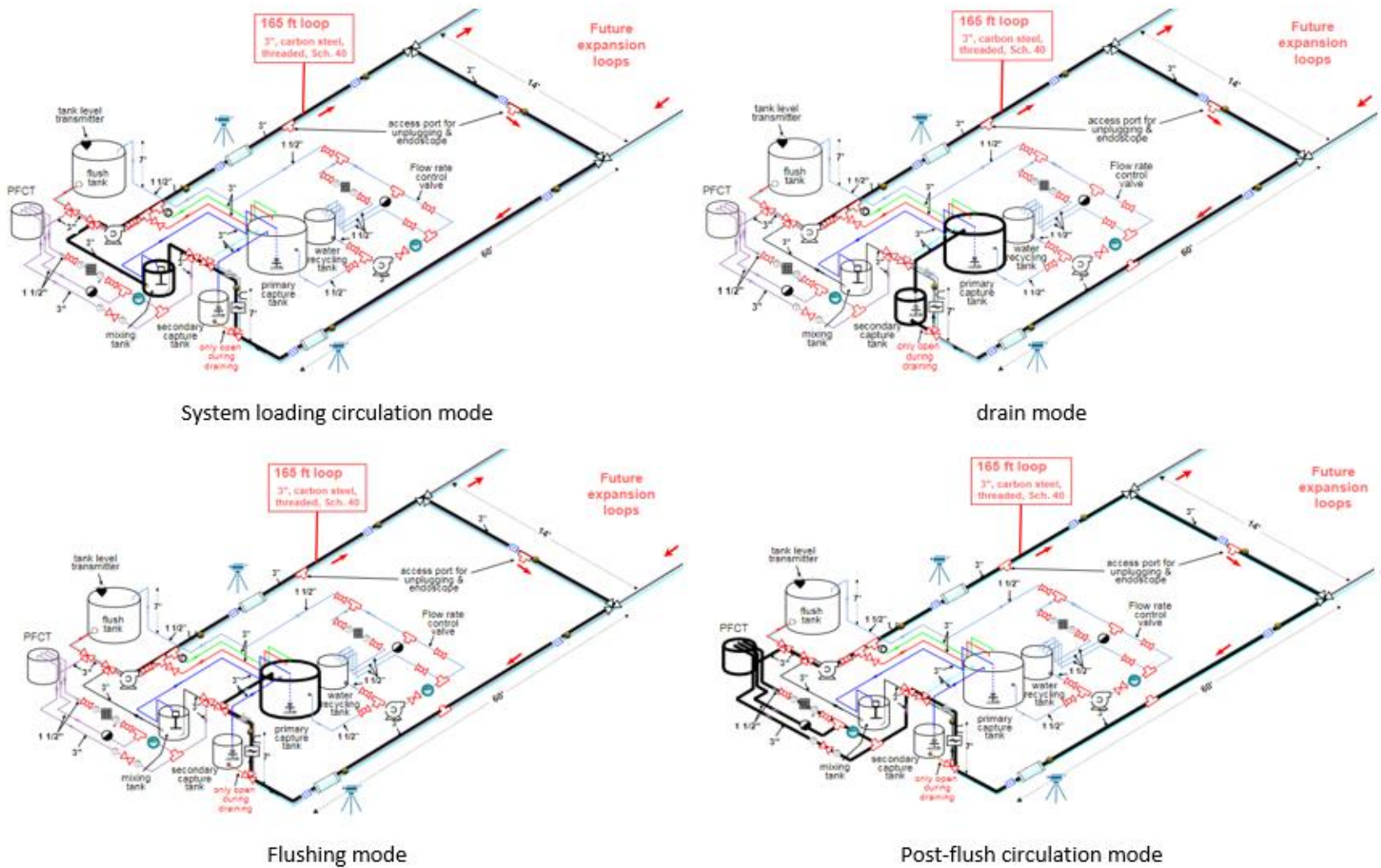
Figure 2. Different modes of the test loop operation.
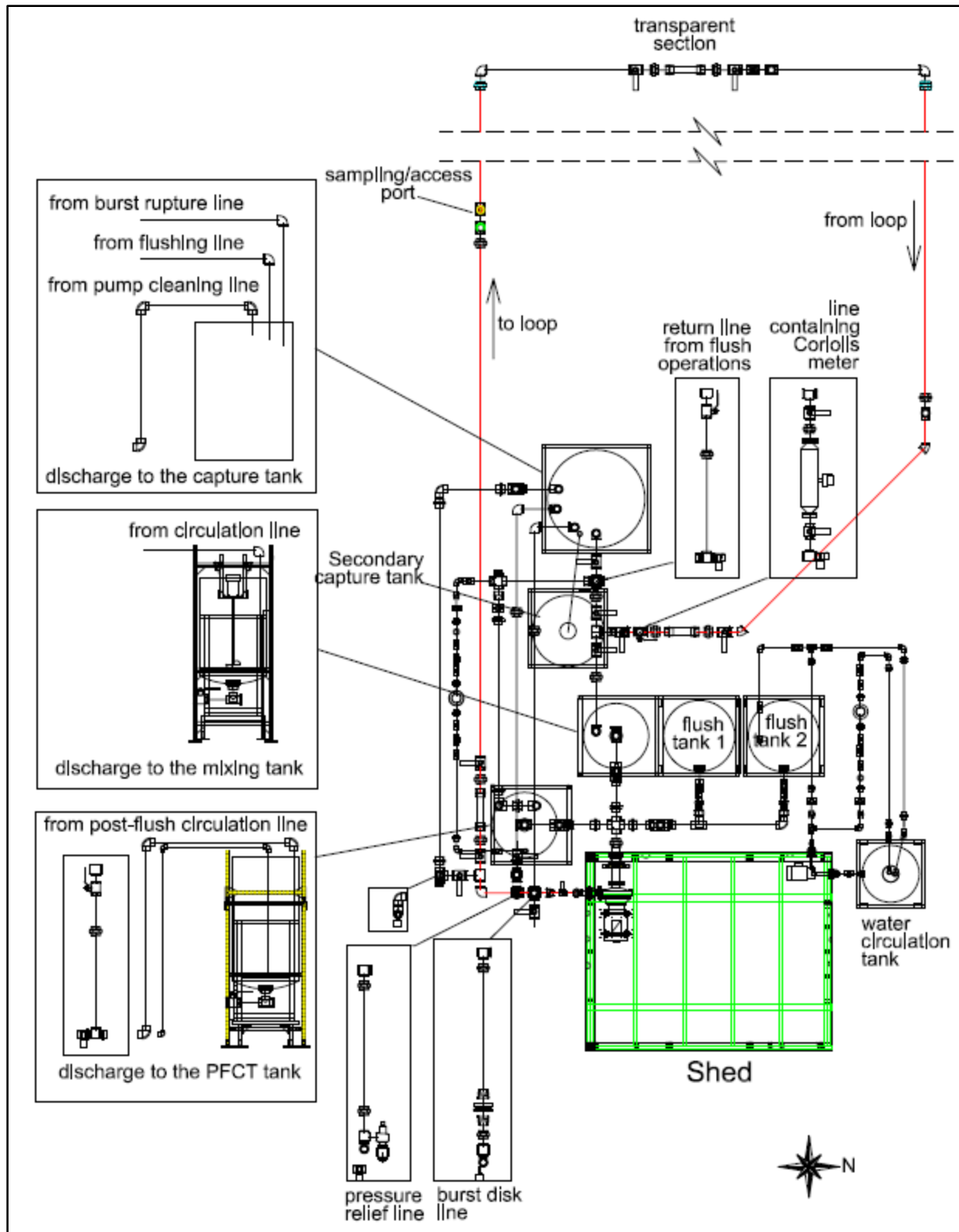
Figure 3. Schematic design of the flushing test loop.
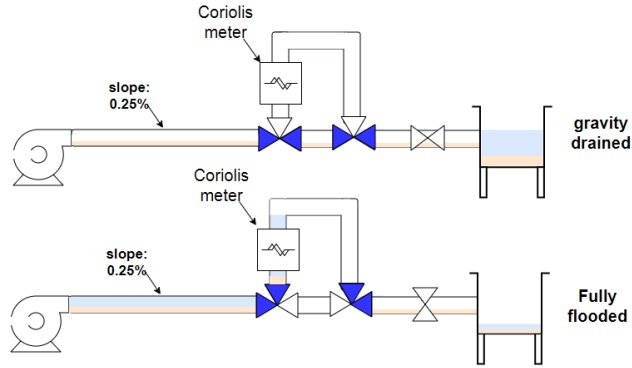
Figure 4. Two initial condition modes for the flushing studies.

This loop is currently under construction at FIU as shown in Figure 5. This figure shows several posts and tank frames constructed for support of elevated tanks and pipelines.
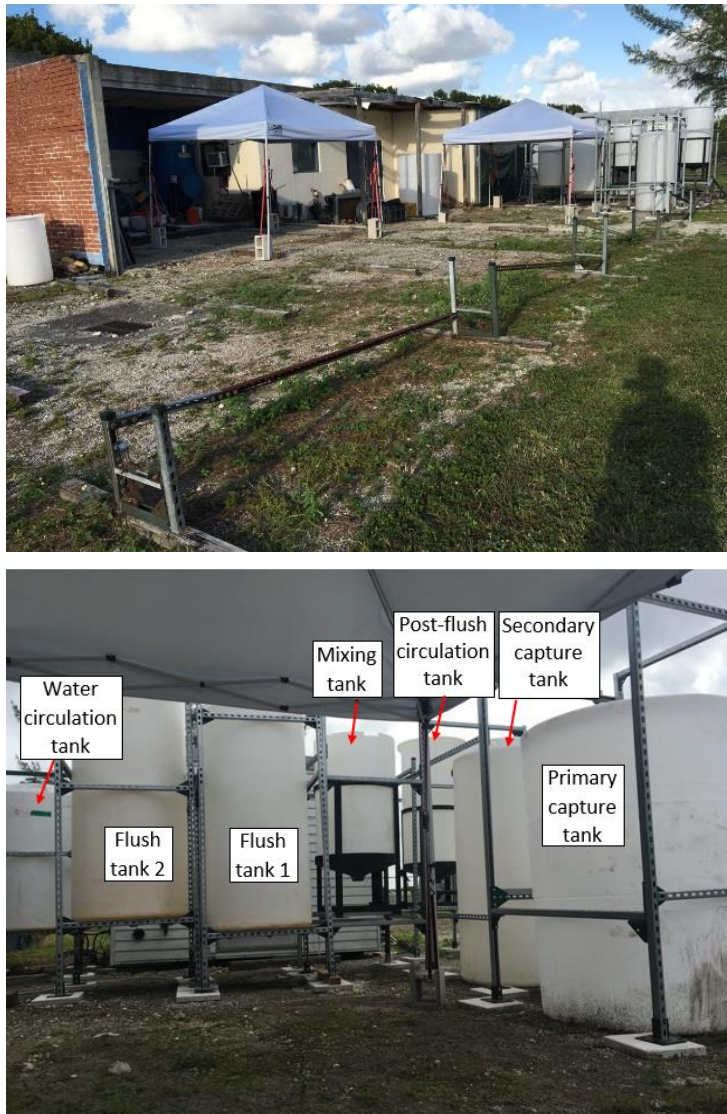
Figure 5. Construction of the flushing test loop.

The selection of the pump for the loop was based on calculations of pressure losses for the target range of flow rates in the flushing tests. A spreadsheet showing typical calculations for the pump is shown in Figure 6.
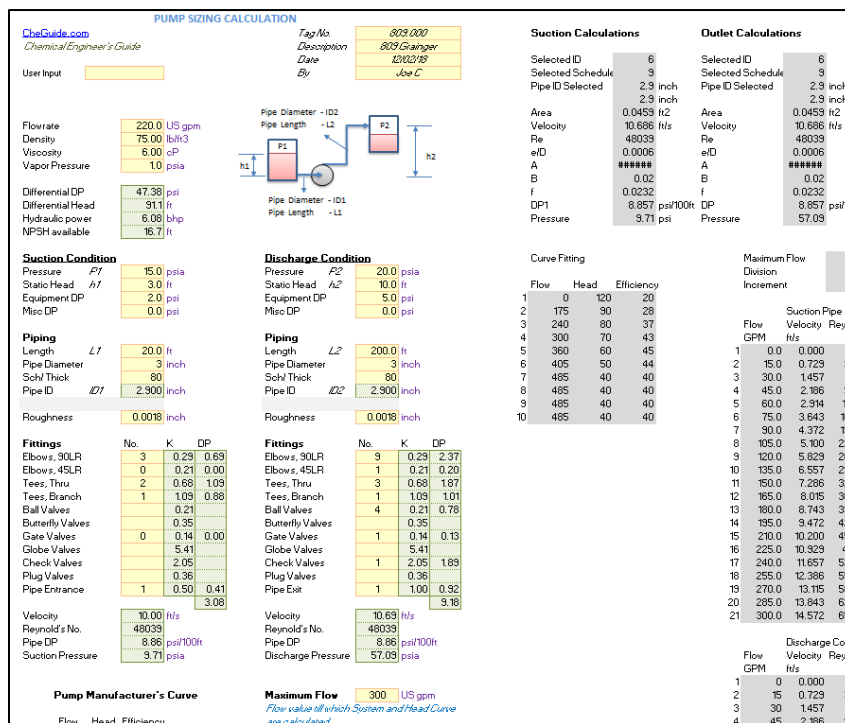
Figure 6. Spreadsheet used for pump calculations.

To obtain safety margins, data reported for a similar 165-ft test loop at PNNL (PNNL-18316 WTP-RPT-189 Rev. 0 and PNNL-17639 WTP-RPT-175 Rev. 0) were referenced. For slurry circulation, FIU focused on data reported for a complex simulant, M1-090109-0905, with similar properties to FIU's target simulant. For flushing, the focus was on pressure gradient data reported for three simulants: 1) low density, low particle size, low fluid rheology (LLL); 2) low density, low particle size, medium fluid rheology (LLM); and 3) low density, high particle size, high fluid rheology (LHH). The LLM and LHH simulants were more challenging than the LLL and were chosen to better understand variations of pressure gradient in initial stages of flushing.

Table 1 shows a comparison between the calculated and reported values for both circulation and flushing operations. This table shows the similarity between reported and predicted required head values obtained from the spreadsheet mentioned earlier. For flushing, values at point A in Figure 7, Figure 8, and Figure 9 were considered. Results show acceptable predictions for LLL (at higher flow rate) and LLM simulants. Larger differences in the case of LLL (lower flow rate) and LHH simulants could be due to variation of density and viscosity in the system. Despite acceptable predictions, application of this spreadsheet for pump size calculations must be approached cautiously, since this tool cannot explain why this system at PNNL had a lower pressure gradient at the same flow rate and density for the LLM simulant compared to the LHH simulant.

Table 1. Pressure Gradient Values Obtained Using a Pump Sizing Spreadsheet for Slurry Circulation and Flushing, (Poloski et al., 2009)

Operation	Simulant ID	Variable	Calculated	Reported
Cirulation[1]	Complex (M1-090109-0905)	Head @ 230 gpm (ft water)	53.1	54
Flushing[2]	Water removing LLL	$\Delta P_{Calculated}$ @230 gpm (psi)	13.42	18
	Water removing LLL	$\Delta P_{Calculated}$ @400 gpm (psi)	34.58	31.7
	Water removing LLM		46.74	48.7
	Water removing LHH		43.46	40
[1] PNNL-18316 WTP-RPT-189 Rev. 0		[2] PNNL-17639 WTP-RPT-175 Rev. 0		
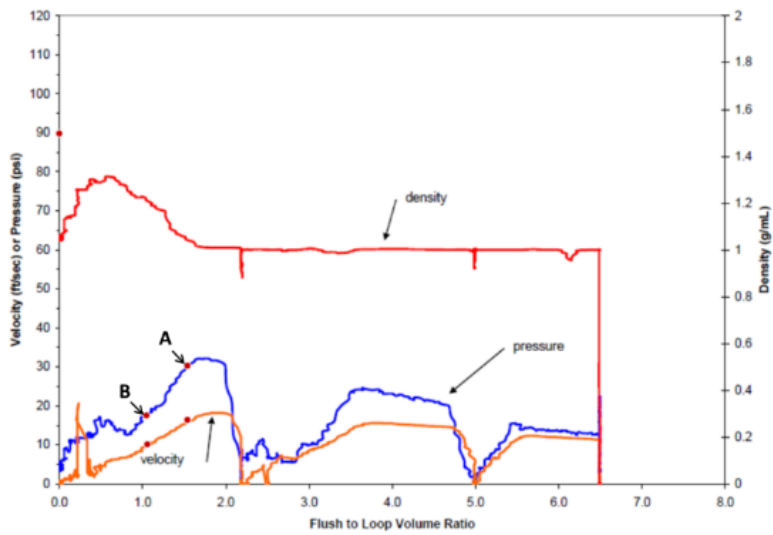
Figure 7. Flow variation during flushing of LLL simulant, (Poloski et al., 2009).
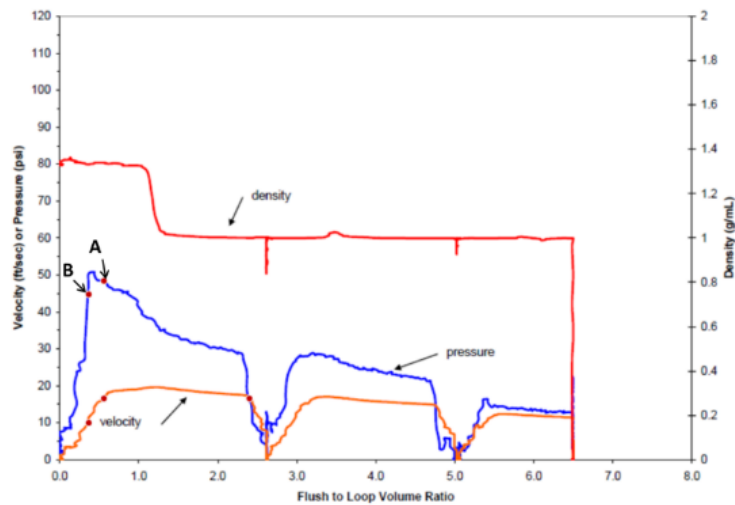
Figure 8. Flow variation during flushing of LLM simulant, (Poloski et al., 2009).
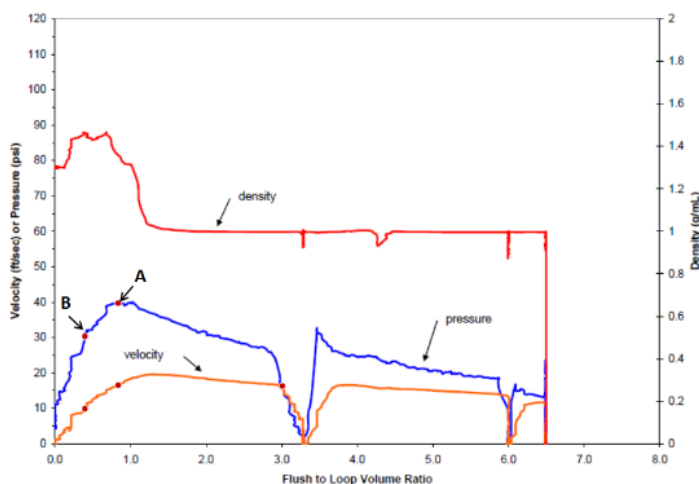
Figure 9. Flow variation during flushing of LHH simulant (Poloski et al., 2009).

In addition, special attention must be paid to the sinitial resistance of the system to an increase of velocity, particularly in a fully flooded system. The selected pump for FIU's test conditions needs to overcome this initial resistance. This initial resistance translated to a 40 psi pressure gradient at point B (showing a pressure peak and descending density) in Figure 8 for the LLM simulant. This value was 30 psi for the LHH simulant in Figure 9. While higher requirements were expected for the LHH simulant with similar density (but higher viscosity and particle size), a lower pressure gradient was reported. The values predicted by the spreadsheet tool were 16.24 psi and 17.24 psi for the LLM and LHH simulants, respectively. The reason for the large discrepancies is likely that inertia and local obstruction effects (granular plugs) are not taken into account in the spreadsheet tool and such factors are added manually.

Table 2 shows the material properties and pressure gradient values reported by Poloski et al. (2009). This table also shows the projected required head after the density factor was incorporated. It is very important to know that the value obtained for the LLL simulant is not conservative since this simulant was rated as Newtonian. Higher viscosity, yield stress, stickiness, and shear requirement for surface erosion of the kaolin clay needs to be included. For this reason, more attention was given to LLM and LHH simulants that had a weight content of kaolin similar to FIU's. The effect of the glass bead content was accounted for through density correction. In addition, a 4 psi pressure drop was estimated for the remaining 51-foot horizontal portion of the system (distance between ports was 114 feet). Also, an 8-foot vertical distance above the pump, which was not part of the 114 feet, was included in this calcuation.

LLM and LHH simulants represented different scenarios during PNNL's flushing experiment. While Figure 8 shows a steep pressure rise as a result of rapid valve opening (according to Poloski et al., 2009), Figure 9 shows a more gentle scenario. It is important that the slurry pump at FIU can support both of these scenarios, especially since the LLM simulant had a similar viscosity and yield stress to FIU's target simulant. This requirement is necessary to ensure that the system can quickly reach the desired flow velocity and flow rate. In addition, it is important that the slurry pump be strong enough to remove local solid accumulations (granular plugs according to Poloski et al., 2009) from the system during flushing. This was successfully shown at PNNL through sequentially charging the system with pressures between 0 to 100 psi (231 feet of water). This

scenario can occur in both fully flooded and drained systems with kaolin at FIU and needs to be accounted for in the pump selection.

Table 2. Projected Pump Head Values Based on Data Reported by Poloski et al., 2009

Simulant ID	LLL	LLM	LHH	FIU's target simulant
Bulk density, kg/L	1.15	1.33	1.3	1.142
Solid concentration, glass bead, wt%	21	18.3	20.6	N/A
Solid concentration, kaolin, wt%	N/A	23.1	18.4	20
Bingham consistency, cP	N/A	6.8	8.7	6
Bingham Yiled stress, Pa	N/A	2.8	6.1	3
d_{50} (d_{95}), µm	6.2, 14.4	6.2, 45.1	120, 200.2	6.3, 49.5
Pressure gradient at 10 ft/s, psi	18 @ S.G. 1.2	45 @ S.G. 1.35	30 @ S.G. 1.33	TBD
Projected pump head at FIU, feet of water, (@ 230 gpm and S.G. of 1.15)	50	93	65	TBD

Based on the estimates mentioned above, FIU considered a 15 hp slurry pump (AMT 427B-95) capable of delivering 230 gpm of water at 93 feet of water. This pump will be controlled via a 15 hp Hopewind HV300 variable frequency drive (VFD) and through software which facilitates remote operations. Figure 10 shows the slurry pump and VFD.

Figure 10. Slurry pump and variable frequency drive for the flushing studies.

A Coriolis meter (Optimass 1000, Krone) will be used to measure density and mass flow rate of the flow during slurry circulation, flushing, and post-flush evaluations modes. The purpose of these measurements will be to adjust concentration inside the mixer tank, to indicate the time for switching between high and low velocity values, and to assess the presence of post-flush solid residues. PulseEcho type ultrasonic transducers (DVF014, NDT systems and HC-SR04, Sainsmart) were purchased to characterize the sediment bed height inside the pipeline before, during, and after flushing operations and to monitor the water level inside the flushing tanks (Figure 11). This ultrasonic tank level gauge will trigger an alarm for termination of the flushing operations when water in the flushing tank drops to the target levels. An existing high-speed

camera (Vision Research v5.0) will be used for initial condition characterization, monitoring of sediment level variations and traces of particles passing through the transparent sections.
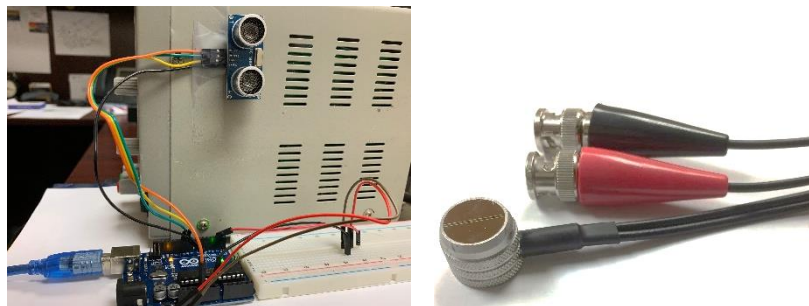
Figure 11. Ultrasonic trandducers for tank level (left) and sediment thickness measurement (right).

The loop will be equipped with safety components to protect the system elements, particularly the slurry pump. Figure 12 shows the pressure relief valve and burst disk which were purchased to avoid over pressurization of the lines and to provide quick venting. The relief valve (Aquatrol Inc., Series 69) was selected for its ability to vent 230 gpm at a set pressure of 85 psig (set pressure is adjustable from 76 to 110 psi, corresponding to 214 to 259 gpm). Selection of the 4-inch burst disk (Graphilor, Series 3) was based on its 180 gpm capacity at the burst pressure of 100 psig.

Figure 12. Pressure relief valves (left) and burst disk (right).

Pressure transducers and gauges will also be used to monitor the system pressure at different locations and detect/locate possible plug formations. This monitoring will help provide precise characterization of the system in terms of pressure losses, protection of the slurry pump, quick unplugging using a drain snake, and on-time cleaning/replacement of filters (used for capturing post-flush solid residual and cleaning the recycling water). In addition, a monitoring system will be designed to continuously monitor the status of the valves in each mode and trigger an alarm as needed.

The utilization of an existing 0.5 hp 32V136 Dayton mixer was also demonstrated. This mixer was integrated into an overhead mounting frame (as shown in Figure 13) over a 28-inch diameter cone bottom baffleless tank. This assembly allows for D/2 vertical offset (D represents tank diameter) from center of the tank to enhance mixing in the absence of baffles. The original 3.5-inch foldable propeller of this mixer was replaced with a 6-inch right-pitched propeller for upward pumping of material inside the tank. Selection of the propeller was based on the need to achieve sufficient agitation for sediment re-suspension from the tank bottom.
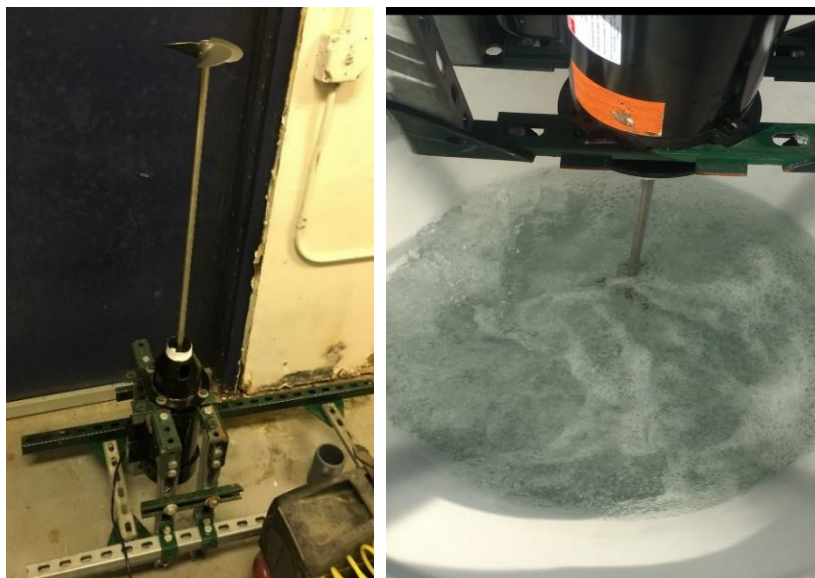
Figure 13. Mixer for the flushing studies.

MATERIALS

Selection of the simulant (17 wt% kaolin in water) for the flushing tests was based on discussions between FIU and engineers from SRNL and PNNL. This mixture was selected to meet the requirements of density (1.15 to 1.22 g/cm^3), viscosity (4 to 12 cP), and yield stress (2.5 to 10 Pascal). Therefore, 200 lbs of EPK kaolin was purchased and used for performance testing of an existing mixer. All components of the test loop, including 3-inch schedule 40 carbon steel pipe fittings and sections, have been purchased. PVC pipe sections and fittings were purchased for transparent sections and some sections which are not part of flushing operations (e.g., part of post-flush circulation and water filtration loops). Water will be used as the flushing fluid in all tests.

EXPERIMENTAL APPROACH

The experimental approach was finalized to include the following investigations:

- Fulfillment of flushing criteria using ultrasonic, visual, and solids entrapment methods.

- Detection of residuals on the pipe walls using PulseEcho transducers, cameras and endoscope (inserted into the pipe loop at different access points).

- Determination of post-flush residuals through mass balance analysis (measurement of accumulated mass of solids inside a filter bag) and density monitoring (using a Coriolis meter) of residuals being recirculated in the loop via fresh water.

A test matrix was developed to achieve the research objectives in regard to initial testing. This matrix, shown in Table 3, includes an overall flush-to-line volume ratio (FTLVR) limited to a maximum of 5 which is less than the maximum FTLVR reported in WTP-RPT-175 Rev. 0 and WTP-RPT-178 Rev. 0 (Poloski et al., 2009 and Yokuda et al., 2009). After initial testing, some of the key parameters may need to be adjusted based on observations during the testing.

Table 3. Matrix for Flushing Test Using a 165-ft Test Loop

Test Number	Flush Mode	Number of flushes	FTLVR (per flush)	Resultant Duration Per Flush (sec)	Resultant FTLVR
1	Constant	1	2	27.4	2
2	Ramped	1	2	-	2
3	Pulsed	1	2	-	2
4	Constant	2	1	13.7	2
5	Ramped	2	1	-	2
6	Pulsed	2	1	-	2
7	Constant	1	3	41	3
8	Ramped	1	3	-	3
9	Pulsed	1	3	-	3
10	Constant	2	1.5	20.5	3
11	Ramped	2	1.5	-	3
12	Pulsed	2	1.5	-	3
13	Constant	1	4	54.8	4
14	Ramped	1	4	-	4
15	Pulsed	1	4	-	4
16	Constant	2	2	27.4	4
17	Ramped	2	2	-	4
18	Pulsed	2	2	-	4
19	Constant	1	5	68.4	5
20	Ramped	1	5	-	5
21	Pulsed	1	5	-	5
22	Constant	2	2.5	34.2	5
23	Ramped	2	2.5	-	5
24	Pulsed	2	2.5	-	5

* Constant mode will target 10 ft/s by default. Ramped mode will start from a high velocity V1 (default: 10 ft/s) and will drop to and stay on V2 (by default: 6 ft/s). Pulse mode will be between a high velocity (default: 10 ft/s) and the maximum velocity (6 ft/s)

To implement the test matrix, FIU developed the following procedural steps:

1. *Initial testing of system components.*
   Initial testing of the system will aim to: 1) ensure smooth operation and accurate functionality of all system elements including pumps, valves, pressure transducers, mixer, and Coriolis meter, etc. as well as the absence of any air pockets or leaks; 2) validate uniformity of the mixtures in the mixing tank and consistency of initial conditions created for each flushing experiment; and 3) test the ability of the ultrasonic sensors in determining the sediment bed thickness inside the pipeline in both static and dynamic conditions.

2. *Initial system loading and air venting.*
   First, 60 gallons of fresh water will be added to the mixing tank. During the addition of the water, the slurry pump will be turned on to circulate the water in the loop. The post-flush circulation tank and filtration line will start receiving water by keeping the corresponding valves open. In this step, air will be removed from the system using a bleed valve mounted at the highest point of the system, Absence of air in the system can be verified by considering the stability of the density signal at the Coriolis meter. The addition of water will be stopped once the water level in the mixing and post-flush tanks reaches 60 gallons.

3. *System loading with water-kaolin mixture at a target concentration.*
   Frequency of the VFD will be increased to achieve a high flow velocity (e.g., 6 ft/s or 10 ft/s) needed for improving mixing in the mixing tank. A table for relating frequency, pump speed, and flow rate will be created. Kaolin will then be slowly added to the mixing tank while running both the slurry pump and mixer continuously. Density will be closely monitored via sampling or a Coriolis meter until the desired concentration is achieved (17 wt% kaolin in water). The slurry pump will then be slowly shut down and a sample will be immediately taken from the mixing tank for rheological measurements.

4. *Creation of initial condition modes.*
   The system will be allowed to gravity-drain (using an on/off valve) if flushing for the gravity drained mode is intended. In this mode, a submersible pump inside the secondary capture tank will be simultaneously powered on to transfer the incoming material to the primary capture tank. The purpose of this is to avoid any interruption in the drain process due to a buildup of hydrostatic pressure inside the secondary capture tank. The drain line will be closed with a ball valve upon completion of the drain mode and the system will be prepared for flushing mode by opening the valve on the Coriolis meter. Sediment characterization will be conducted by measuring the sediment height via PulseEcho sensors and cameras.

   For initial condition modes, efforts will focus on creating repeatable sediment beds inside the pipeline in both fully-flooded and gravity-drained systems. In the initial testing, material composition used to create sediment beds (mixing tank content) as well as the loop length will be fixed (a 165 ft loop will be used). Bed parameters such as height, solids concentration, and rheology will be measured to ensure about consistency of initial conditions between tests. FIU will control parameters such as the rate of slurry pump shut-down and delay time (between the end of system loading to the start of flushing test) which affect the sediment buildup to attain consistent initial conditions.

5. *Flushing operations.*

To start flushing, the frequency of the VFD will be preset to the recorded values corresponding to 10 ft/s and the slurry pump will be started. Flush velocity will be controlled according to three functions during the tests: 1) a constant value, 2) step (dual constant values), and 3) pulsating. A constant value function will be used to set the flush velocity to 10 ft/s. In the dual functioning mode, FIU will start with a velocity of 10 ft/sec and decrease the velocity to 6 ft/s after the peak density is reached at the Coriolis meter. The third function will be to alternate between 6 ft/s and 10 ft/s velocities. In all cases, flushing will be terminated upon reaching the target value for water flushing volume according to the test matrix.

To ensure smooth and safe operation of the slurry pump and other test loop components, the pressure will be continuously monitored via pressure transducers installed in several locations of the loop. The pipe loop will be equipped with an alarm system to alert the operator in case the pressure difference between the discharge and suction sides of the pump approaches 50 psi. This system will also create alarms in the event that the pressure in the system approaches 100 psi. In the first set of tests, flushing operations will be terminated upon a drop in the water level in the flush tank to the target values indicated by the FTLVR values in Table 3. A pair of water level sensors will continuously monitor the water level in the flush tanks and create an alarm at the target FTLVR.

6. *Post-flush evaluations*

Post-flush evaluations will be conducted to measure how much solid is left in the pipe loop immediately after termination of the flushing runs. FIU will first inspect the transparent pipeline section and then use an endoscope inserted at the access points and the PulseEcho transducer to inspect the non-transparent pipeline sections. Then, the slurry pump will be turned on to circulate material inside the post-flush evaluation loop. This process will allow gradual filtration of the particles and is protected by a bypass loop. FIU will continuously monitor the density of materials in the circulation loop (by checking the Coriolis meter readings and sampling from the post-flush circulation tank) and will terminate the process as soon as the density approaches the water density. At the end of the process, FIU will remove the sediment inside the filter to determine the mass of the accumulated material. This process will also help to clean the slurry pump.

7. *Water and slurry retrieval from the primary capture tank.*

Retrieval of the water and slurry from the primary capture tank will follow the post-flush evaluations to give the solids time to settle. Initial experiments have shown that larger particles will settle within 2 to 3 hours, creating two distinct layers with 3.6% (dilute) and 30% (concentrated) volumetric solid concentrations. FIU will start decanting the water from the upper layer using a submersible pump which will be manually placed near the interface between the top and bottom layers. One-hundred gallons of this water will be sent to a water circulation tank where a filtration loop will gradually filter out the solids. FIU will monitor the density of samples taken from the water circulation tank and, once clear, the water will be sent to one of the flush tanks. Transfer of the concentrated layer to the mixing tank will be done by placing the submersible pump at the bottom of the primary capture tank. This pump, which is equipped with a powerful agitator, will be moved as needed to various locations along the tank bottom surface.

FIU also developed a plan to eliminate the risks associated with possible mispositioning of the valves in the system. A pair of contact switches will be activated by the valve handle in the on and off positions and a microcontroller board (Arduino Mega) will read the voltage output from these switches. A program written in an integrated development environment (IDE) will be used to collect and compare the position data from each valve to the system configuration for each operational mode selected by the user. All system configurations will be predefined and programmed into this indicator system. Therefore, an alarm will indicate an incorrect valve position.

INITIAL TESTING

Results of testing a settling suspension of 22% by volume kaolin in water is shown in Figure 14. Testing was conducted to extract information about the upper (dilute) and lower (concentrated) sediment layers after 2 hours of settling time. Calculated concentrations for the upper and lower layers were 3.6 and 30 vol %, respectively. After 48 hours, a completely clear layer was observed above the concentrated layer. At this point, tilting the tube to large angles did not disturb the kaolin layer, showing a strong cohesion (Figure 15). At the horizontal level, particles started to shear off and mix with the water as soon as the edge of air-water interface reached the packed kaolin-water layer. Testing showed that the concentration in this thick layer was as high as 45 vol %.
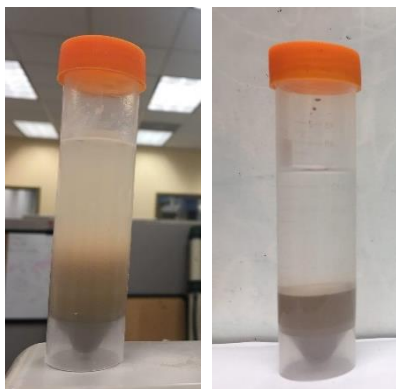
Figure 14. Kaolin suspension testing - sample after 2 hours (left) and 48 hours (right).

Figure 15. Test of cohesiveness of a fully settled kaolin bed in water.

Performance testing of the mixer was conducted by extracting one sample from the top and one sample from the bottom (through a valve) of the mixing tank while the mixer was in operation (Figure 16). The densities of the extracted samples were analyzed (indicative of percent solids) for the tank filled with 30 and 60 gallons of 17 wt% kaolin-water. FIU found no significant differences between the density samples for each tank loading. In addition, results at different loadings were almost identical (less than 1 percent difference), validating the performance of the mixer.

Figure 16. Performance testing of the mixer with 60 gallons of material in the tank.

FIU also tested the density of a sample extracted from the bottom of the tank (through a ball valve) after 4 days of completing the mixing test. The objective was to test the flow and density of kaolin-water exiting the tank after full settlement (no mixer operation) and sufficient aging. The mixture was found to easily flow at 0.34 gpm (at a very small valve opening) and at a density of 1.1362 gr/cm^3.

Table 4. Performance Testing of the Mixer

Density of mixture during mixer operation (± 0.02 gr/cm3)				Density of mixture 4 days after mixing (± 0.02 gr/cm3)
30 gallons		60 gallons		60 gallons
top	bottom	top	bottom	bottom
1.04 gr/cm^3	1.04 gr/cm^3	1.05 gr/cm^3	1.04 gr/cm^3	1.1362 gr/cm^3

PulseEcho Testing

Bench-scale ultrasonic PulseEcho testing was conducted using a dual element 0.5 fingertip NDT transducer with center frequency of 1 MHz and Tektronix oscilloscopes (THS720A and TDS3034). The goal was to measure the time-of-flight of sound waves in the absence and presence of various kaolin-water mixtures. These tests were intended to demonstrate the accuracy of the transducers in measuring the sediment height inside a test spool. Initial testing was conducted for calibration purpose using aluminum pieces of different thickness (3, 12, and 40 mm). Initial results showed that a 6.2 µs time gap existed between the start of the excitation signal and the start of the first echo. This time delay is a typical representative of material thickness by a factor of two, as it shows the time of flight measurement of waves traveling to and back from the end of the material. This time distance was approximately 9.2 µs and 18 µs for the 12 mm and 40 mm pieces, respectively. These results failed to show a proportionality between the time delays and the thickness of the pieces.
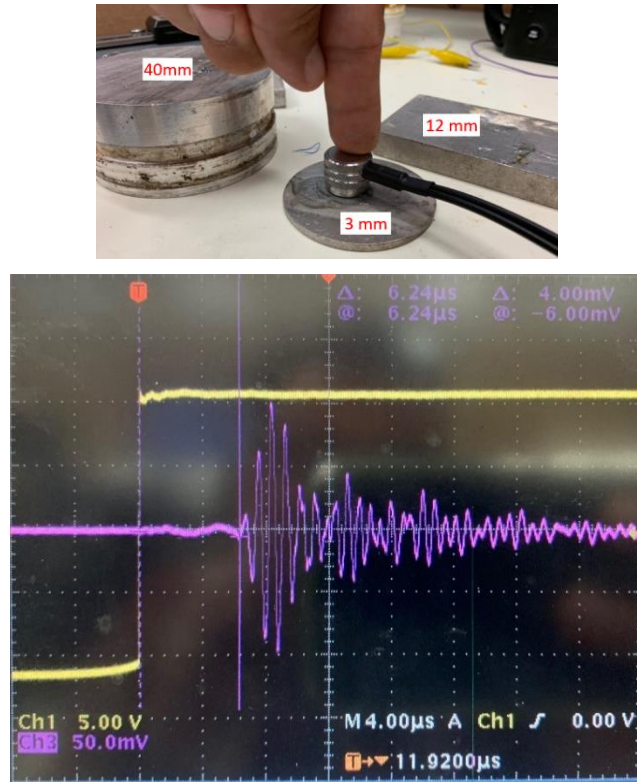
Figure 17. Test of PulseEcho Transducer for Thickness Measurement.

Therefore, FIU tested the time delay of the transducer to respond to the excitation wave (square wave generated by the signal generator) and echoed sound waves. The test was performed to measure how fast the transducer reacted to voltage signals (to create sound waves) and vibrations (to create voltage signal). FIU first tested a pair of fast-response single element Ultran transducers (Figure 18) and found a total of 490 ns time delay. As the transducers were identical, half of the delay time (~0.25 µs) was assumed to be created during reaction to the voltage signal and the same amount during reaction to the sound echoes.
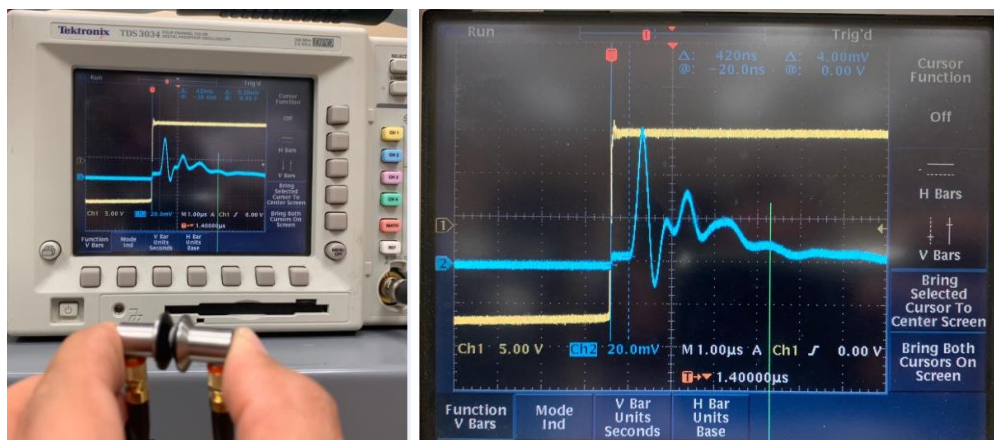
Figure 18. Test of Ultran transducer for response delay measurement.

In the next step, FIU used the Ultran transducer to show the response delay time of the NDT PulseEcho transducer (both transducers were placed adjacent to each other). In one test, the NDT

transducer was excited by the signal generator and the Ultran transducer showed the waveform and time delay generated by NDT transducer (left image in Figure 19). In another test, the Ultran transducer was excited by the signal generator and the NDT transducer showed the waveform and time delay generated by NDT transducer (right image in Figure 19). In both cases, a delay time of about 2.8 µs was observed. By considering a 0.25 µs delay time of the Ultran transducer, a 2.55 µs time delay was considered for the NDT transducer in its pulse and received modes. Therefore, time delay values will be modified to 1.14, 4.4, and 12.9 µs. The updated ratios correlate strongly with the material thickness. Slight deviations can be related to variations in material density between the aluminum pieces (ρ_{3mm}=2.85 gr/cm^3, ρ_{12mm}=2.66 gr/cm^3, ρ_{40mm}=2.67 gr/cm^3).
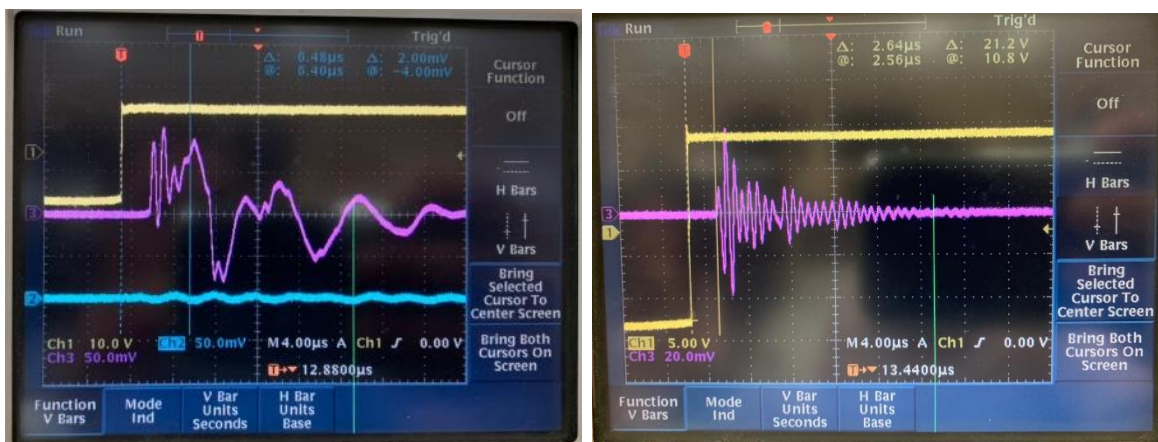
Figure 19. Test of PulseEcho for thickness measurement.

Next, ultrasonic testing was performed to measure sediment thickness, as shown in Figure 20. FIU used PVC pipe (schedule 40) for its stronger acoustic match with the sediment. Tests were conducted with and without the presence of sediment (10 mm layer of uniform kaolin in water with 17 wt % concentration) in the pipe. Blue curves in Figure 20 show the echoes received by the transducer. The time difference between the first and second echoes significantly increased (7.2µs) with the addition of the sediment. This time shift was 4.8 µs for a 7-mm thick layer, demonstrating the proportionality between the increase of sediment thickness and the increase of time between the first and second echoes. Thus, this time difference may be used to determine the sediment thickness in fixed concentrations of mixture. Another observation was a significant increase of strength of the second echo with the addition of sediment layers. This effect can be explained by considering the close acoustic match between PVC and sediment (allowing sound energy to mostly transmit through the PVC-sediment interface instead of reflecting) and strong acoustic mismatch between PVC and air (causing a major energy reflection from the PVC-air interface). This finding was in accordance with results published by Lee (2010).
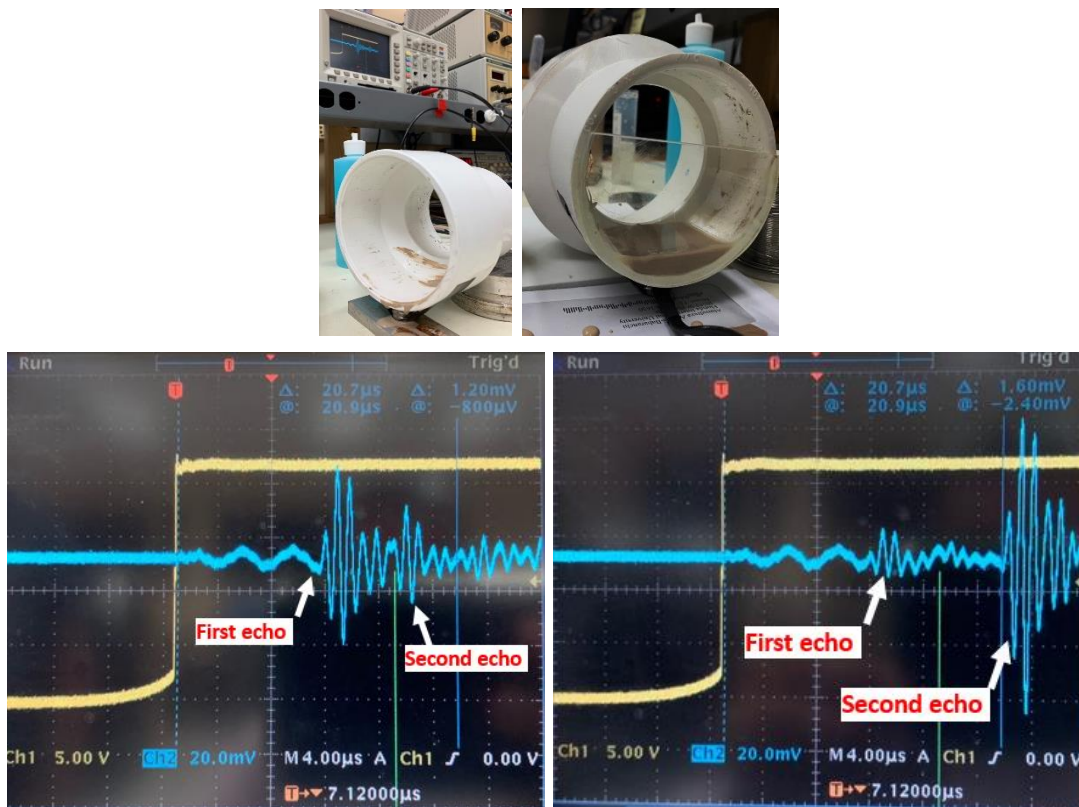
Figure 20. Test of PulseEcho with (right) and without (left) sediment.

Testing was also performed on a spool piece that was provided to FIU for initial bench-scale testing. This spool was previously used in PNNL's ultrasonic tests and, as shown in Figure 21, has two flattened sections with thicknesses of 2 to 3 mm. Results of this test are shown in Figure 22 and indicate distinctive echoes for the thicker flat section. However, for the thinner section, FIU only observed small modulations in the noise signal (the signal generated by the receiver part of the transducer when it is not connected to any surfaces). This dampening effect was probably caused by destructive effects in the near-field-zone of the transducer (entire pipe wall thickness was in the near-field-zone).
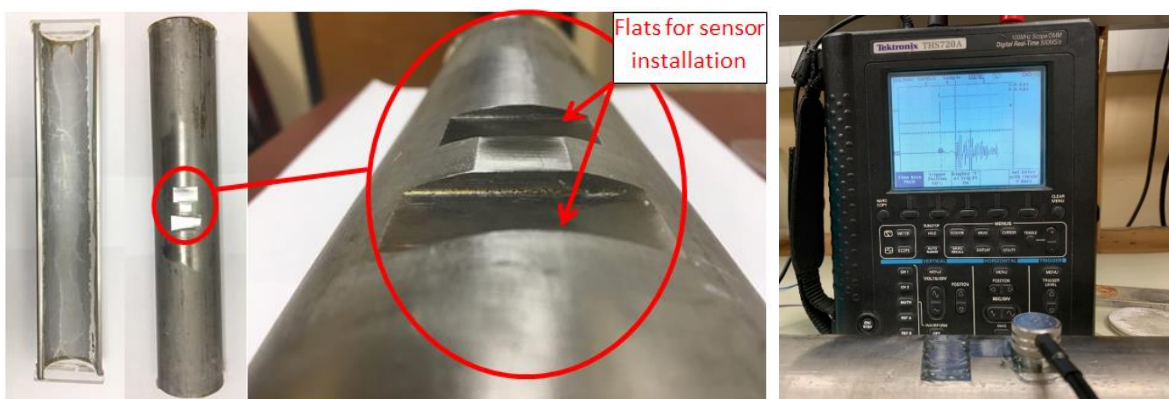
Figure 21. Spool piece considered for ultrasonic tests at FIU.
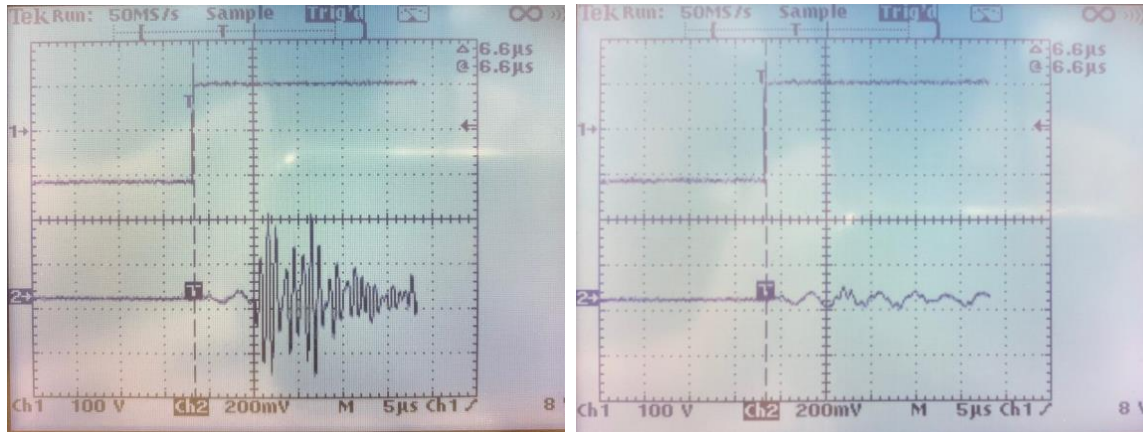
Figure 22. Sound echoes detected by the ultrasonic sensor on the ticker (left) and thinner (right) flats.

Ultrasonic testing was also performed in the presence and absence of sediment placed inside the stainless-steel spool piece. For this pipe material, the same results in Figure 22 were reproduced, showing no differences in time and amplitude of the echoed waves. This lack of difference can be related to the inability of waves to travel into the sediment due to the large acoustic impedance difference between the pipe and sediment material. Use of higher amplitude sound waves (increasing peak-to-peak voltage) can increase the amount of energy transmitted to the sediment and potentially increase the strength of detectable echoes sound waves.

CONCLUSIONS AND FUTURE WORK

Details of a test loop designed for flushing experiments at FIU was presented. All piping components and instruments were purchased for this loop and this test loop is currently under construction. A test matrix was also developed along with the steps and details of conducting the flushing tests. Results of initial settling tests shows a minimum wait time of 2 hours to allow most of particles settle in the loop (needed to create a sediment bed) and inside the capture tank (needed to maximize kaolin retrieval and minimize filtration during water circulation). Results also suggest that long delays between the end of the bed creation process and start of flushing should be prevented. This will help to minimize effects of bed compactness inside the pipes and fittings. Performance testing of the mixer showed satisfactory level of homogeneity in the mixing tank. We also found that after four days of material settling (no agitations) inside the mixing tank, the settled kaolin could easily flow out of the tank due to the large hydrostatic pressure above the discharge port. This high flow rate discharge of material occurred with a density relatively lower than that of a compact bed at a no flow condition. This will allow for pumping even after long resting times. Initial testing of a 1 MHz PulseEcho transducer using PVC spool revealed that sensor was able to provide indications of sediment layer presence and thickness. Testing conditions (10 volts maximum amplitude for the excitation signal and 1 MhZ transducer) failed to indicate sediment presence in the case of a stainless-steel spool piece. Future work includes full construction of the test loop (currently pending space reallocation) and ultrasonic testing using a higher amplitude signal generator. We will also complete the design and construction of a valve position monitoring system. Finally, efforts will also include creation of repeatable initial conditions and the start of initial flushing tests according to the developed test matrix.

REFERENCES

1. Bontha J.R., Adkins H.E., Denslow K.M., Jenks J.J., Burns C.A., Schonewill P.P., Morgen G.P., Greenwood M.S., Blanchard J., Peters T.J., MacFarlan P.J., Baer E.B., Wilcox W.A., 2010, Test Loop Demonstration and Evaluation of Slurry Transfer Line Critical Velocity Measurement Instruments, PNNL-19441 Rev. 0

2. Bontha J.R., Adkins H.E., Denslow K.M., Jenks J.J., Burns C.A., Schonewill P.P., Morgen G.P., Greenwood M.S., Blanchard J., Peters T.J., MacFarlan P.J., Baer E.B., Wilcox W.A., 2010, Test Loop Demonstration and Evaluation of Slurry Transfer Line Critical Velocity Measurement Instruments, PNNL-19441 Rev. 0

3. Denslow K.M., Jenks J.J., Bontha J.R., Adkins H.E., Burns C.A., Schonewill P.P., Bauman N.N., Hopkins D.F., 2011, Hanford Tank Farms Waste Certification Flow Loop Phase IV: PulseEcho Sensor Evaluation, PNNL-20350 FINAL

4. Hall M. N., 2006, Minimum Flow Velocity for Slurry Lines, 24590-WTP-GPG-M-0058, Rev 0.

5. Hansen E.K., 2015, WTP Pretreatment Facility Potential Design Deficiencies - Sliding Bed and Sliding Bed Erosion Assessment, SRNL-STI-2015-00014, Revision 0

6. Kazban R., Poloski A., 2016, Plugging and Wear of Process Piping at The Waste Treatment and Immobilization Plant, Document ID: DNFSB/TECH-40

7. Lee Kang, 2010, Ultrasonic Technique for Measuring the Thickness of Scale   on the Inner Surfaces of Pipes, Journal of the Korean Physical Society, Vol. 56, No. 2, February 2010, pp. 558-561

8. Nguyen V.C., Fountain M.S., Enderlin C.W., Fuher A.J.L., Pease L.F., 2016, One System River Protection Project Integrated Flowsheet-Slurry Waste Transfer Line Flushing Study, RPP-RPT-59600, Rev. 0

9. Poloski A.P., Bonebrake M.L, Casella A.M., Johnson M.D., MacFarlan P.J., Toth J.J., Adkins H.E., Chun J., Denslow K.M., Luna M.L., Tingey J.M., 2009, Deposition Velocities of Newtonian and Non-Newtonian Slurries in Pipelines, PNNL-17639, WTP-RPT-175 Rev. 0

10. Yokuda S.T., Poloski A.P., Adkins H.E., Casella A.M., Hohimer R.E., Karri N.K., M.Luna, Minette M.J., Tingey J.M., 2009, A Qualitative Investigation of Deposition Velocities of a Non-Newtonian Slurry in Complex Pipeline Geometries, PNNL-17973, WTP-RPT-178 Rev. 0

TASK 18.2
Development of Inspection Tools for DST Primary Tanks

EXECUTIVE SUMMARY

In August of 2012, traces of waste were found in the annulus of the AY-102 double-shell tank (DST) storing radioactive waste at the Hanford Site, prompting the need for developing inspection tools that can identify the cause and location of the leak. To help in this effort, FIU is investigating the development of inspection tools able to access the tank's secondary containment, while providing live visual feedback. This effort has led to the development of two inspection tools that includes a magnetic wheeled miniature motorized rover that will travel through the refractory cooling channels under the primary tank, and a pneumatic pipe crawler that will inspect the tank ventilation header piping. Both inspection routes lead to the central plenum under the primary tank.

The magnetic wheeled miniature tool is a remote controlled rover with four wheels directly driven by independent micro DC motors. It is equipped with front and rear cameras to provide live visual feedback of the inspection tasks and maneuvering. To avoid debris, the device will travel upside down magnetically attached to the bottom of the primary tank. It will also have to traverse over weld seams with heights ranging from 0.25 to 0.375 inches. A generic sensor hood has been designed to allow different sensors to be integrated via a common hard wired interface. The miniature tool is tethered to provide the power and communication links to and from the operator. To reduce operational fatigue, a semi-autonomous control is incorporated to assist the operator in steering the miniature tool during inspections.

System testing for the inspection tool has been carried out at the full-scale sectional mockup facility built at FIU. A system demonstration has also been performed for the WRPS site engineers during their visit to FIU. Feedback from the engineers for the improvement of the system are currently being incorporated. These include studies of the minimum magnetic force required for traversing weld seams, investigation of magnetic tank track designs as well as the incorporation of dual cameras for the inspection tool.

The pneumatic pipe crawler is an inspection tool that can navigate through 3- and 4-inch diameter pipes and provide visual feedback while traveling through pipelines in excess of 100 feet and multiple 90 degree elbows. Recent updates to the crawler include a new sensor module that can provide information regarding environmental conditions within the pipeline and a mapping of the interior surface of the line. The sensor module is a carousel type device that can rotate 360 degrees and is placed near the front of the crawler. The module can house a number of sensors including temperature, pressure, radiation, LiDAR, optical camera and an inertial measurement unit (IMU). The intent of the module is to improve the functionality of the crawler by providing environmental conditions within the pipe and internal surface topography maps that can assist in understanding potential wear, pitting or thinning of the pipe.

In addition to the 3- and 4-inch crawler, FIU is developing a 6-inch crawler that utilizes the same principles as the smaller unit. The objective of this tool is to navigate through the 6-inch drain lines leading to the drain channels within the foundation underneath the secondary liner of the DSTs. This crawler will house a miniature rover that will be deployed at the end of the drain pipe, where

it connects to the foundation.   The miniature rover will operate upside down, via magnets, underneath the secondary liner within the drain slots and provide visual information regarding the condition of the secondary liner. Thinning of the secondary liner has been noted from the annulus of the some of the DSTs, but it is unclear if the thinning is isolated to locations near the annulus.

INTRODUCTION

In August of 2012, traces of waste were found in the annulus of the AY-102 double-shell tank storing radioactive waste at the Hanford Site, prompting the need for developing inspection tools that can help assess the structural integrity of the DST primary liner. In addition, evaluations of the DST secondary liners within the tank annulus have also shown thinning of the secondary liner. This has prompted the development an inspection tool for the secondary liner as well.

Figure 23 shows three possible entry points for inspection in a typical DST (AY-102):

1. refractory air slots through the annulus,
2. leak detection piping, and
3. ventilation header piping.
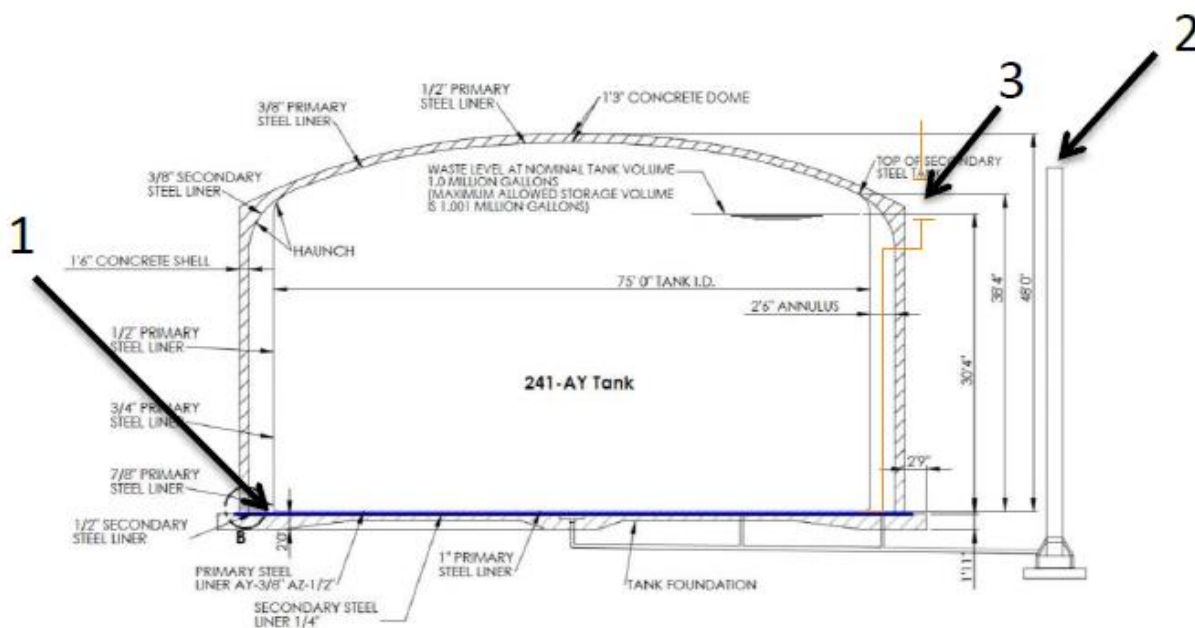
Figure 23. Inspection entry points of the AY-102 double-shell tank.

Among the inspection tools that are currently being developed and tested at FIU are:

*   a ***magnetic miniature rover*** that will travel through the refractory air slots,
*   a ***pneumatic pipe crawler*** that will inspect the ventilation header piping, and
*   a new ***marsupial crawler*** that will inspect the secondary liner.

The new marsupial crawler has a design that includes a pneumatic pipe crawler that travels through the 6" leak detection piping and houses a rover that has similar features as the magnetic miniature rover.

MAGNETIC MINIATURE ROVER

Background

FIU is developing a technology that will access the primary tank floor of DSTs at Hanford through the annulus and refractory air slots (Figure 24) and provide visual feedback of the conditions within the air slots. The refractory air slots range from 1 inch to 3 inches in width and provide a complex maze to navigate through, including four 90° turns to reach the center of the tank (Figure 25). Pictured is documentation on AY-102, a tank possessing one of the more difficult inspection paths due to the layout of the refractory cooling channels; other double-shell tanks contain channels with layouts that resemble a web structure with much larger angles at the turns rather than sharp 90° turns (Figure 26).
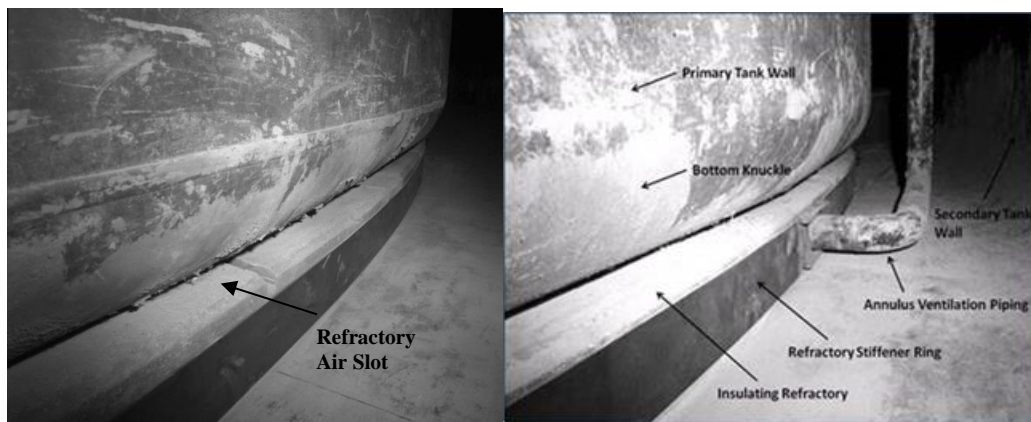
Figure 24. Side view of primary tank and refractory air slot.
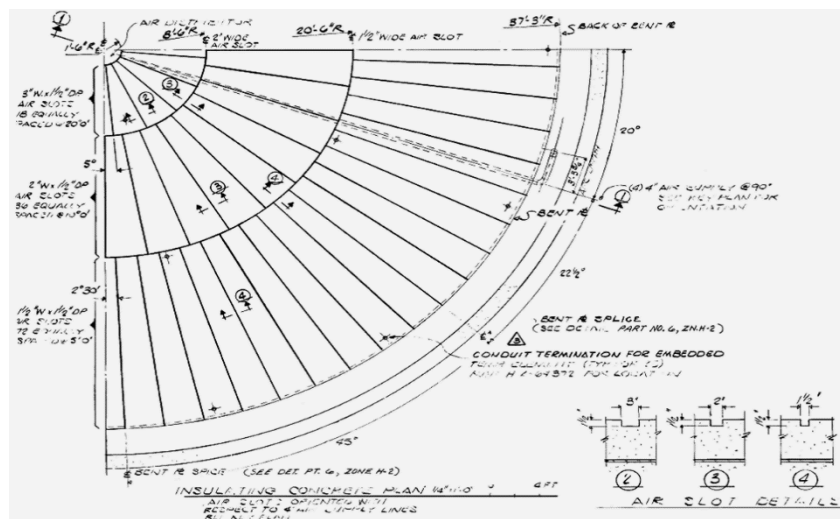
Figure 25. Refractory air slot layout and description for AY-102.
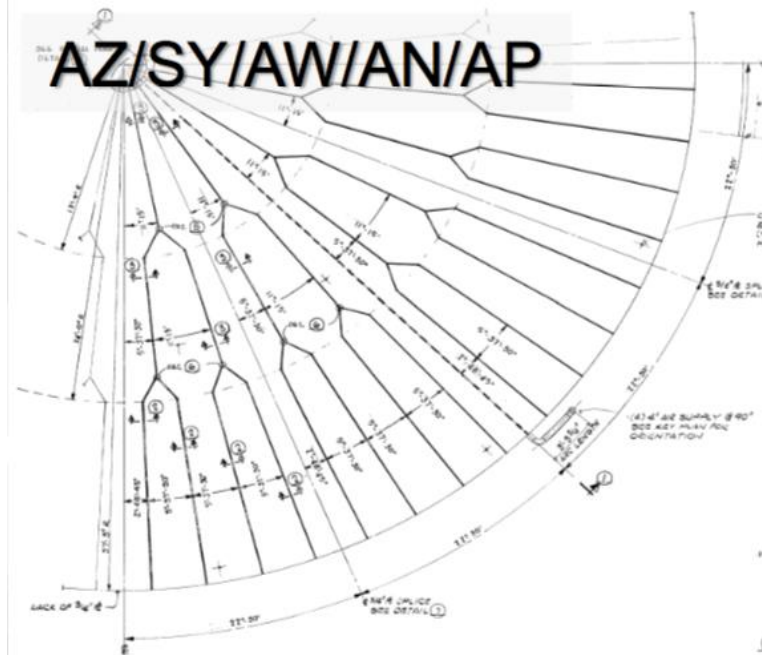
Figure 26. Refractory slot layout for Tank type AZ, SY, AW, AN and AP.

Technology demonstration

During a visit by the site engineers from the WRPS in February 2018, the miniature inspection tool was demonstrated in the full-scale DST mockup and was able to traverse the full distance of the sectional mockup, from the annulus to the central plenum (Figure 27). Problems did arise due to the uneven surfaces created by the steel plates. The plates did not align perfectly, which created gaps that the tool had trouble traversing. This was temporarily solved with the placement of high-powered magnets at the joints between the plates, which forced the plates to align. Due to the tool's geometry, the front PCB sometimes comes into contact with the plate prior to the wheels, which prevented the tool from easily traversing the gaps.
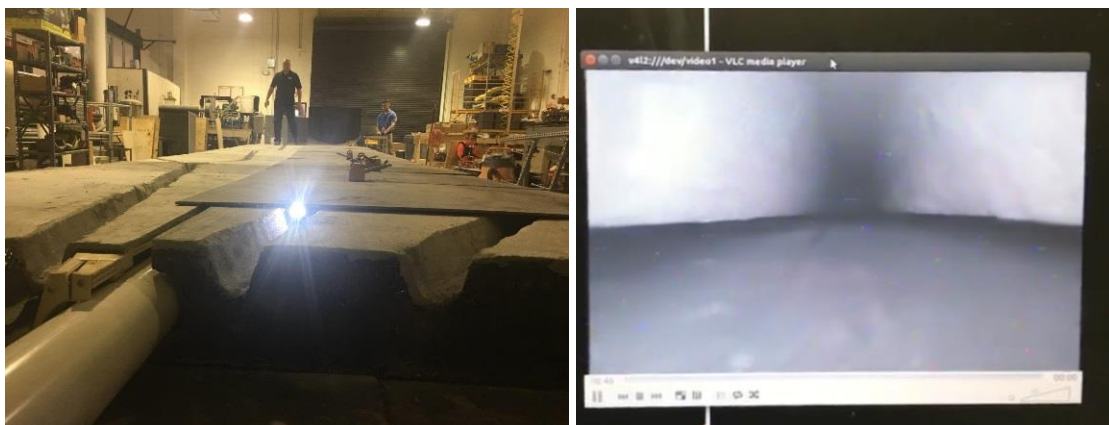
Figure 27. Demonstration of the mini inspection tool traversing from the entry to the end of the mockup (left) and image/video captures from the mini inspection tool's onboard camera (right).

The feedback from the WRPS engineers after the demonstration has proven to be extremely beneficial for FIU because it helped to identify two additional, yet critical operational requirements for the mini inspection tool. The first requirement is for the inspection tool to traverse the weld seams that are located underneath the actual tanks. According to the site engineers, the weld seam heights can range from 0.24 to 0.375 inches. The second requirement is for the inspection tool to have a backward facing camera to aid in reversing maneuvering during the inspection tool's retrieval, after the inspection task has been completed. During the demonstration, retrieving the inspection tool without any visual feedback to the operator was shown to be challenging.

Numerical studies of maximum magnetic force while traversing weld seams

FIU set up a numerical experiment using Matlab to calculate the maximum magnetic force of the magnets that line the bottom of the rover, based on the height of the weld seam and the distance the rover has traveled. Since the magnetic force falls off exponentially with increasing distance from the surface, it is critical to ensure that the mini inspection tool still have sufficient magnetic force with increasing seam heights. Figure 28 shows the numerical study setup and results. FIU varied the weld seam height from 0 to 0.5 inches, while decreasing the chassis length offset (simulating the tool moving forward, causing an increase in the distance between the tool's bottom and the tank surface). The results showed that the mini inspection tool still has sufficient magnetic force even with a seam height of 0.5 inches. Since the inspection tool navigates upside-down, gravitational force will not aid the tool in pivoting over the center point of the weld seam. FIU's preliminary study showed that there is a very small margin for the magnetic force (before and after the pivoting point) to cause the tool to pivot forward so that the front wheels can regain traction and allow the tool to continue its maneuver.
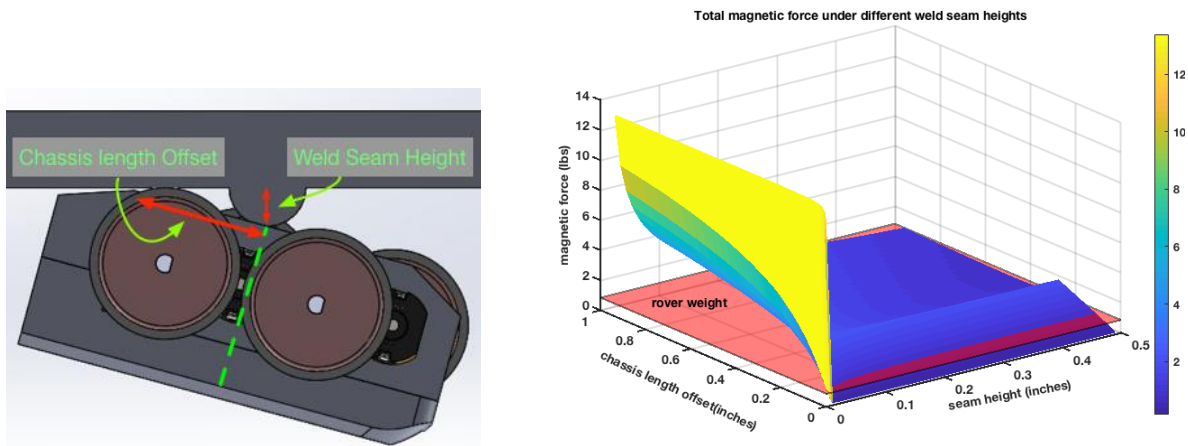
Figure 28. Setup for the numerical study showing the weld seam height and chassis length offset (left) and the results from the computation (graph above the rover weight plane) showing that the mini inspection tool has sufficient magnetic force to overcome its weight (right).

Feasibility studies of magnetic tank track design

Instead of relying on the magnets attached underneath the inspection tool, of which the attraction force decreases drastically with increasing clearance, the magnetic tank track design enables the magnets to be in contact with the surface at all times, even when the tool is traversing over weld seams. Figure 29 shows the CAD drawing of the magnetic tank track system that was designed as part of the feasibility study. Due to the width constraint for the inspection tool, the width of the

track only measures 0.25 inches. FIU envisions at least 4 magnets will be in contact with the surface on each side of the inspection tool. With each magnet providing approximately 1 pound of attraction force, the magnetic tank track system would provide approximately 8 pounds of attraction force for the inspection tool.
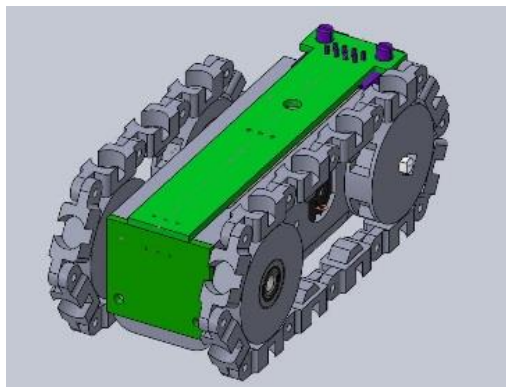
Figure 29. The CAD drawing of the scaled-down version of the inspection tool.

Due to the scaling down of the tank track system, the design of the joint of the track links poses challenges in terms of size and material strength to support the operation of the inspection tool. Several iterations of the design have been performed to identify suitable linking mechanisms, as well as materials to be used to ensure the required strength. Figure 30 shows three different designs using pin (top left), bearing (top right) and rivet (bottom) designs. The rivet design was selected based on the ease of assembly and lower expected maintenance. Nylon was selected as the best fabrication material to ensure structural strength at the miniature scale required.
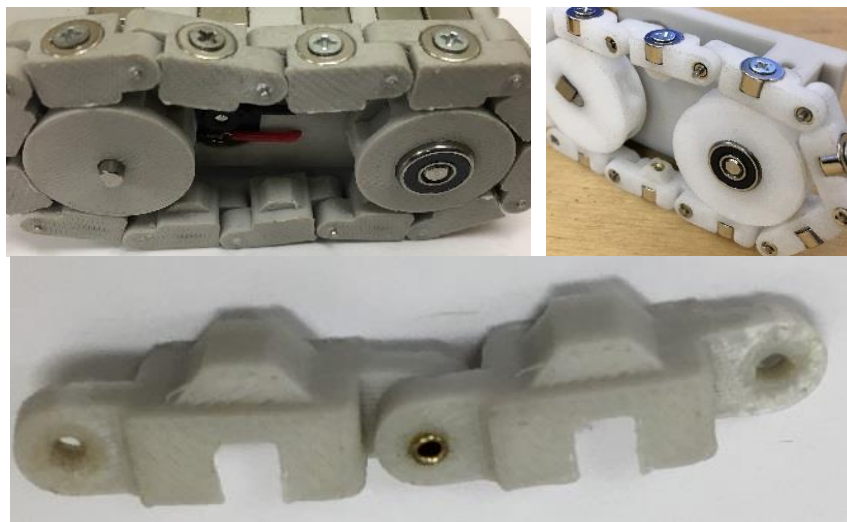
Figure 30. Pin design (top left), bearing design (top right), and rivet design (bottom).

As a comparison, FIU has also adjusted the current inspection tool to have a chamfer in the front, in order to help overcome the weld seam. As the development of both a chamfered and tank tread version of the mini inspection tool was continued (Figure 31), the links for the tank treads were 3D printed with nylon and magnets were attached so that the tank maintains direct contact with the traveling surface. Stronger magnets were also attached to the underside of the rover in order to

increase the overall adhesion force to the steel plates. Changes to the tank design were also explored in order to overcome the weld seams that line the refractory slot ceiling.
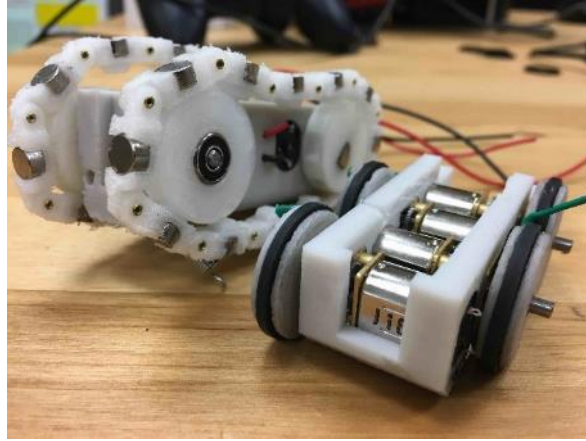
Figure 31. Tank tread (left) and chamfered (right) versions of the mini inspection tool.

Five weld seams of varying heights (0.1, 0.25, 0.33, 0.5, and 0.75 inches) were created along a 3-foot steel bar in order to simulate the obstacles in the actual tank (Figure 32). The tank tread version, along with the chamfered version of the mini inspection tool, were both tested with varying degrees of success. The chamfered version, fitted with a large rubber O-ring that connects the wheels on each side of the inspection tool, was able to traverse all of the weld seams when right-side-up. Operating upside-down, it managed to traverse both the 0.1 and 0.25 inches weld seams, but not the larger heights. The magnetic force was the limiting factor for this design. The magnetic force calculations previously performed showed that the attraction force of the magnets drops sharply with an increasing gap. The tank tread design was unable to overcome any of the seams, most likely due to the stiffness of the links in the system. This design effort will be put on-hold until a more suitable material and miniature link mechanism are identified. Figure 33 shows the bench-scale testing of both versions of the inspection tool traversing over weld seams of different heights.

Figure 32. Weld seams of increasing height from 0.1 to 0.75 inches.
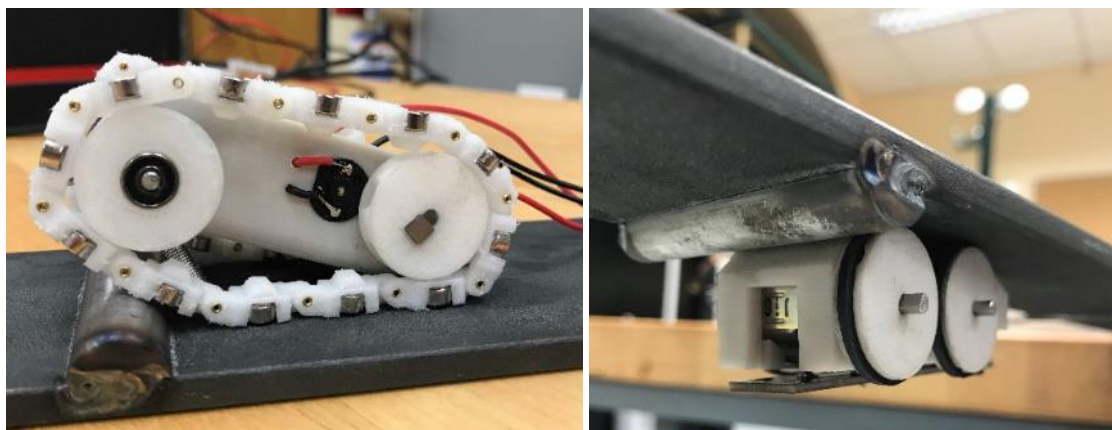
Figure 33. Bench tests of two different versions of the inspection tool traversing over weld seams of different heights.

Incorporation of rear facing camera

An alternate design for the chamfered version was also designed and fabricated for housing a different connector and a rear PCB. The new flatter connector will free up room for the rear PCB to be mounted. In addition, the design will also allow the connector to be covered and secured within the inspection tool's housing, thus providing a better protected and secured connection. The rear PCB has both a camera and multiple LEDs attached in order to provide video feedback when the unit is moving backwards. The modified version of the mini inspection tool, together with the 3D printed chassis and newly fabricated PCB boards are shown in Figure 34.
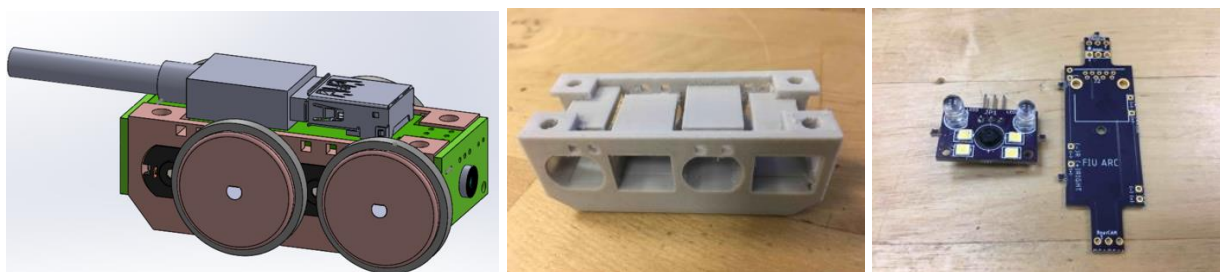
Figure 34. Mini inspection tool with dual camera design and chamfered chassis (left), the 3D printed chassis (middle) and newly fabricated PCB boards (right).

The fully assembled, modified version of the mini inspection tool is shown in Figure 35. The major difference from the previous version of the mini inspection tool is the backward-looking camera, as well as moving the tether connector to the top of the inspection tool, to provide space for the second camera. The tool is fully functional and is currently being tested in the full-scale mockup facility at ARC as well as with traversing weld seams.
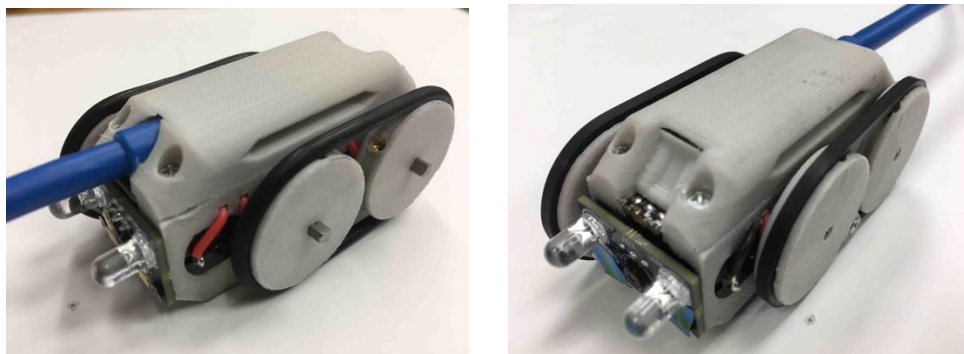
Figure 35. Fully assembled mini inspection tool with dual cameras.

One of the concerns expressed by the site engineers was the strength of the tether connection since the inspection tool must be capable of being pulled out in case of system failure. This critical fail-safe measure will ensure that no external objects are left behind, which could potentially obstruct the air flow that is used to maintain the tank temperature. The modified mini inspection tool has the connector located at the top of the tool, and the connection is tightly secured with two supporting screws and the hoop. Figure 36 shows the screw holders that are used for the screws to secure the hoop and the tether connector to the inspection tool. Tests were conducted to ensure the strength of the tether when it is pulled (Figure 36). The tether and the connector were able to withstand a pull-force of about 65 lbs. without breaking. FIU is also considering incorporating a bus drop grip on the tether to increase the safety buffer.

Figure 36. Screw holders at red arrows (left) for securing the hoop and the connectors to the inspection tool and performing a pull test for tether strength (right).

Semi-autonomous control

FIU reviewed the video footage from the deployment of the inspection tool at the sectional full-scale mockup facility and noted that due to the close proximity of the inspection tools' camera to the tank bottom, and wider refractory slots of AZ/SY/AW/AN/AP tank configuration, the previous approach of using image segmentation to identify navigable region is no longer suitable. Figure 37 shows the camera views in the slot mockup that mimics the narrower top surface the slot for the AY tank configuration as well as the wider top surface of the slot for other tank configurations. The narrower slot configuration poses a challenge to determining a clear navigable path for semi-autonomous control of the technology.
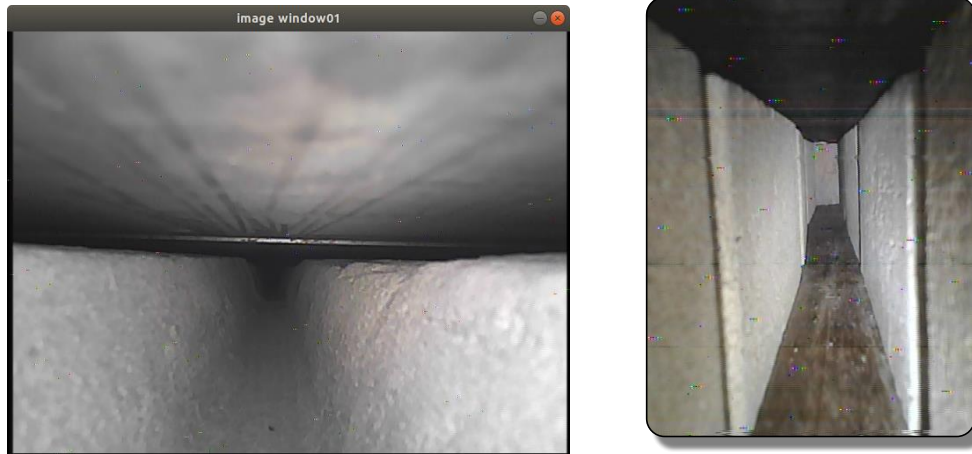
Figure 37. Narrower top surface of the slot mockup based on the AY tank configuration (right) and the wider top surface of the slot mockup based on other tank configurations (left).

Instead of segmenting the top surface of the tank, FIU took advantage of the channel's geometry and the lighting conditions on the refractory slots when illuminated by the inspection tool's lighting source as another alternative for navigable path identification. The approach employed the inverse perspective transformation of the camera's image to identify the central location of the slot. Figure 38 illustrates the idea of using the inverse perspective transformation. It transforms the camera's image, taken at the real camera's position, to an image that appears as if it was taken from a top view camera. The results from the transformation of the video footage taken at the sectional full-scale mockup can be seen in Figure 39. The approach managed to identify the center location of the slot and the inspection tools' current heading (blue and red circles shown in Figure 39). The horizontal difference between these two circles can be used to control the mini inspection tool to perform lane-keeping during semi-autonomous operation.
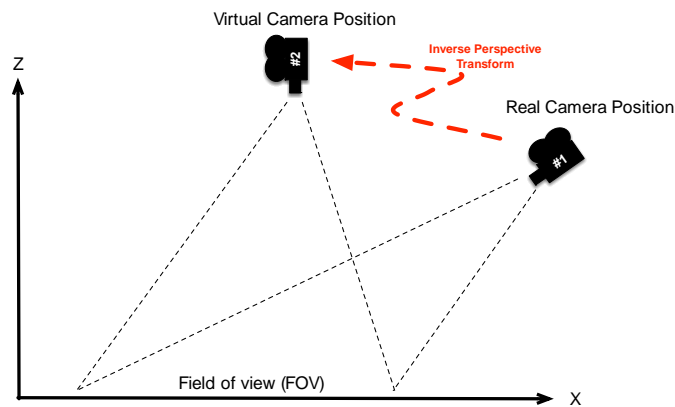
Figure 38. Inverse perspective transformation to transform the camera's image, taken at the real camera's position, to an image as if it was taken at the virtual camera position.
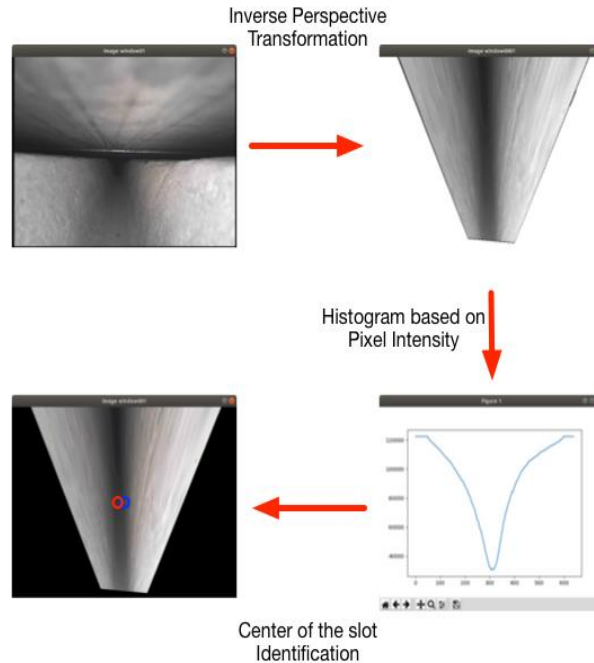
Figure 39. Video captures from the inspection tool's camera (left top) undergo inverse perspective transform (right top). After that, a histogram based on the resultant pixels' intensity was constructed (right bottom), and the valley of the histogram was identified as the center location of the refractory slot (left bottom). The blue circle is the slot center while the red circle shows the inspection tool's current heading.

The proportional integral derivative (PID) controller for the newly implemented inversed perspective lane identification was also developed and tested at the mockup facility. Figure 40 shows the performance of the resultant PID controller, during a forward and backward transact. The controller was able to keep the inspection tool close to the center of the detected lane. The minor fluctuation of the control performance was due to the dead zone of the mini inspection tool's servo motors and does not affect the semi-autonomous operation.
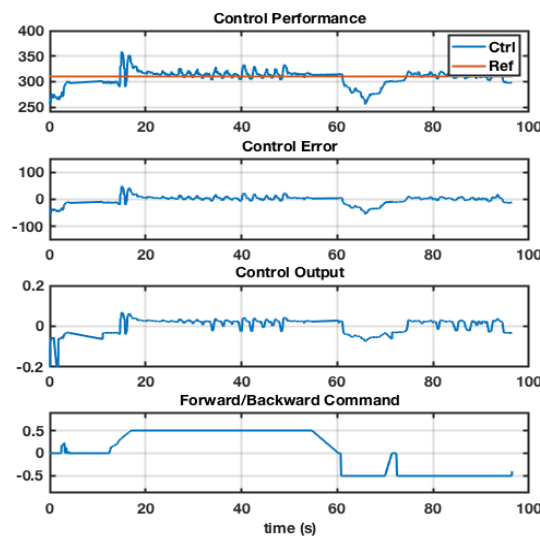
Figure 40. Control performance of the PID controller for the inversed perspective lane identification system.

Knowing the mini inspection tool's location along the refractory slot is critical in associating the location information with any potential anomalies found during an inspection. Even though the location can be approximated by measuring the tether length, it does not account for potential tether slacks from the location of deployment. FIU also investigated the application of monocular simultaneous localization and mapping (SLAM). FIU adopted the monocular SLAM approach proposed by Raul, et. al. [1], and calibrated the camera using the mini inspection tool's onboard camera. Figure 41 shows the preliminary results from the SLAM performed (offline) using the video images obtained by the mini inspection tool during a test at the full-scale sectional mockup facility at FIU. Field experiments will be conducted to ensure that the SLAM can be performed online, and to validate the accuracy of the location information generated.
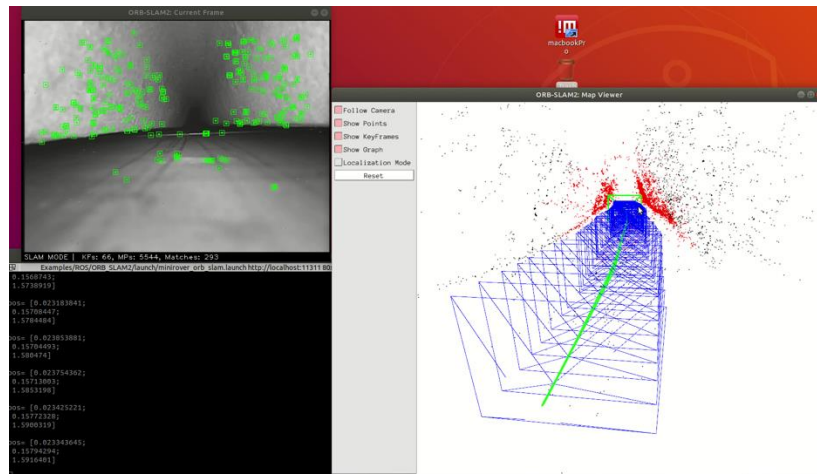
Figure 41. Screen capture of the SLAM performed using the visual images obtained by the mini inspection tool during a test at the sectional full-scale mockup facility.

PNEUMATIC PIPE CRAWLERS

3- and 4-inch pipe crawler

Since a leak was discovered within Hanford tank 241-AY-102 [2], FIU has been developing a pipe crawler with the objective of providing visual feedback of the primary liner of DSTs near the central plenum. The crawler would need to navigate through the air supply line header to one of the four supply lines leading to the central plenum. The path requires traversing through over 100 feet of 3- and 4-inch diameter pipes with multiple 45 and 90 degree elbows as shown in the figures below. A detailed description of the crawler development and testing can be found in references [3] and [4].

The current design for the pneumatic pipe crawler is a worm-type robot with a modular design, composed of interchangeable cylindrical modules connected with flexible links. Figure 42 shows of one of the more recent designs of the system.
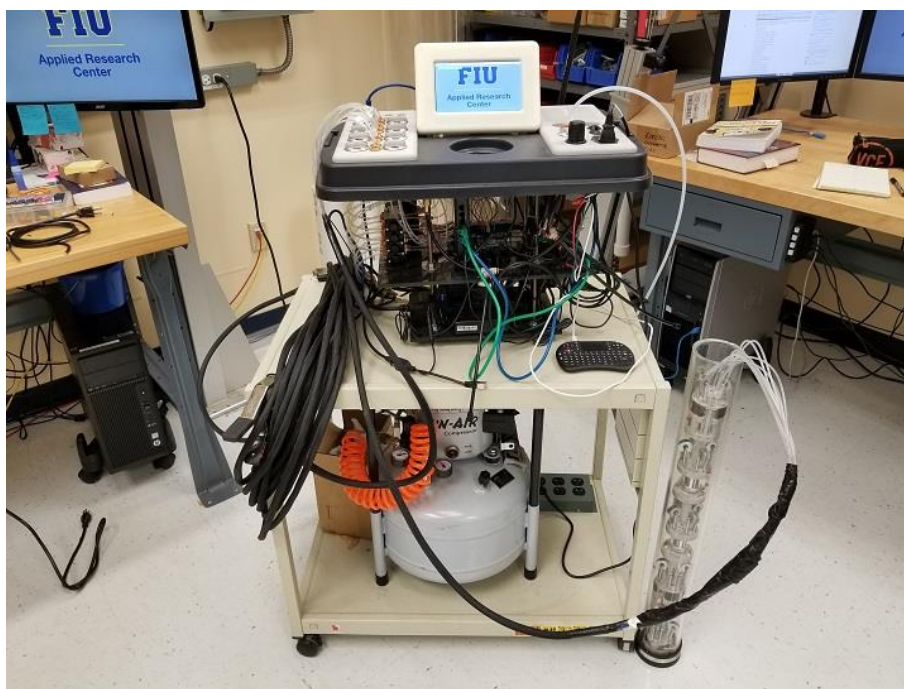
Figure 42. FIU's pneumatic pipe crawler.

Minor changes were implemented in the pneumatic crawler design, including a streamlined camera module, and extension modules with a larger stroke. The following figure shows the new streamlined camera module, redesigned to better handle obstacles and geometrical changes in pipes and fittings.

Figure 43. Redesigned camera module.

The 3/4" stroke pneumatic cylinders of the extension modules were also replaced by equivalent actuators with 1-1/2" stroke each, which significantly improved the device speed and navigation thru elbows. The figure below shows the current crawler with the minor design modifications.
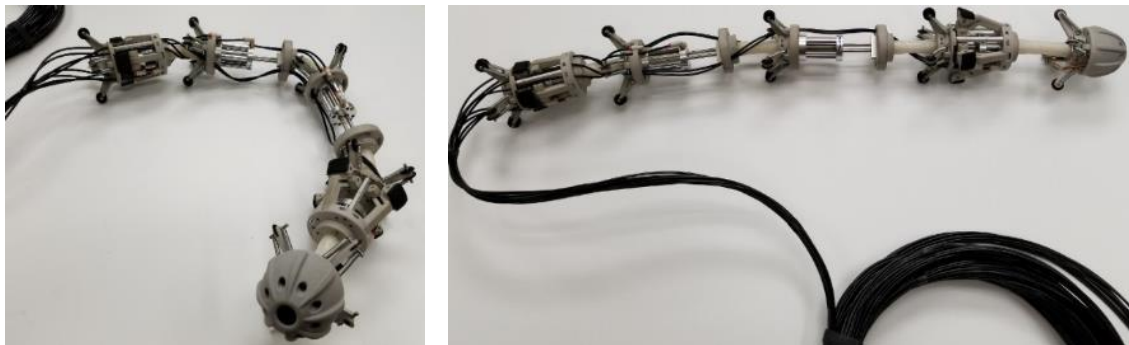
Figure 44. Current design of the crawler.

Recently, the objectives for the pipe crawler have been broadened to include general inspection of pipelines. With this objective in mind, an instrumentation module is being integrated with the crawler to provide additional information about the environment and integrity of the pipelines.

Figure 45 illustrates commonly occurring anomalies that compromise the structural integrity of pipelines. Due to the complexity of their mechanisms, the designed module hosts a set of different sensors necessary for proper evaluation and prognosis. This section includes a description of the module design and the sensors included in the module to help diagnose these anomalies. It also describes the assembly process and the testing conducted to validate the sensors and the module.
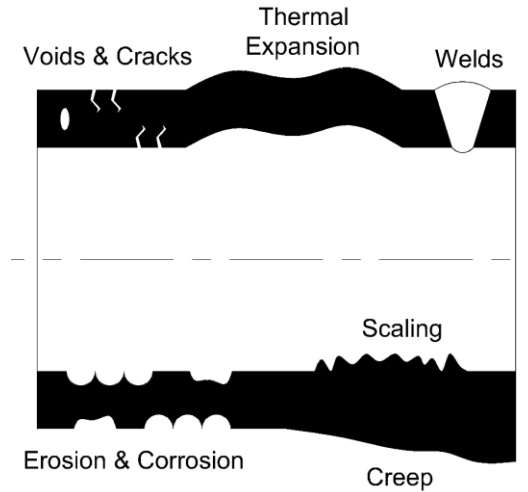
Figure 45. Common pipeline integrity issues.

Instrumentation Module

The sensor module was designed with the objective of improving the capabilities, robustness and operational feedback of the pipeline crawler. The module is a carousel type device that uses a spinning drum for evaluating the circumference of the internal surface of a pipe. A conceptual design is shown in Figure 46 which includes nine panels that can be used to mount sensors.
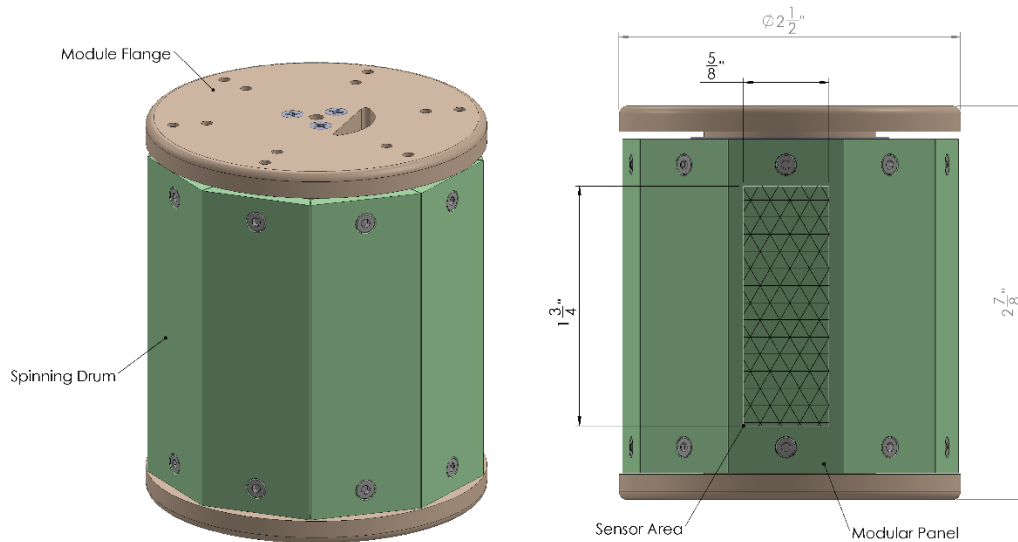
Figure 46. Instrumentation module.

In this prototype, the instrumentation module is placed behind the camera module of the crawler. Positioning the module in this location eliminates the need for the pneumatic lines that supply the gripper and the expansion modules to pass through the instrumentation module, simplifying the construction and maximizing space. Figure 47 shows a rendering of the instrumentation module integrated into the pneumatic pipe crawler.
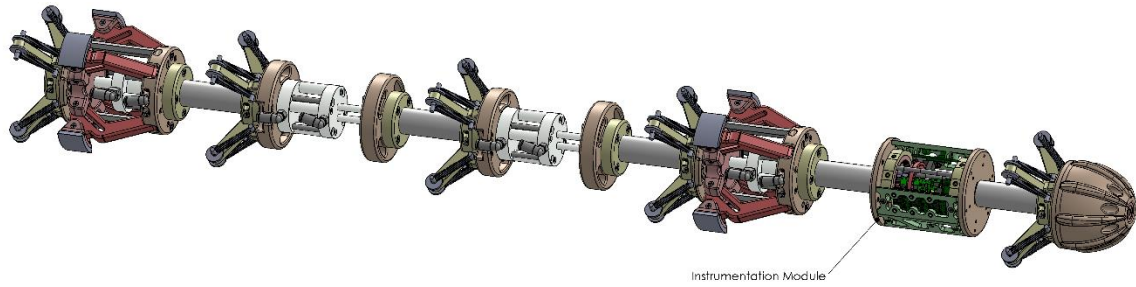
Figure 47. Pneumatic crawler.

The rendering of the module's rotating drum with one of the nine panels installed is shown in Figure 48. An optical encoder is installed on one panel and there is the potential to install eight additional sensors.
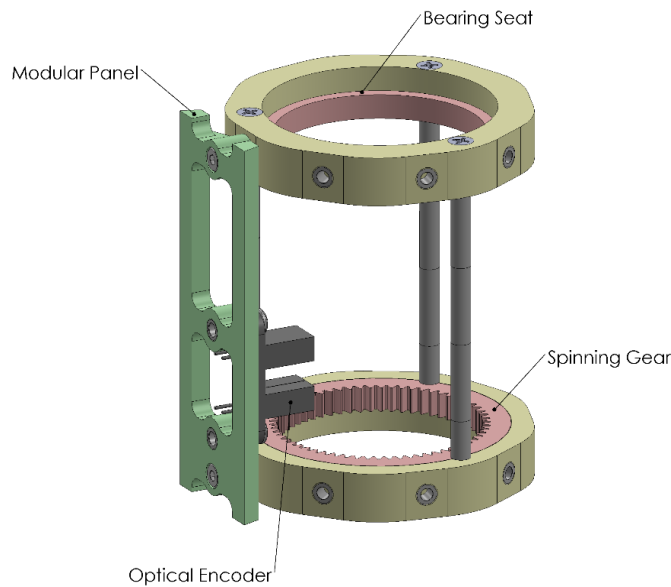
Figure 48. Module's spinning drum.

The basic components in the module are shown in Figure 49. The design includes:

    a) a set of spur gears, similar to a planetary gearbox, to provide the spinning movement,
    b) an optical encoder to track the rotational position and the speed of the drum, and
    c) an inertia measurement unit (IMU) to provide an estimation of the position and the orientation of the module.
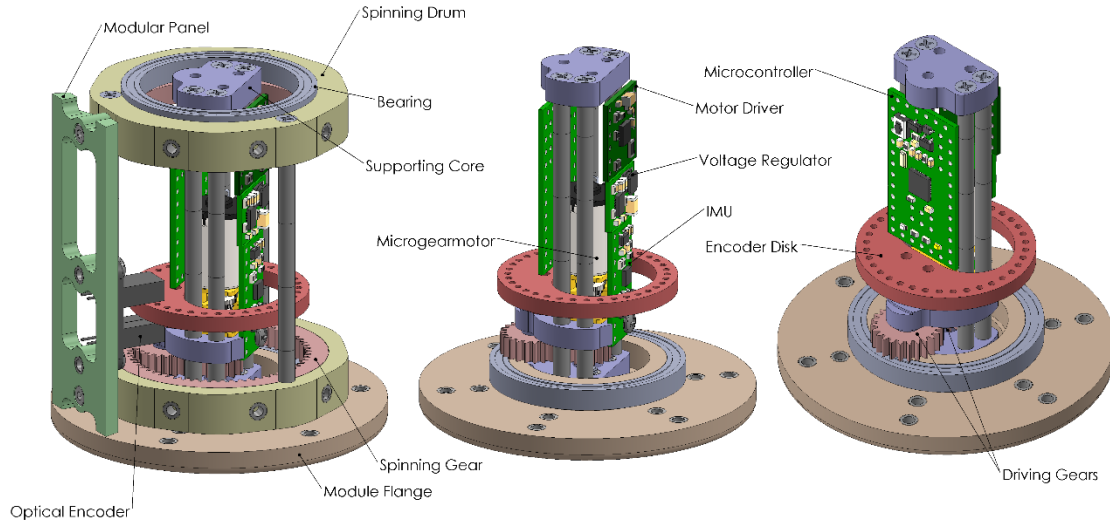
Figure 49. Module's basic components.

The current prototype of the instrumentation module is illustrated in Figure 50, which uses the following off-the-shelf sensors:

- a BME280 atmospheric sensor to measure barometric pressure, humidity, and temperature,
- a LSM6DS33 inertial measurement unit (IMU) to measure position and orientation,
- three VL6180X proximity (LiDAR) and ambient light sensors to measure pipeline circumference,
- a generic miniature NTSC video camera to stream surface images, and
- a RD2014 radiation sensor.
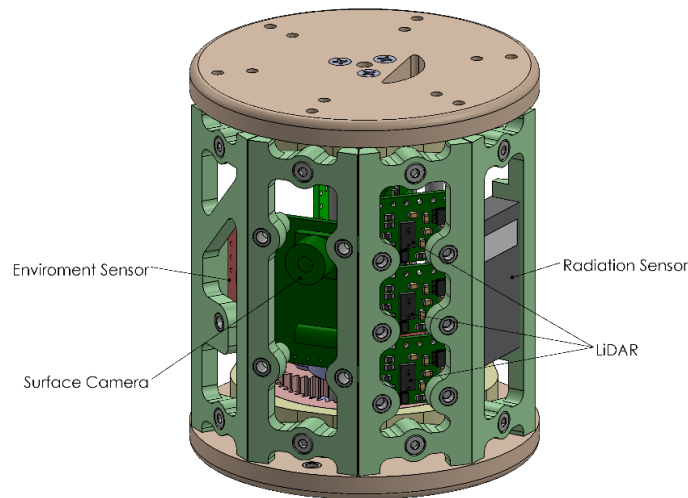
Figure 50. Instrumentation module.

All controls and the data stream from the instrumentation module to the pneumatic crawler's control box is handled using RS-485 communication, which is a half-duplex serial network that runs throughout the inspection tool, connecting all of the microcontrollers. Images from the surface camera is streamed using an additional analog video line, similar to the front camera.

The module consists of a cylinder that includes top and bottom flanges, the motor housing and panels that attach to the sides of the module.

The module with the sensors installed is shown in Figure 51. The left picture shows the LiDAR sensor, the middle shows both the radiation sensor and the environmental sensor which includes temperature, humidity and pressure and the right picture shows the camera.
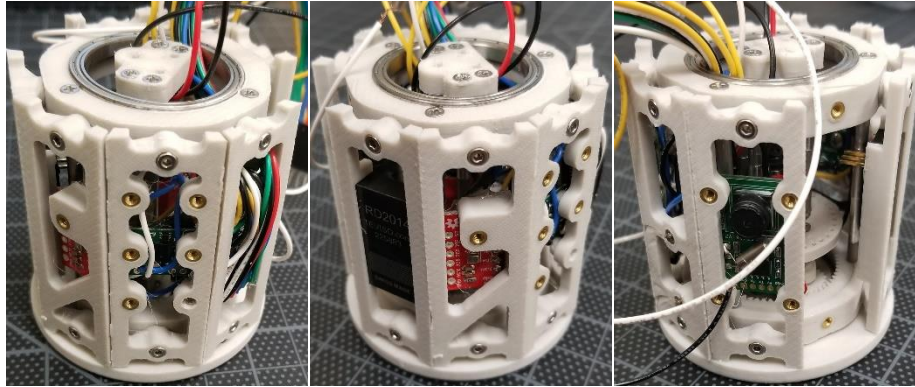
Figure 51. Installed sensors: LiDAR (left), radiation and environmental sensor (center) and camera (left).

It should be noted that the module structure is 3D printed and can easily be modified for a number of other types of sensors. Currently, the wiring from the sensors to each of their control boards takes up a significant amount of space and restricts the rotation of the module. Efforts continue to streamline the wiring of the sensors and the connections to the module microcontroller as well as to develop a slip ring to improve wire management and increase available spacing.

The sensor module is shown in Figure 52 and depicts how it fits within the pneumatic crawler. As noted previously, the sensor module is placed behind the front camera and before the forward gripper module. This eliminates the requirement of having to pass the pneumatic lines through the sensor module.

Figure 52. Crawler with sensor module.

Module Evaluation

The sensor module is controlled by several embedded microcontrollers, which manage and control the communication of all sensors in the unit. A serial network connects all microprocessors throughout the inspection tool to the portable control box via the tether. Table 5 lists the sensors currently utilized in the module and their respective specifications. It should be noted that these sensors are commercial-off-the-shelf products and were selected based on cost to demonstrate the functionality of the module. In the future, more precise sensors will be considered for deployment.

Table 5. Sensor Specifications

Sensor	Measurement	Range	Resolution	Unit	Model
Environmental	Temperature	-40 – +85	±1	°C	BME280
	Pressure	30 – 110	±0.1	kPa	
	Humidity	0 – 100	0.008	%RH	
Inertial measurement unit (IMU)	Acceleration	±2, ±4, ±8, or ±16	±0.004	g	LSM6DS33
	Angular velocity	±125, ±245, ±500, ±1000, or ±2000	±10	°/s	
Radiation	Beta, gamma and X-rays	0.0001 – 100	±10%	mSv/h	RD2014
Camera	Surface imaging	640 x 480	VGA	Pixel	Generic
Light Detection and Ranging (LiDAR)	Circumferential mapping	10 – 100	±1	mm	VL6180X

To evaluate the ability of the LiDAR to scan the internal surfaces of pipes, a template representing a pipe was designed and is shown in Figure 53. The 3D printed template simulates sections of 3- and 4-inch diameter pipes with measurable irregularities.
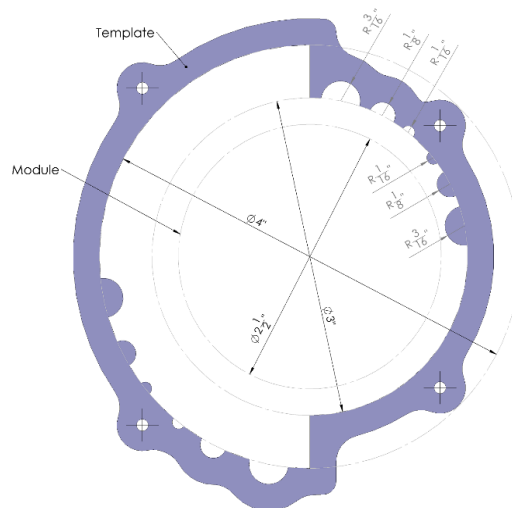
Figure 53. Scanning template.

During scanning tests, the module was secured at the center of the template frame as illustrated in Figure 54. To evaluate the module, the unit was rotated 360 degrees and scans were taken to determine if the sensor could detect the changes in the surface. Figure 55 indicates the LiDAR location and demonstrates how a typical scan was conducted.
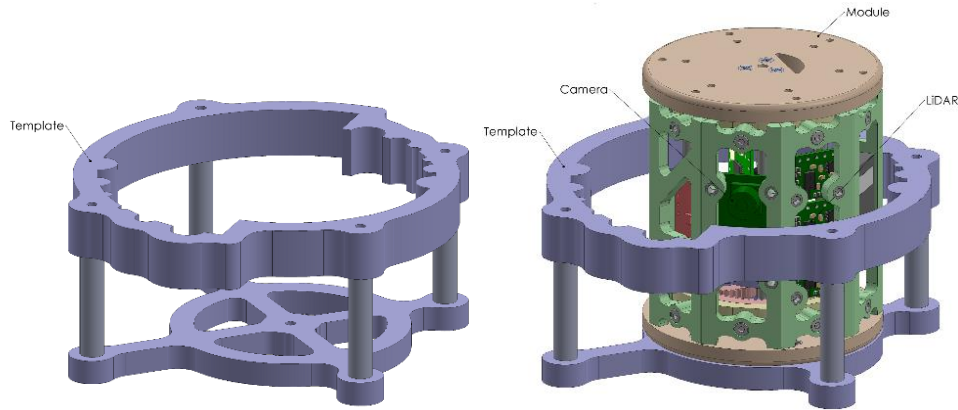
Figure 54. Scanning testbed.
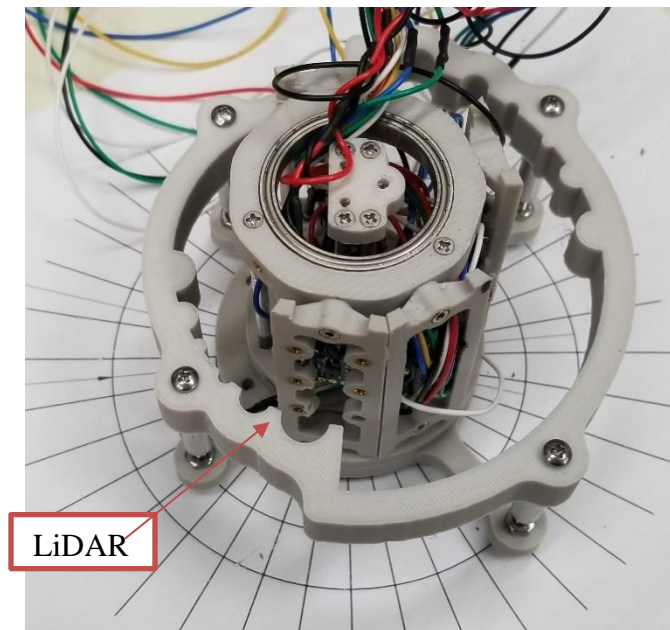
Figure 55. LiDAR testbed.

The preliminary results, shown in Figure 56, demonstrate the module and sensor's potential to detect pipeline anomalies and material buildup. Both the raw and filtered data are provided in the figure. As noted previously, FIU plans to investigate higher resolution scanners that would increase the circumferential scanning resolution of the module, to ultimately provide a valuable tool for surveying pipelines with small diameters.
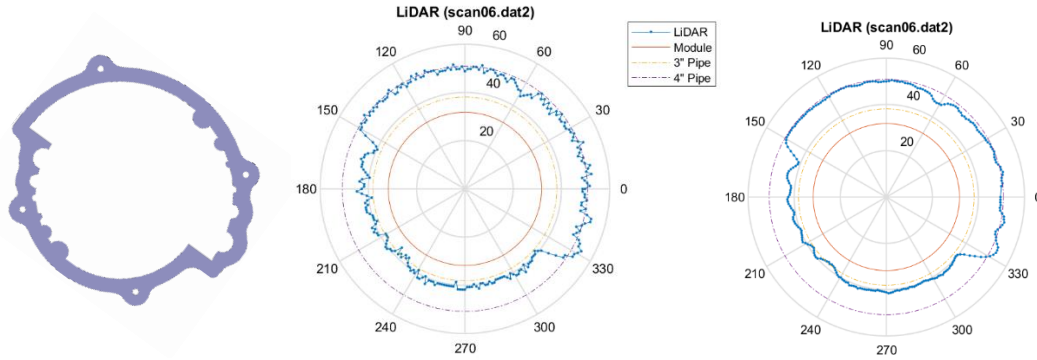
Figure 56. Preliminary circumferential scanning, raw data (left) and filtered data (right).

In addition to testing the LiDAR, the module's circumferential camera was also evaluated for its functionality. A circumferential camera can be a valuable tool when inspecting the localized surface conditions for damage and modes of corrosion and erosion. Figure 57 shows the camera location during the testing and evaluation.
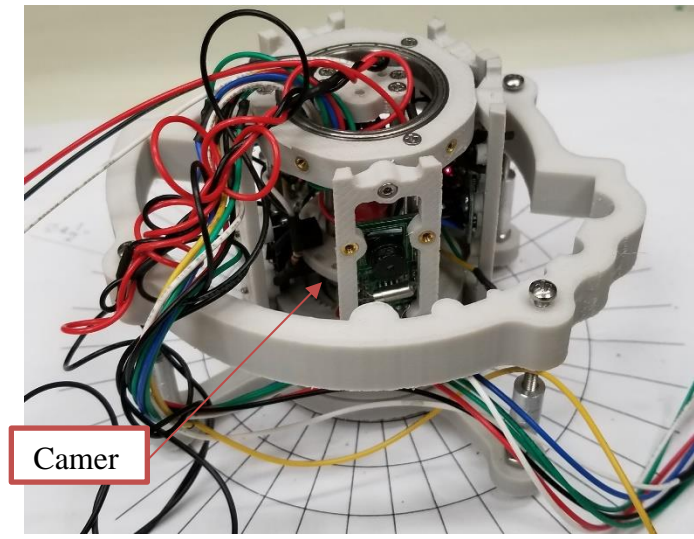
Figure 57. Circumferential camera.

To evaluate the imaging capabilities of the camera, the module was placed within a 4-inch diameter pipe section and rotated 360 degrees. The camera recorded the internal surface over the entire circumference. Figure 58 shows screen captures of the surface at various locations around the circumference. As with the LiDAR scans, these tests were intended to demonstrate the capabilities of the module and sensors. A more sophisticated camera with zoom control and improved image quality is needed. High quality imaging and LiDAR data would allow accurate mapping and three-dimensional reconstruction of pipeline surfaces.
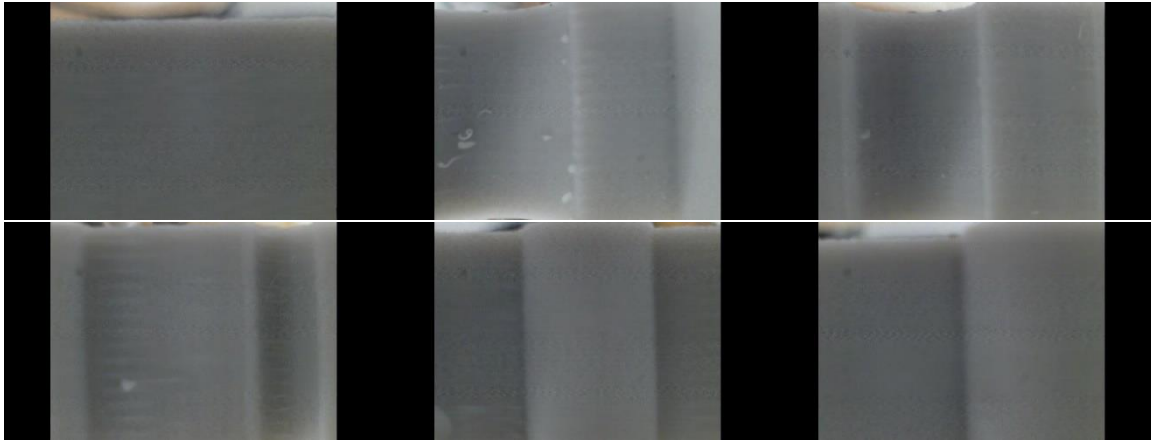
Figure 58. Preliminary circumferential scanning.

From the testing images (Figure 57), the wiring of the sensors is clearly an issue that needs to be addressed. The wiring takes up a significant amount of space within the module and limits the ability of the unit to rotate more than 360 degrees. To avoid wire entanglement, future efforts will focus on incorporating a slip ring to allow for continuous rotation of the module.

The sensor module also includes an IMU sensor installed at the center of the module. The sensor provides information including the orientation of the unit. Figure 59 shows a sample of the data in which movements demonstrated consecutive rotations about the yaw, pitch and roll axes of the crawler. The orientation results were calculated, based on the accelerometer and the gyroscope readings, using an implementation of the Madgwick's Attitude and Heading Reference System (AHRS) algorithm. This algorithm utilizes an extended Kalman filter to fuse data from the gyroscopes and the accelerometers provided by the IMU.
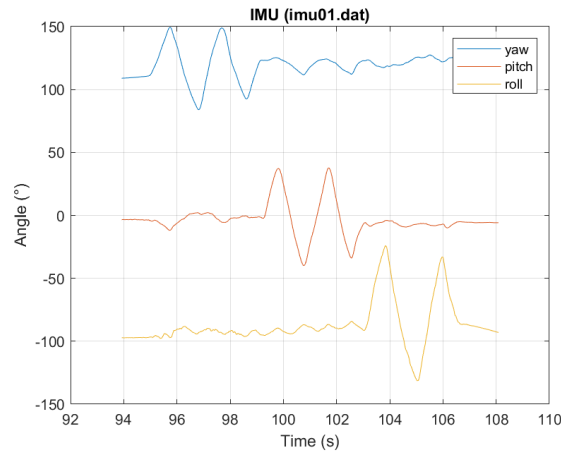
Figure 59. IMU movement.

Marsupial Crawler

Recent concerns about the structural integrity of the containment foundation of DSTs had prompted the need for developing specialized tools to inspect for potential thinning of the secondary liners at the bottom of the tanks under the refractory pads. The access points for these inspections is the leak detection system integral to the tank's concrete foundation. Figure 60

illustrates the types of leak detection systems at Hanford' DSTs. In all configurations, a 6-inch drain pipeline provides access to the drains slots under the tank through a leak detection pit.
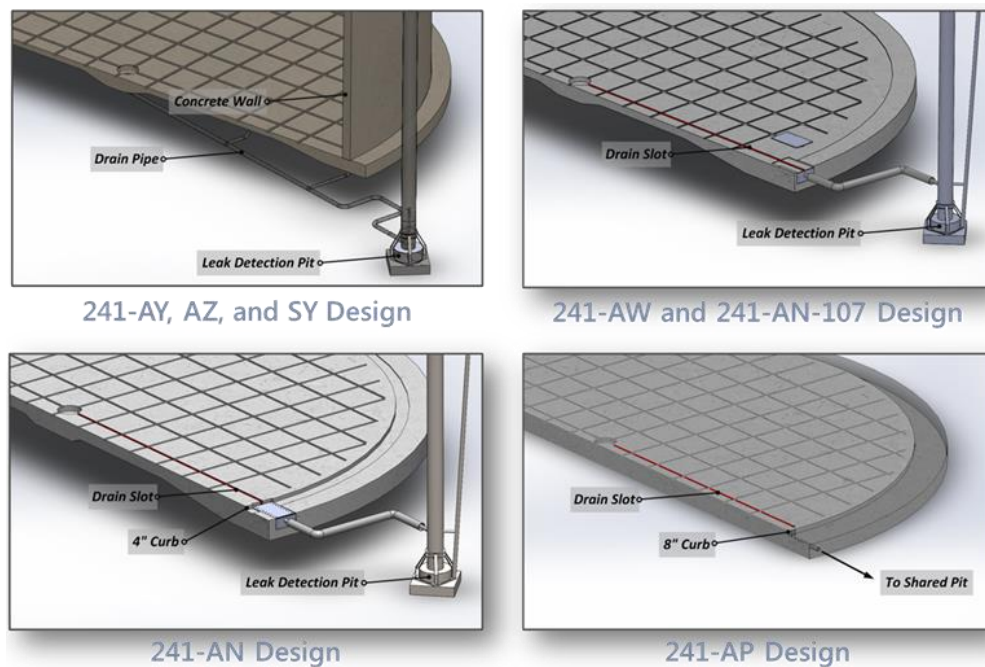
Figure 60. Leak detection systems at Hanford' DSTs.

To address this need, a novel inspection tool has been designed based on lessons learned from previous crawlers developed at FIU. The tool, in design, is a robotic marsupial system that uses a mother pipe crawler to navigate through the 6" drain lines and deploys a miniature child-rover into the drain slots. With this configuration, the pipe crawler will be responsible for managing the tether of the child-rover and to rescue the miniature unit in case of failure.

The rendering of the conceptual design of the primary pipe crawler is shown in Figure 61. This 6" crawler operates on the same peristaltic principles as the 3-inch system previously developed at FIU [2] that travels through the air supply line to the central plenum.
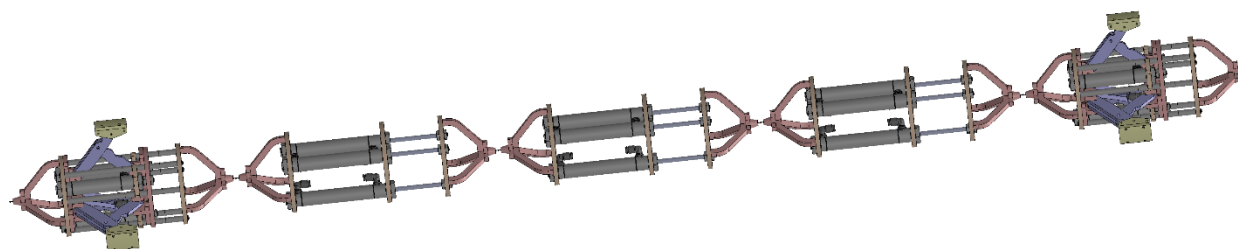
Figure 61. FIU's 6-in peristaltic crawler.

The crawler's current design has two front and back gripper modules and three middle expansion modules. The modules are attached with articulating joints that allows the unit to maneuver through pipe bends. In each module, the actuators are radially distributed allowing a hollow core convenient for carrying payloads, instrumentation and cabling. Figure 62 illustrates this concept showing the conceptual design and a prototype of the gripper module.
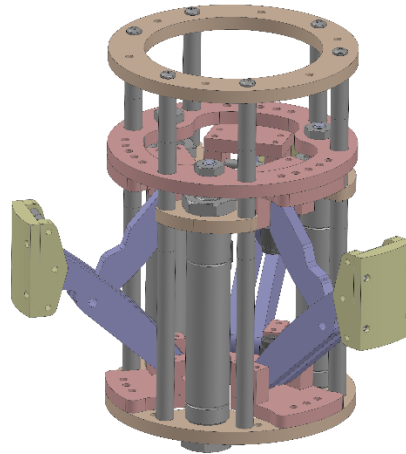
Figure 62. Conceptual design of the 6-inch crawler gripper.

The first prototype of a mother-crawler prototype is shown in Figure 63, which also illustrates the peristaltic locomotion similar to the other tools developed at FIU.

Figure 63. Mother-crawler prototype.

The final design will include a new front module to house the magnetic miniature inspection rover. Preliminary designs use a scissor-lift mechanism to deploy the miniature unit from the pipe to the bottom of the liner plates. The existing middle modules will carry a modified cable management system for the miniature rover and the necessary embarked control hardware.

The current testing prototypes of the miniature child-rover is shown in Figure 64. The unit design has been enhanced with wheel encoders and an inertial measurement unit (IMU). These sensors will improve the unit localization and dead-reckoning navigation (position estimation using sensed speeds over elapsed time and course) during tank inspections.
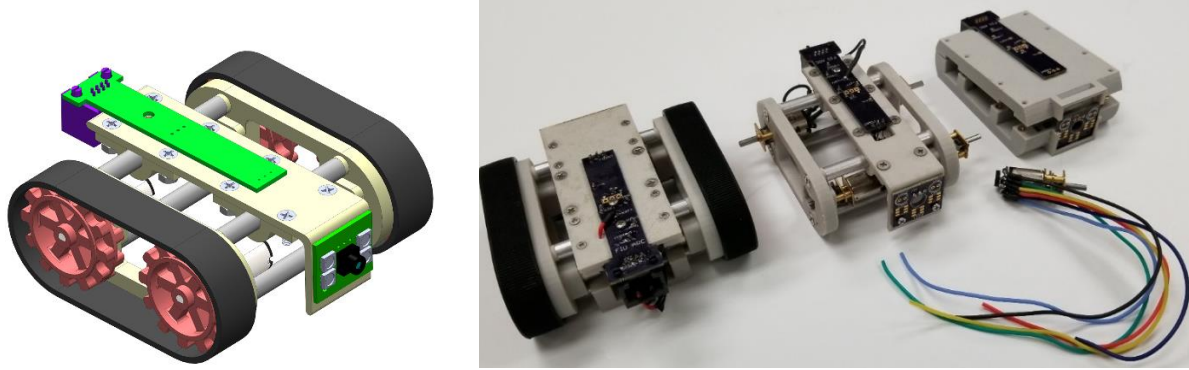
Figure 64 . Miniature child-rover prototypes.

The integration of other sensors into the child-rover is also being considered, including environmental, radiation, LiDAR and a surface camera. The integration will take advantage of the sensor and software framework developed for the pipe crawler instrumentation module described previously.

In addition, alternate articulating joint designs are being investigated, with the objective of improving the modules connections and the units ability to maneuver through pipe bends and obstructions, improving mobility in tension and compression. Currently, the team is investigating:

- a rigid prismatic joint connected by a metal cable,
- a ball joint, and
- a bistable-like joint mechanism.

Figure 65 shows the rigid prismatic joint part of the original design, which is being tested. The addition of springs to the design is being explored due its potential to improve the discrepancy between the joint behavior during compression and tension.
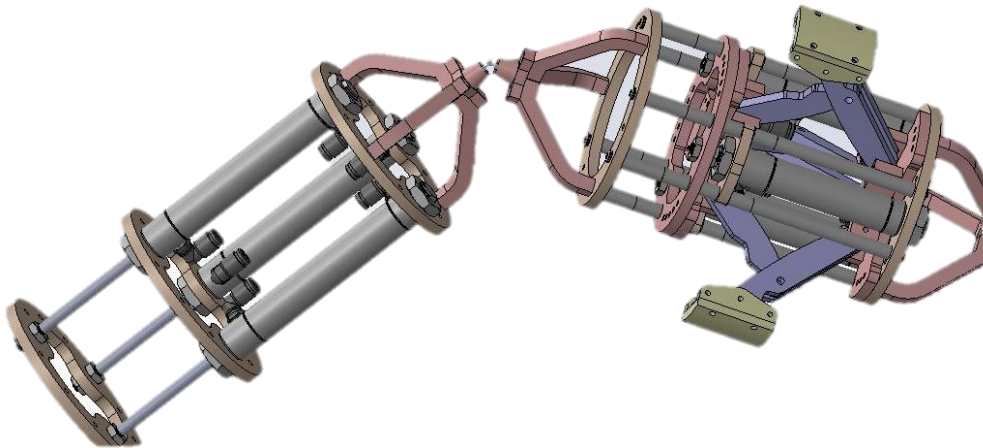
Figure 65. Rigid prismatic joint.

A concept similar to tendons (flexible but inelastic cords) and socket joints is also being investigated. Figure 66 shows a simplified version that uses a ball and socket connection, which provides a rigid connection eliminating the displacement between modules, while also providing an ample desired range of motion and good strength under compressive load. However, the design

is not as robust considering its complex shape the limitations of 3D printed materials. This also affects the part strength under tensile loads, which can potentially be solved using different reinforced printed materials.
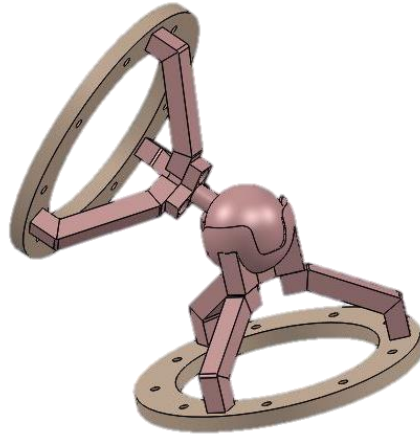
Figure 66. Ball socket joint.

Another alternate design being investigated uses a bistable-like joint mechanism. Figure 67 illustrates a preliminary configuration, which can provide the same range of motion as the ball socket-joint, while being rigid and robust, presenting adequate strength to tensile and compressive loads. However, concerns with the overall length of the mechanism might affect its viability and motility while traversing pipe bends. Another concern is that the design might require an additional slip ring.
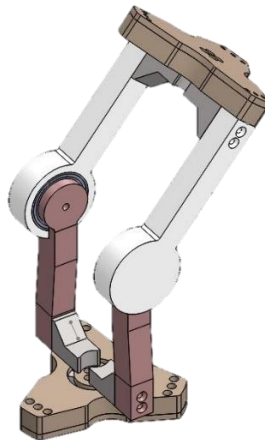
Figure 67. Bistable joint.

The team is currently procuring a bench-scale mockup to test the unit to simulate the conditions of the DST's original leak detection system.

DST FULL-SCALE SECTIONAL MOCKUP

In the previous year, FIU began the construction at ARC for a full-scale sectional mockup of the DSTs at Hanford. The testbed will allow for the testing of FIU inspection tools in addition to other industrial technologies delivery systems and robotic devices. The mockup design was extensively coordinated with the site engineers at WRPS, and extra care was taken to assure a high correlation between the mockup and in-field conditions. The testbed has a modular design that can reproduce different inspection conditions in Hanford tanks. This includes various configurations of:

a) the refractory pad,
b) cooling channels,
c) supply airlines and
d) plate thicknesses.

Defects such as damaged welds and *in situ* bottom cracks can also be simulated. Figure 68 illustrates the current mockup design.
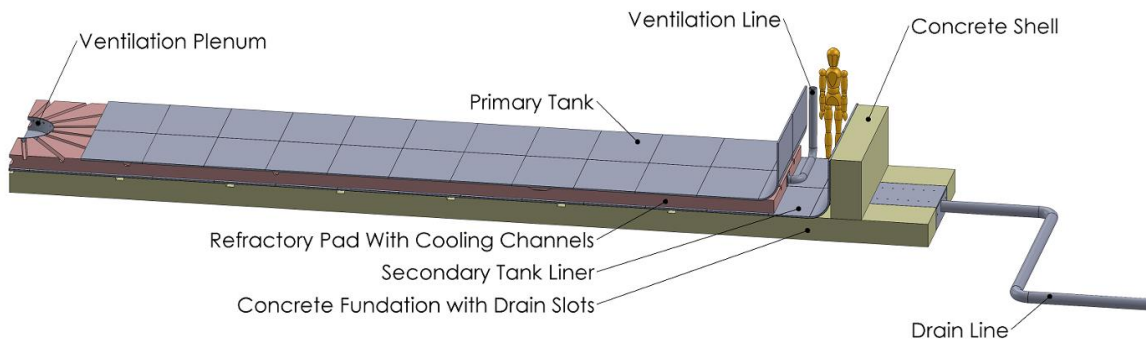
Figure 68. Current mockup design.

The mockup not only includes the ventilation channels in the refractory pad of the primary tank, but it also includes the leak detection system in the foundation slab of the secondary tank liner. The full structure is 8 ft wide and 37.5 ft long and emulates the following elements of the tank:

- concrete foundation with draw slots,
- 6" drain line,
- concrete shell,
- secondary tank liner,
- refractory pad with cooling channels,
- 4" ventilation line,
- primary tank, and
- tank center plenum.

Figure 69 shows the existing leak detection configurations used in the double shell tanks at Hanford. FIU's mockup is based on the 241-AN, 241-AW and 241-AN-107 designs which constitute a majority of the configurations.
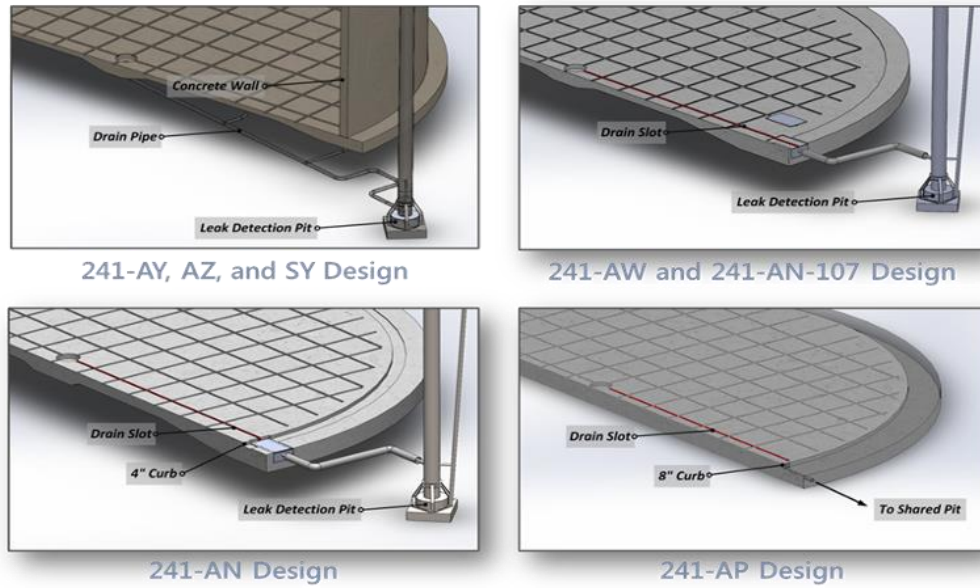
Figure 69. Existing configuration of the DST's leak detection system.

As illustrated in Figure 70, the mockup covers approximately 7% of the DST's foundation with the 8-ft swath.
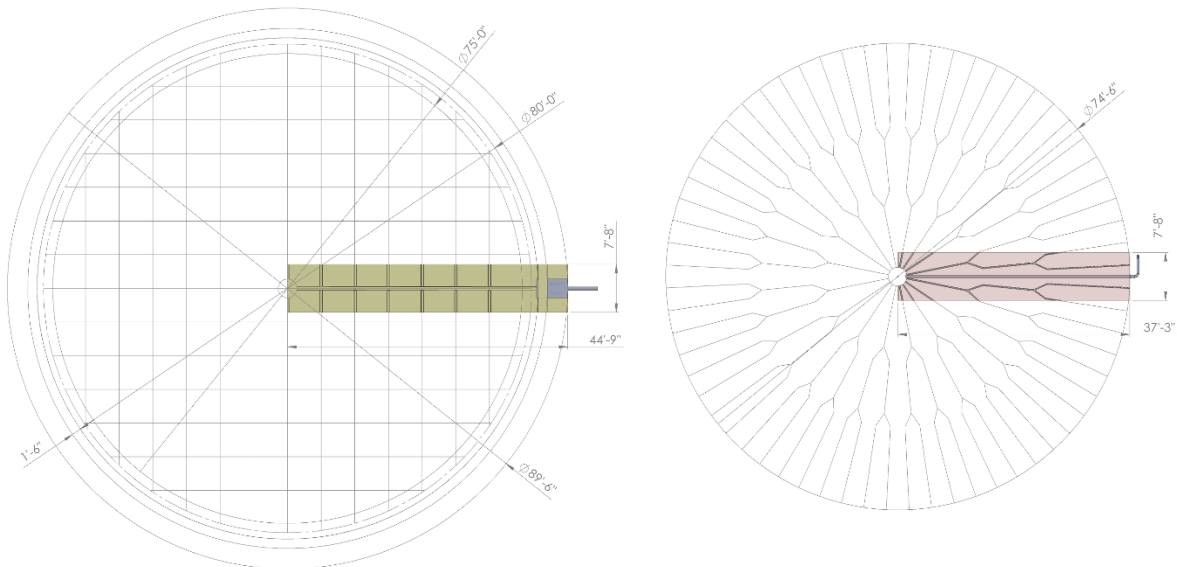
Figure 70. Layout of the tank foundation drains (left) and cooling channels (right).

Figure 71 shows the layout of the concrete foundation in the mockup under the secondary tank liner. The foundation leak detection system has a maze of sloped drains. In the mockup, the drains are sloped and angled according to the double shell tank's shop drawings, and they are suitable to address corrosion issues in the inspection of the bottom of the secondary tank liner.
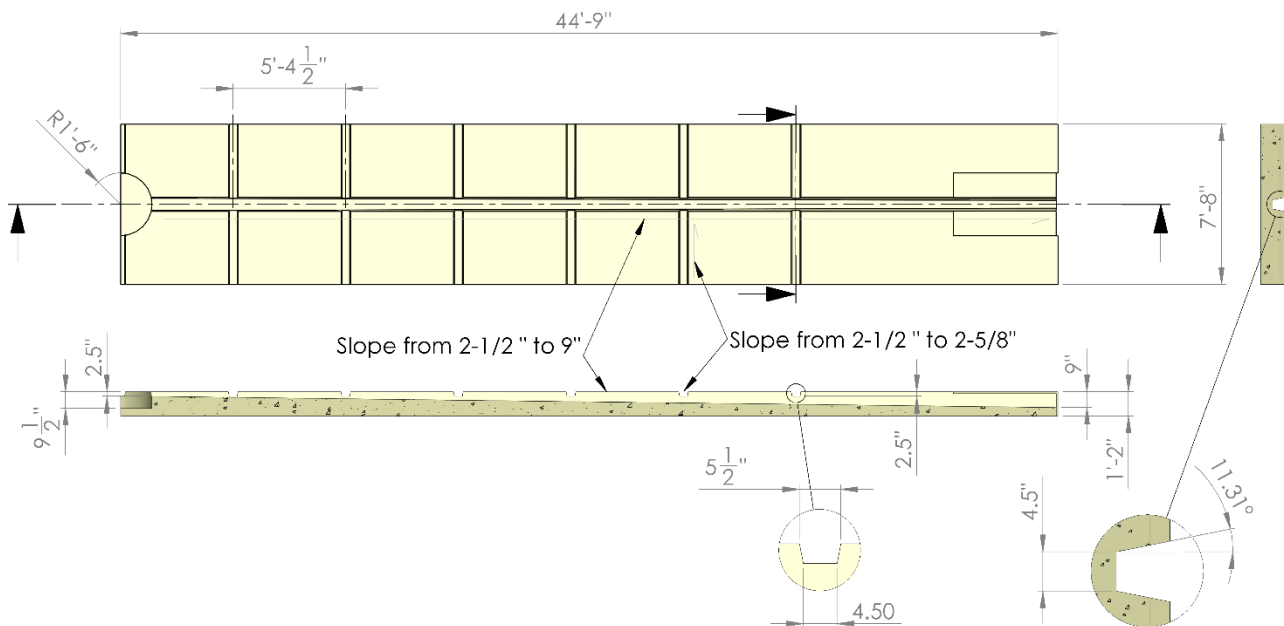
Figure 71. Concrete foundation with drain slots.

Figure 72 shows the layout of the refractory pad in the mockup under the primary tank. The mockup has two full length cooling channels reaching from the tank annulus to the center plenum. This configuration is suitable for testing emitter-receiver sensor technologies, such as long-range guided ultrasonic waves, which would require multiple sensors simultaneously located in both channels. The refractory mockup also includes one of the carbon steel 4" ventilation pipe lines, the only feasible way to provide access to the tank central plenum.
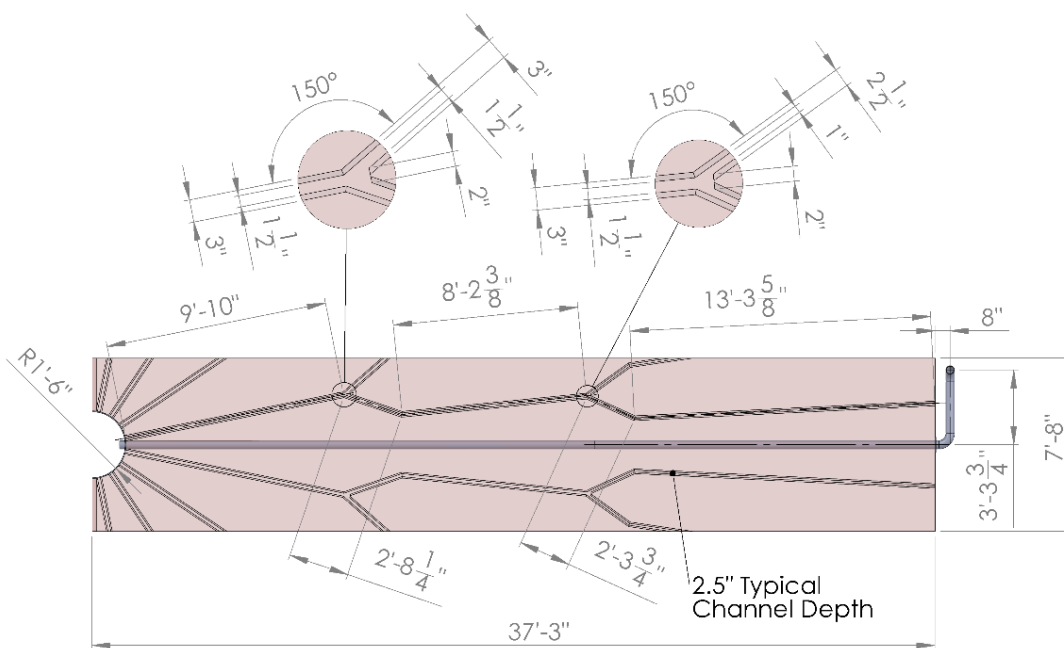
Figure 72. Refractory pad with cooling channels.

Figure 73 shows the mockup of the central plenum, which is also constructed in accordance with the DST drawing provided by WRPS.
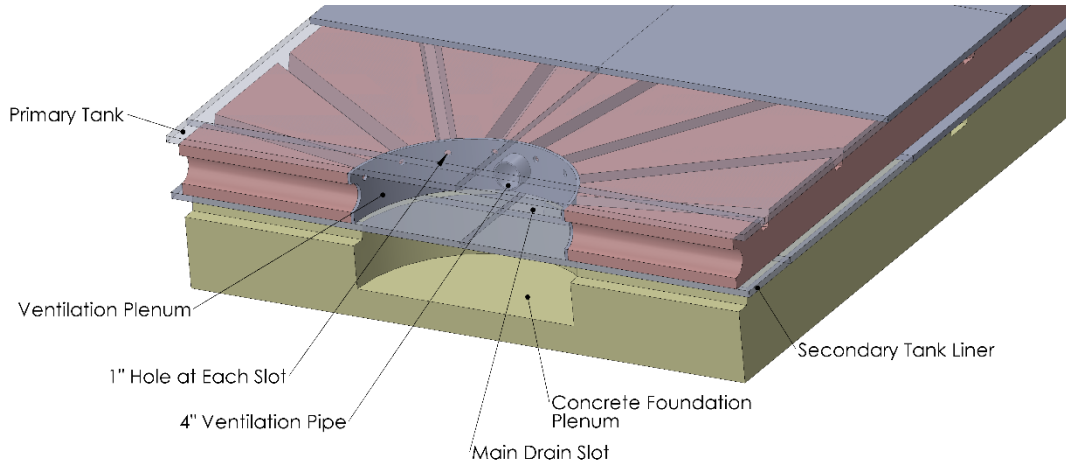
Figure 73. Tank central plenum.

During the past year, FIU focused on completing the constructing the refractory slots. Staring with Figure 74, the pictures show subsequent stages of the mockup refractory pads during construction.

Figure 74. Progression of refractor channels.

The refractory channels were cut and assembled according to the layout in Figure 75 and were installed into the wood frame of the modules.
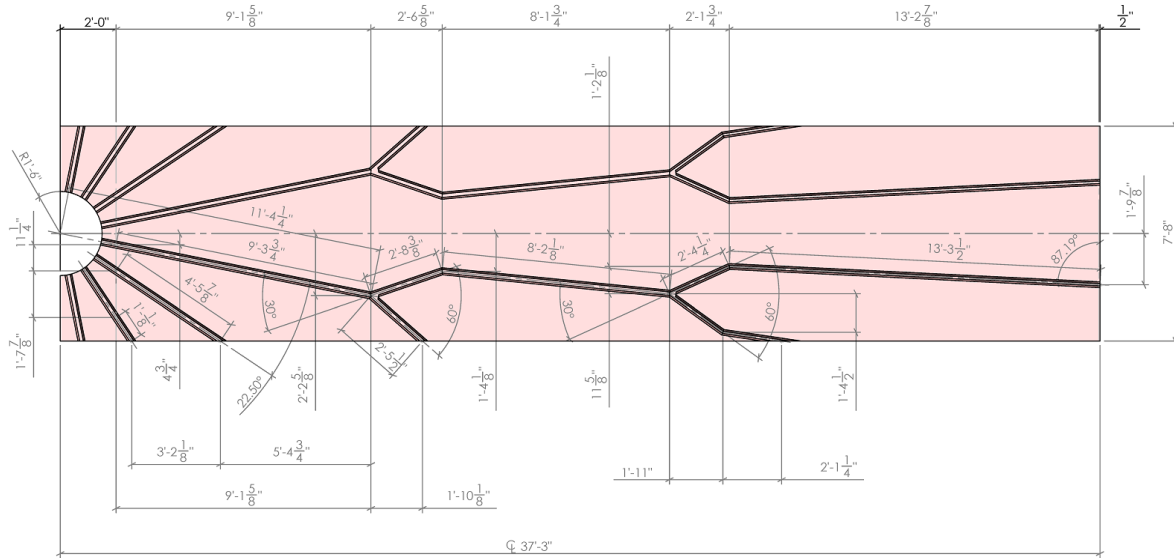
Figure 75. Refractory channel layout.

Figure 76 shows details of the supporting structure used in the refractory channel development. During the construction process, 3D printed templates were employed to ensure accuracy in the slot dimensions according to the refractory shop drawings.
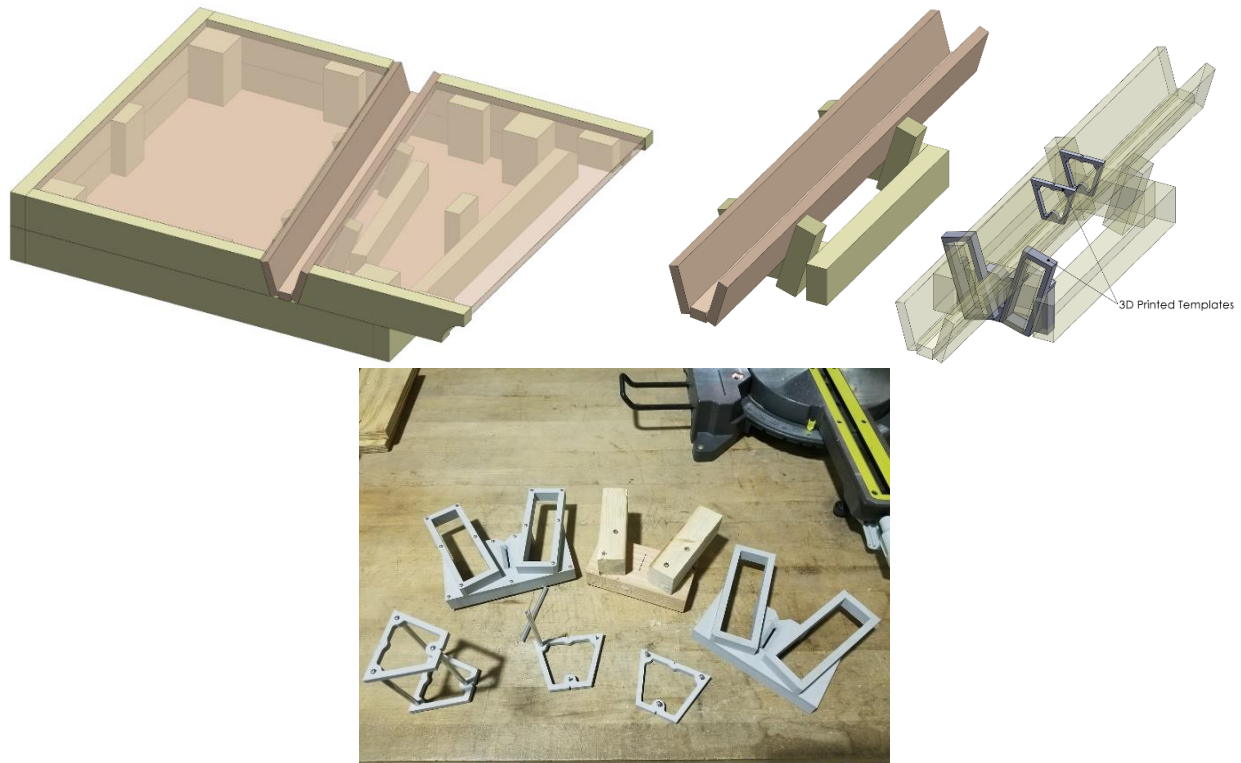
Figure 76. Refractory channel supporting structure.

After the slots were constructed, the necessary grooves were cut from the refractory foundation and the channels were inserted as shown in Figure 77.
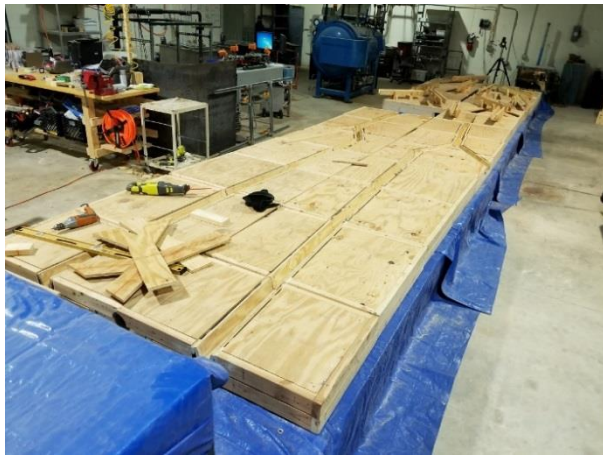
Figure 77. Framing for the refractory slots.

Figure 78 provides details of the procedures followed for the construction of the refractory channel modules. This includes use of a self-leveling line laser and 3D printed templates which were employed to guarantee accuracy in the slot dimensions (according to the refractory pads shop drawings).
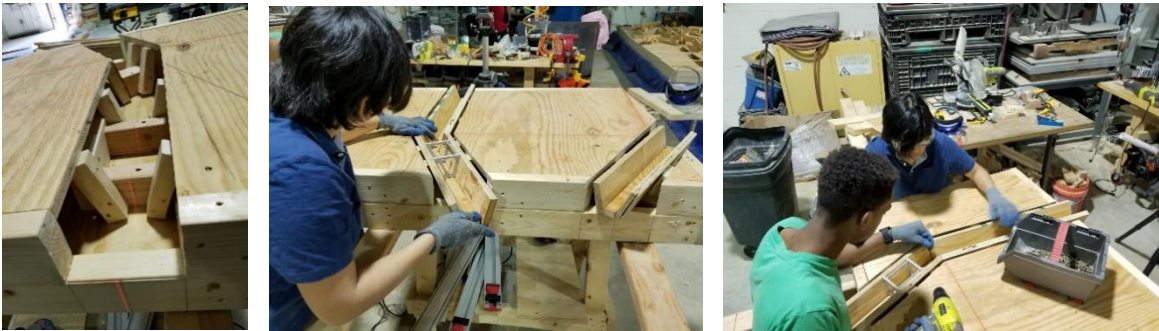
Figure 78. Refractory channel construction.

During construction (Figure 79), the profiles of the cooling channels were oversized by 1/2". The extra clearance accounts for the concrete coating, which utilizes the same process that was used to create the foundation and the drain slots. A moister barrier of roofing felt paper was wrapped over the outside wood frame, and a self-furred diamond metal lath was used as reinforcement. In addition, protruding 1/2" side panels were installed as a guide, which was needed to mold the concrete to an exact thickness. After the modules were completed, these panels were removed. A second thin layer of concrete will be manually applied using 3D printed profiles to fine tune the channel dimensions according to the DST's CAD drawings.

Figure 79. Refractory channel construction.

Figure 80 shows final images of full-scale sectional mockup, which was inspected by engineers from WRPS during their visit to FIU in February 2018. In general, the test bed was very well received, but it was noted that some of the heights of the refractory sections were not aligned. This will be addressed with simple modifications to the final layer of concrete on each section.

Figure 80. Construction of the full-scale HLW DST test bed.

CONCLUSIONS AND FUTURE WORK

The miniature rover inspection tool was successfully demonstrated to the site engineers from WRPS. Feedback from the engineers have been extremely helpful in identifying additional requirements for the inspection tool: (1) ability to traverse weld seams of different heights located underneath the actual tanks, and (2) a back-facing camera to aid the reverse maneuvering of the inspection tool, as well as (3) a more secure connector for the retrieval of the inspection tool in case of failure.

Numerical studies have been conducted to calculate the maximum magnetic force of the inspection tools' magnets when it is traversing the weld seams. The results showed that there is a very small margin for the magnetic force to cause the tool to pivot forward to allow the front wheel to regain traction and continue its maneuver. Feasibility studies have also been carried out to investigate the use of a magnetic tank track design, so that the track will always be in contact with the surface. However, due to the current limitations in terms of materials and link mechanisms, the results from the prototype requires improvement.

In parallel, a front- and back-chamfered version of the inspection tool that houses two cameras was also developed. The improved version also has a connector located at the top of the inspection tool so that it can be tightly secured by the inspection tool's hood. The front- and back-facing camera provides the operator with visual feedback for both the forward and backward maneuvers. This version of the inspection tool is currently being tested and the newly designed connector was able to withstand at least 65 lbs of pull-force. Furthermore, the chamfered version was able to traverse over a weld seam with height of 0.25 inches.

To ease the inspection operation within the narrow refractory channels, semi-autonomous control of the inspection tool has been designed and is being fine-tuned. Images from the inspection tool's camera were processed to implement lane-keeping capability. This freed the operator from having to keep the inspection tool in the center of the channels, allowing them to focus their attention on the inspection tasks at hand.

Preliminary testing of the semi-autonomous operation has been conducted at the full-scale sectional mockup facility at ARC. Test results showed that the PID controller was able to maneuver the inspection tool along the central region of the refractory slots. Work is ongoing to improve the performance of the semi-autonomous control, as well as make use of the onboard cameras' feedback for SLAM.

Future work includes developing a 150-ft tether that is able to reliably provide power and communication to the mini inspection tool. This is to facilitate the deployment of the mini inspection tool through the 3- and 4-inch annulus, where the deployment of a delivery platform is not feasible. Work is also ongoing to ensure that the resultant system is field deployable, for a potential field deployment at the Hanford Site.

FIU has also developed a sensor module that augments the capability of the current pneumatic pipe crawler. Previously, the crawler could only provide visual feedback of the inside of a pipe. Although this information is very valuable for assessing areas of concern within a pipe, the new

sensor capabilities provide the framework for gathering detailed information regarding the conditions within the pipe and the internal surface topography.

The new module is a carousel type unit that can rotate 360 degrees, providing information as the crawler navigates through pipelines. The module frame is 3D printed and currently houses off-the-shelf sensors. In this prototype, the module is placed in front of the crawler's forward gripper for easier integration. The sensors currently installed on the module include: radiation, temperature, humidity, video camera, IMU, and LiDAR sensors. Due to the module's novel design, it can be customized to integrate other sensors as needed.

The module was tested to validate that it rotated properly and that the sensors functioned. Although this first prototype did function as designed, there are a few areas in which the prototype can be improved. In the future, FIU will streamline the wiring of the sensors and its connection to the microcontroller and incorporate a slip ring for wire management. FIU will also investigate including higher resolution sensors to improve the quality of the images and data.

In addition, FIU is designing a novel specialized tool to inspect metal plate thinning of the secondary liner at the bottom of DST's at Hanford. The access points for the inspection will be the leak detection system integral to the tank concrete foundation. The tool under design is a robotic marsupial system that uses a mother pipe crawler to navigate through the 6" drain lines to deploy a miniature child-rover in the drain slots.

Lastly, a full-scale sectional mockup of the DST floor was designed and constructed. FIU has worked with engineers at Hanford to ensure that the structure meets the needs of the sites in terms of accurately representing the geometry of the actual tanks. The mockup has been used to evaluate FIU's current inspection tools but can also be used to evaluate future inspection technologies, sensors and robotic devices in operational conditions equivalent to those at Hanford.

REFERENCES

1. Rau ́l Mur-Artal and Juan D. Tardo ́s. ORB-SLAM2: an open-source SLAM system for monocular, stereo and RGB-D cameras. *IEEE Transactions on Robotics*, 33(5):1255–1262, 2017

2. Engeman, J.K., Girardot, C.L., Harlow, D.G., Rosenkrance, C.L. , 2012, Tank 241-AY-102 Leak Assessment Report, Washington River Protection Solutions, RPP-ASMT-53793, Rev.0

3. DiBono, M., Abrahao, A., McDaniel, D., Lagos, L. and Tan, Y., 2018, Engineering Scale Testing of Robotic Inspection Tools for Double Shell Tanks at Hanford, Proceedings of the Waste Management Symposia 2018, Phoenix, AZ.

4. Abrahao, A., Fekrmandi, H., Gocke, E., Sheffield, R. and McDaniel, D., (2016) Development of Inspection Tools for the AY-102 Double-Shell Tank at the Hanford DOE Site, Proceedings of the Waste Management Symposia 2016, Phoenix, AZ

TASK 19.1
Pipeline Corrosion and Erosion Evaluation

EXECUTIVE SUMMARY

A fitness-for-service (FFS) program has been implemented by Washington River Protection Solutions (WRPS) to assess the structural integrity of pipelines, tanks and tank farm waste transfer systems. The purpose of the program was to inspect primary piping, encasements, and jumpers for corrosion/erosion. As recommended, at least 5% of the buried carbon steel DSTs waste transfer line encasements were inspected. The data has been collected for a number of these system components and analyzed.

Previous efforts from FIU included the evaluation of ultrasonic transducers that can provide real-time thickness measurements for transfer system components. Initially, a market study was conducted on various commercially available ultrasonic transducer systems according to the requirements listed by the WRPS/DOE personnel. Out of the many options, some of the sensors were procured and tested. Since the data acquisition systems were expensive; two of the viable options were down selected. One of the down selected UT sensor systems, from Permasense, has been acquired and bench-scale validation tests have been conducted.

During this past year, a custom designed pipe loop system was installed using 2- and 3-inch pipe sections. The Permasense sensors were transferred from the bench-scale set up to the engineering scale test loop. An initial set of experiments was conducted on the pipe loop. To generate erosion in the pipe loop, a sand and water slurry (10% by volume) was circulated through the loop. This resulted in significant erosion and the Permasense sensors were able to successfully capture the measurements.

Additionally, erosion coupons developed by SRNL were procured, customized and installed into the flow loop to detect erosion on a small scale. These coupons were made to be flush with the inside diameter of the pipe to detect erosion in the low grade carbon steel material while the sand water mixture was eroding the inner sections of the pipe loop. A gravimetric method (mass change) was used to detect erosion in the coupons.

INTRODUCTION

The Hanford Site Tank Farm has implemented a Fitness-for-Service (FFS) program for the Waste Transfer System. The FFS program, based on API-579-1/ASME FFS-1, examines the structural parameters of the waste transfer systems in order to develop erosion/corrosion rates for relevant system components. The FFS information is acquired from opportunistic evaluations of pipelines that have been removed from service. FIU-ARC engineers work closely with key Hanford high level waste (HLW) personnel and the contractor, Washington River Protection Solutions, LLC (WRPS), to support the FFS program, deliver solutions for sensor evaluations, as well as conduct bench-scale testing followed by data acquisition and analysis for corrosion and erosion assessment.

The objective is to assist DOE and WRPS in providing realistic estimates of the remaining useful life of the components and to incorporate those estimates into future design plans. Previous efforts at Hanford included the installation of sensors on a number of the POR 104 components, to provide real-time pipe wall thickness measurements. Due to various limitations, alternative approaches for remote permanently-mounted pipe wall ultrasonic thickness measurement systems are being investigated.

FIU efforts to support this scope have included investigating key options available in the market for remote permanently-mounted ultrasonic transducer (UT) systems for HLW pipe wall thickness measurements. Specific applications include straight sections, elbows and other fittings used in jumper pits, evaporators, and valve boxes. FIU assessed the use of various ultrasonic systems that are either commercially available or used previously at Hanford and selected the most promising systems for further evaluation. One of the two down selected systems (Permasense UT sensor system) was acquired and initial bench-scale validation testing was conducted. Following the initial bench scale tests, engineering scale testing was implemented on an in-house designed and installed test loop. The design loop has been established using 2- and 3-inch diameter straight and bends pipe sections to mount the sensors. The loop was eroded using sand-water slurry and the Permasense sensors were used for thickness measurements.

Currently, FIU is in the process of conducting the second phase of testing on the erosion loop based on the lessons learned from the previous testing. Further validation of the SRNL coupons is also being implemented simultaneously.

The research will provide information that will assist engineers with understanding the failure potential of HLW transfer components due to corrosion and erosion. This information can assist in determining if and when lines need to be removed, saving time and resources on unneeded excavation of transfer lines. This information can also assist engineers with designing new transfer systems by establishing more detailed/accurate guidelines governing the life expectancy of the transfer system and its components.

EROSION TESTING USING PERMASENSE UT SENSORS AND SRNL EROSION COUPONS

After efforts by WRPS to obtain real-time thickness measurements using a pipe wrap system were found to be difficult [1], FIU began investigating alternative approaches to obtain the thickness measurements. Some of the operating parameters for the sensors include their need to be able to take measurements via permanent mounting and be installed in confined spaces. To this end, FIU investigated a variety of ultrasonic sensors for measuring the thickness of 2- and 3-inch diameter pipes. A majority of the companies that carry relevant transducers did not have products that met the site needs. In particular, most sensors evaluated required the use of a liquid couplant. For this application of long-term real-time measurements, a dry couplant is more practical.

After initial discussions with WRPS engineers, FIU purchased an Olympus 45MG digital ultrasonic thickness gauge [2]. The system is a dual crystal transducer that comes with a two-step reference block and a liquid couplant sample. Hence, a dry couplant was purchased and tested. The results showed that the dry couplant was unable to provide accurate readings. In addition, vacuum tests were also conducted to eliminate the air gap between the test piece and the sensor surface. These results were also found to be highly inaccurate.

Other options without the use of a gel couplant were then investigated. Four of the options considered were: Ultran sensors, Permasense sensors, Acellent smart sensors, and electromagnetic acoustic sensors (Innerspec EMAT). Descriptions of the UT sensors and the experiments conducted have been presented in previous reports. The down selected Permasense UT sensor system and its bench-scale validation testing has been described in the previous year's report.

In addition, SRNL developed a replaceable erosion/corrosion coupon that detects the mass loss due to erosion using a gravimetric method. It is also designed to obtain and study the surface roughness profiles from wear and pitting corrosion. The coupon can hold a pencil UT sensor for real-time measurements. In the previous year, the coupons were tested for erosion based on weight loss. This year, the coupons will be tested for weight loss and surface roughness changes in the profiles.

Permasense Guided Wave Sensors and Testing

The guided wave sensors from Permasense have been acquired and bench-scale testing has been conducted with details presented in the previous year's report. During this year, the custom designed loop was installed and engineering scale testing has been initiated. Details of the test loop and results are presented in the next section.

Experimental Test Loop

For the engineering-scale test loop is shown in Figure 81. It consists of 2- and 3-inch pipe sections welded together with a reducer. The loop is approximately 25 ft in total length and incorporates a by-pass for flow control to compensate for the lack of VFD on the pump. The Permasense sensors have been installed in four critical sections of the loop, including the 2-inch and 3-inch straight and bend sections. Also, one of the sensors is installed upside down to cover the bottom section of the pipe loop where gravity might lead to the settlement of sand particles during longer periods of

testing. A flow meter has been installed in the 2-inch straight section to measure the flow rate during testing (Figure 82). One of the challenges faced during testing is the suspension of sand particles in the tank and the test loop. For this, a mixer has been researched, selected, acquired and installed as shown in Figure 82. Additionally, a stand has been designed and built using unistruts to support the mixer as shown in Figure 83.

Figure 81. Erosion Pipe loop with sensors.

For the next phase of this effort, the Permasense sensors will be tests under real-time conditions by slow and gradual erosion for a period of 2-3 months. Additionally, the sensors will be checked for changes in environmental conditions. These conditions will include high temperatures and humidity. An environmental chamber will be placed surrounding the sensors and temperature and humidity sensors will be installed for continuous monitoring over a period of 1-2 months.

Figure 82. Flow meter [4] (left) and mixer and supporting stand (right).

Figure 83. Sand water mixer [5].

SRNL Coupon Testing

With support from SRNL, FIU testing included their coupon system developed for monitoring erosion and corrosion. These are small ½-inch diameter stainless steel coupons weighing about 0.3 oz. (Figure 84). The SRNL coupons were installed into the pipe sections based on the specified assembly and checked for flushing from the inside of the pipe using an endoscope. The endoscope images and video showed an approximate gap of 1.8 mm as shown in Figure 85. Since the coupons obtained from SRNL were unable to be flush with the pipe inner diameter during assembly, the front diameter and the flange were trimmed down to 0.310 inch and 0.020 inch thickness, respectively. The coupons before and after trimming are shown in Figure 84 and the endoscope image of the coupons inside the pipe are shown in Figure 85. Figure 86 shows the coupon with polymer sleeves and A-lock fitting ferrules assembly as well as the assembly installed on the flow loop.

Figure 84. Coupon surface to be milled (left) and coupons before and after machining (right).

Figure 85. Endoscope image of the pipe with original coupon (left) and machined coupon (right).
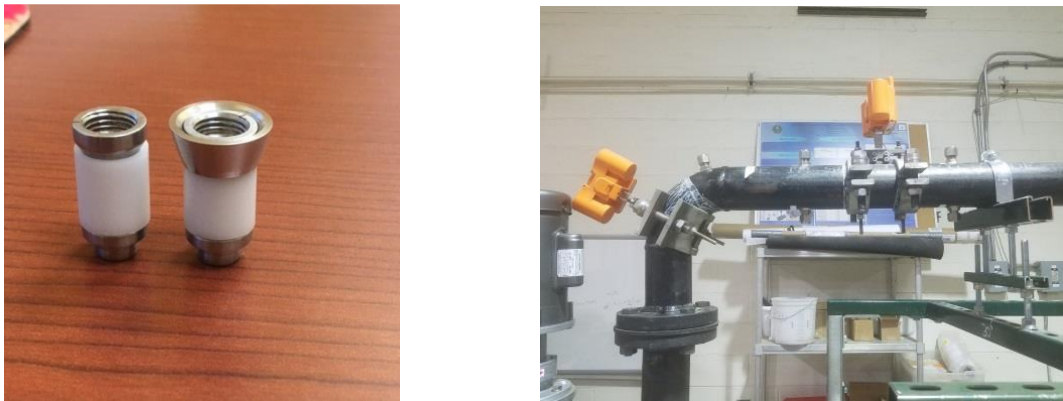
Figure 86. Coupon (left) and coupon installed on an elbow (right).

Results and Discussion

The simulant selected for testing was sand and water slurry. The initial concentration of sand for the initial test was intended to be 10% by volume. Sample test results obtained during the engineering-scale testing are shown in Figure 9 and Figure 10. Water was initially circulated for several hours followed by sand-water mixture testing. The real-time wear rate is captured for about 800 hours. As seen in Figure 87, the UT sensor detected a maximum wear rate of about 0.2 mm in the 2-inch elbow. Similarly, a thinning of 0.09 mm has been observed in the 2 inch straight section (Figure 87). In the 3-inch elbow section, a thickness change of 0.04 mm was observed while in the 3-inch straight section, there was a thinning of 0.03 mm (Figure 88) and then the readings returned to the initial value of 5.42 mm after about 400 hrs. It is evident from the graphs that the sensor measurements from the 2-inch sections remained the same after about 100 hrs but the 3-inch elbow took 400 hrs to stabilize. This could be due to an anomaly in the sensor readings. The sensors have been reset and calibrated for accurate readings.
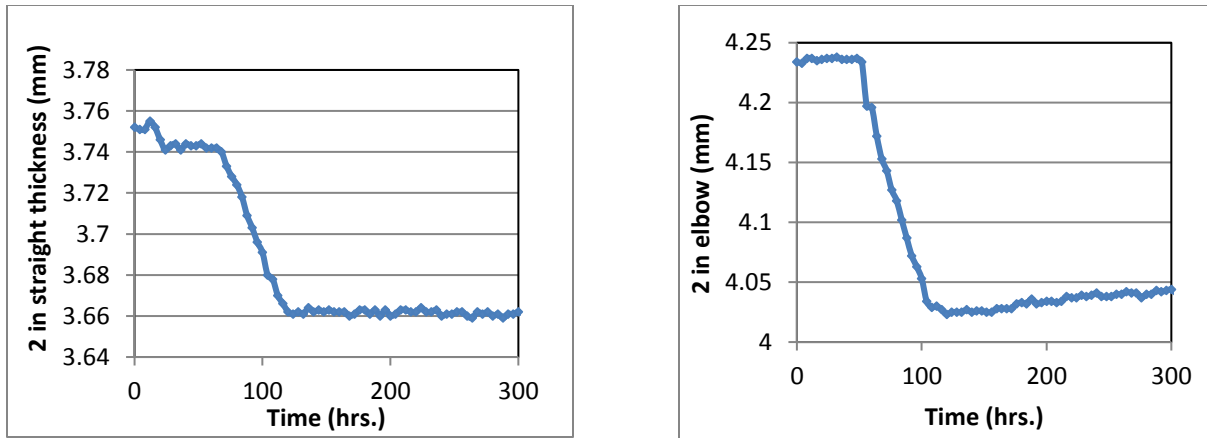
Figure 87. UT thickness change: 2-inch straight section (left) and 2-inch elbow section (right).
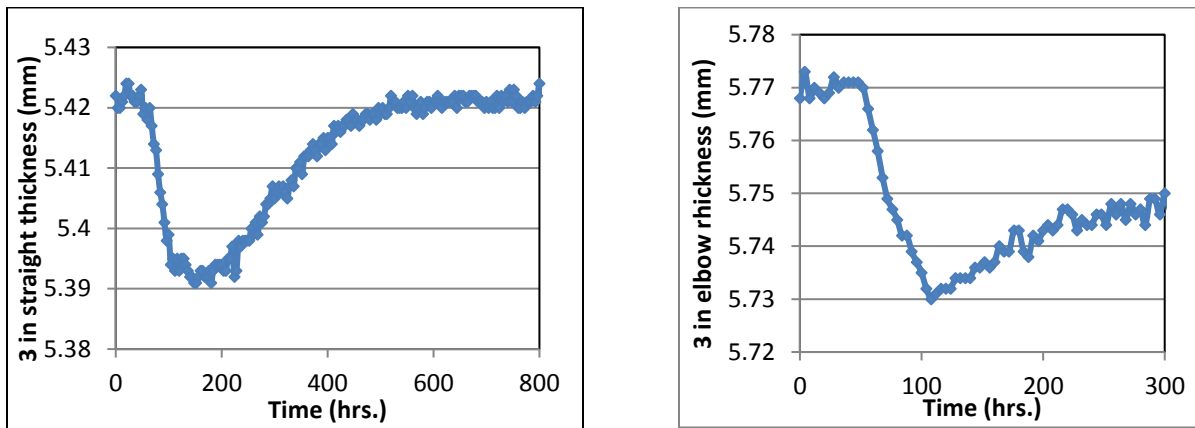
Figure 88 . UT thickness change: 3-inch straight section (left) and 2-inch elbow section (right).

The results indicate a sudden drop in thickness values. This could be attributed to the rapid increase in concentration of sand particles in the mixture. This happened during the experiment when the sand accumulated at the bottom of the tank and the inlet to the pump was close to the bottom. This caused the sand-slurry (high concentrations of sand) to be circulated into the loop which resulted in dramatic wear rates. The pump was shut down after about 90 hrs of operation since the large erosion rates resulted in a leak near the pump's exit. The thickness values captured by the sensors after 100 hrs of operation remained mostly stable. The Permasense sensors could capture the changes in thicknesses up to 2 decimal places in units of mm. This establishes the precision and accuracy of the wave guided sensors for remote monitoring.

The SRNL coupons also showed erosion during the experiments. To quantify the erosion, the coupons were weighed at the beginning and end of the experiments. Results are shown in

Table **6**. As seen from the table, the maximum weight loss was in coupon 5 with a loss of 663.2 mg while the minimum weight loss was in coupon 4 with a loss of 277.3 mg. These coupons were located near the 3-inch bend and the 3-inch straight (top) sections. This is as expected since the maximum erosion happened near the 3-inch bend while the least erosion was on the upper surface of the 3-inch straight section.

Table 6. Erosion in SRNL Coupons

Coupon	Initial Weight (mg)	Final Weight (mg)	Weight loss (mg)	Weight loss (%)
1	8424.9	8031.4	393.5	4.6
2	8406.2	7844.4	561.8	6.6
3	8493.3	7910.4	582.9	6.8
4	8339.7	8062.4	277.3	3.3
5	8487.0	7823.8	663.2	7.8

CONCLUSIONS

During this performance year, the wave guided UT sensor system from Permasense has been validated using the bench-scale tests conducted at FIU-ARC. Results obtained from the bench-scale testing led to the engineering-scale testing.

The engineering-scale tests were conducted on a flow loop developed in-house using 2-inch and 3-inch pipe sections. The loop was aged using the simulant-sand water mixture. A literature review of the sand erosion determined the amount and particle sizes needed for the mixture. The initial engineering-scale tests were conducted using 10% by volume sand.

Additionally, FIU is testing the erosion coupons developed by SRNL to measure small-scale erosion, particularly pitting and erosion corrosion. The erosion coupons have been sized to accommodate five different critical sections on the 3-inch pipe loop and the tests resulted in rapid erosion. Measurements were conducted based on mass change (gain/loss) of the coupons.

Currently, FIU is in the process of conducting the second phase of testing using the Permasense sensors and evaluating the SRNL coupons for pitting and erosion corrosion based on steady flow conditions in the loop. Additionally, the Permasense sensors will be evaluated for their ability to monitor environmental conditions, including temperature and humidity. For practical implementation, an environmental chamber will be built to enclose the sensors on the test loop.

REFERENCES

1. B. J. Vasquez, RPP – RPT – 55812, Engineering Evaluation of Remote Permanently Mounted Pipe Wall Ultrasonic Thickness Measurement Devices, Rev 0, Washington River Protection Solutions, Richland, WA.

2. Aravelli, A., McDaniel, D. and Davila C., "Assessment of Guided Wave Ultrasonic Transducer Systems for Wall Thickness Measurements", Summary Document submitted to DOE –EM under Cooperative Agreement # DE-EM0000598 (FIU-ARC-2016-800006470-04c-242).

3. www.permasense.com

4. https://www.mcmaster.com/catalog/124/609

5. https://www.dynamixinc.com/mixers-by-model/dmx

6. Philip T. and Jake D., "Monitoring and simulation resolves overhead corrosion – online corrosion monitoring in tandem with simulation modelling identified the root cause of corrosion in a crude unit overhead", www.eptq.com – PTQ Q1 2016.

7. https://www.grainger.com/ec/pdf/4YU37_1.pdf.

8. Wood R. J. K and Jones T. F., "Investigations of sand–water induced erosive wear of AISI 304 stainless steel pipes by pilot-scale and laboratory-scale testing", Wear, Vol. 255, Issue 1-6, Aug-Sep 2003, Pg. 206-218, http://www.sciencedirect.com/science/article/pii/S0043164803000954.

9. Naz., M. Y., Ismail, N. I., Sulaiman, S. A., Shukrullah, S., "Characterization of erosion of gas pipelines by dry sand," Instrumentation Science and Technology, 2017, VOL. 45, NO. 1, 62–72. http://dx.doi.org/10.1080/10739149.2016.1194295

10. Morris, K., "Investigation of Various Water Sources on the Corrosion of Carbon Steel and Aluminum", 2017, Honors Research Project, Dept. of Chemical Engineering, University of Akron, OH, USA.

11. http://hghouston.com/resources/technical-newsletters/corrosion-in-caustic-solutions

12. Lu, B., " Erosion-Corrosion in Oil and Gas Production", Research and Reviews in Materials Science and Chemistry, Vol. 2, Issue 1, 2013, Pages 19-60, ISSN 2319-6920.

13. Aravelli, A., McDaniel, D., Davila, C., "Real-time Erosion-Corrosion Detection in Waste Transfer Pipelines using Guided Wave Ultrasonic Sensors", Proceedings of the Waste Management Symposia 2018, Phoenix, AZ, March 18-22, 2018.

TASK 19.2
Evaluation of Nonmetallic Components in the Waste Transfer System

EXECUTIVE SUMMARY

Nonmetallic materials are used in the United States Department of Energy's Hanford Site Tank Farm waste transfer system. These materials include the inner primary hoses in the hose-in-hose transfer lines (HIHTLs), Garlock® gaskets, ethylene propylene diene monomer (EPDM) O-rings, and other nonmetallic materials. These nonmetallic materials are exposed to β and γ irradiation, caustic solutions as well as high temperatures and pressure stressors. How the nonmetallic components react to each of these stressors individually has been well established. However, simultaneous exposure of these stressors has not been evaluated and is of great concern to Hanford Site engineers.

FIU engineers worked closely with key Hanford HLW personnel to develop an experimental test plan to determine how these nonmetallic components react to various simultaneous stressor exposures. The materials selected for testing included of EPDM and Garlock® coupons, EPDM HIHTL inner hoses and EPDM O-rings as well as Garlock® gaskets. An experimental test loop was constructed and the components were aged for durations of 180 and 365 days. The system can accommodate eighteen component assemblies. Each assembly consisted of one EPDM HIHTL, one EPDM O-ring and one Garlock® gasket. There were three assembly aging sets, one for each temperature. Each set has six assemblies in it; three for each of the two time periods.

Prior to aging of the components, a sample set was tested to obtain various baseline mechanical properties as per ASTM standards. The aging of the materials involved exposing each sample to a 25% NaOH solution at ambient (100°F), operating (130°F) and design temperatures (170°F) for durations of 180 and 365 days. After aging/conditioning, the mechanical and material properties of the aged samples were measured and compared with the baseline results to obtain an understanding of degradation caused by the stressors. This report provides results from the mechanical property testing of EPDM and Garlock® material coupons as well as the blowout/leak testing for HIHTL after a 365-day aging period. Results showed a significant degradation was observed in the bursting pressure of the hoses. The burst pressure decreased by 28.75% for the sample aged at 170°F, while samples aged at 130°F and 100°F had approximately 5.70% and 1.34% loss in burst pressure, respectively. Meanwhile, the material coupon results indicated a 91% and 89% reduction of average tensile strength for the Garlock® and EPDM samples, respectively. In addition, analysis using a scanning electron microscope with energy dispersive X-ray spectroscopy (SEM-EDS) was conducted on the EPDM inner hose samples to determine how far the NaOH penetrated into the ethylene propylene diene monomer (EPDM). Results show that some level of sodium hydroxide has penetrated into the inner hose.

INTRODUCTION

Nonmetallic materials are utilized in the waste transfer system at the Hanford tank farms; these include the inner hose of the hose-in-hose transfer lines (HIHTLs), Garlock® gaskets and ethylene propylene diene monomer (EPDM) O-rings. These materials are exposed to simultaneous stressors including β and γ radiation, elevated temperatures, caustic supernatant as well as high pressures during normal use. In 2011, the Defense Nuclear Facilities Safety Board recommended to the U.S. Department of Energy (DOE) to conduct post service examination of HIHTLs and Teflon gaskets to improve the existing technical basis for component service life. Suppliers of the nonmetallic components often provide information regarding the effects of some of the stressors, but information is not provided for simultaneous exposure. An extensive test plan was developed by Sandia National Laboratories to understand the simultaneous effects of the aforementioned stressors [1]; however, this test plan was never executed. Additional studies conducted by Lieberman provides information on HIHTLs at elevated temperature and pressure but little information is gained regarding the synergistic effects with the caustic supernatant [2]. FIU has been tasked with supporting this effort by conducting multi-stressor testing on typical nonmetallic materials used at the Hanford tank farms.

This report provides the mechanical property testing of EPDM and Garlock® material coupons as well as the blowout/leak test results for HIHTL, EPDM O-rings and Garlock® gaskets after a 12-month aging period. In addition, the experimental test loop used to age the test specimens is described.

EXPERIMENTAL TESTING

All material samples had their baseline mechanical performance and properties tested as per ASTM standards prior to any exposure. Once the baseline properties were determined, each material sample was aged, which involved exposing each sample to a chemical simulant at ambient (100°F), operating (130°F) and design temperatures (170°F) for durations of 365 days. Note that in the previous year, the aging occurred for 180 days. Tests were conducted on both material coupons as well as in-service configuration assemblies. After aging/conditioning, the mechanical properties of the samples were again measured as per ASTM standards.

In-Service Configuration Aging

The in-service configuration aging experimental setup consisted of 3 independent pumping loops with two manifold sections on each loop (Figure 89). Each of the 3 loops was run at a different temperature (100°F, 130°F and 170°F). Each manifold section held three test samples and was used for a corresponding exposure time of 6 months and 1 year. Each test sample consisted of a HIHTL hose section, an EPDM O-ring and a Garlock® gasket placed in a series configuration. Isolation valves on each manifold allowed for removal of samples without affecting the main loop and the rest of the samples. The temperature of the chemical solution circulating within each loop was maintained at a preset temperature by an electronically controlled heater. A 25% sodium hydroxide solution was used as a chemical stressor that circulated in each of the loops. The chemical stressor's pH was checked every 30 days to ensure that the concentration levels remained consistent.
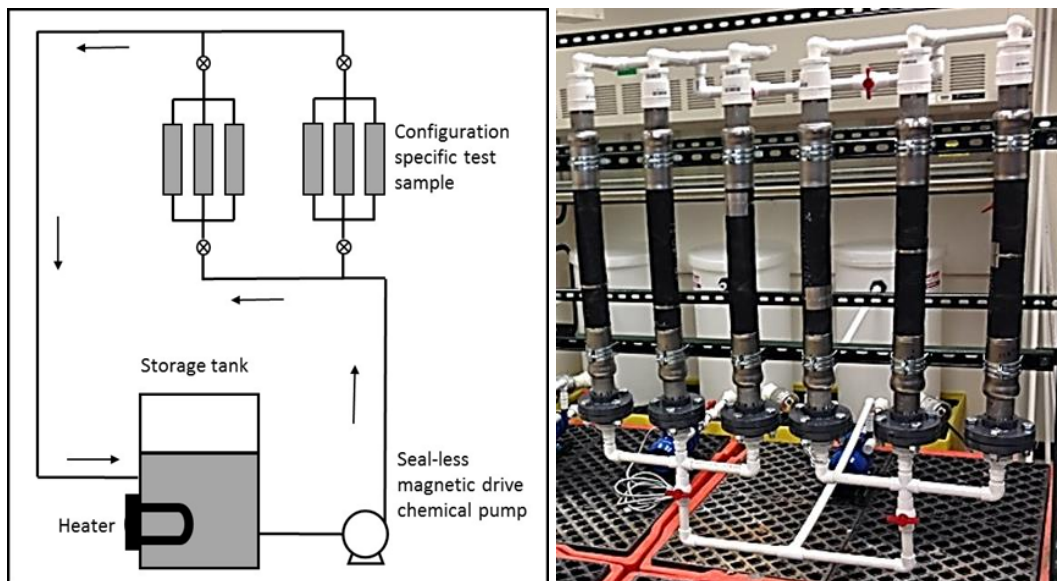

Figure 89. In-service component aging loop.

The coupon aging experiment setup consisted of one coupon aging vessel submerged in each of the three test loop's storage tanks (Figure 90). This resulted in exposing the coupons to the same conditions as the in-service configuration tests; the circulating fluid is the same 25% sodium hydroxide solution. Each vessel contained 6 coupons (3 of each type of EPDM and Garlock® materials) and was submerged in the bath for duration of 365 days.

Figure 90. Coupon aging vessel (left) and EPDM & Garlock® coupons (right).

12-Month Testing Results

Material Tensile Testing

Three of the EPDM and Garlock® samples were aged in each of the three loop tanks maintained at 100°F, 130°F and 170°F. All procedures used for testing were derived from the ASTM D412-16 standard [3]. Figure 92 and Figure 93 show results from the tensile strength tests for the Garlock® and EPDM coupons, respectively, including the results from the 6-month aging experiements.
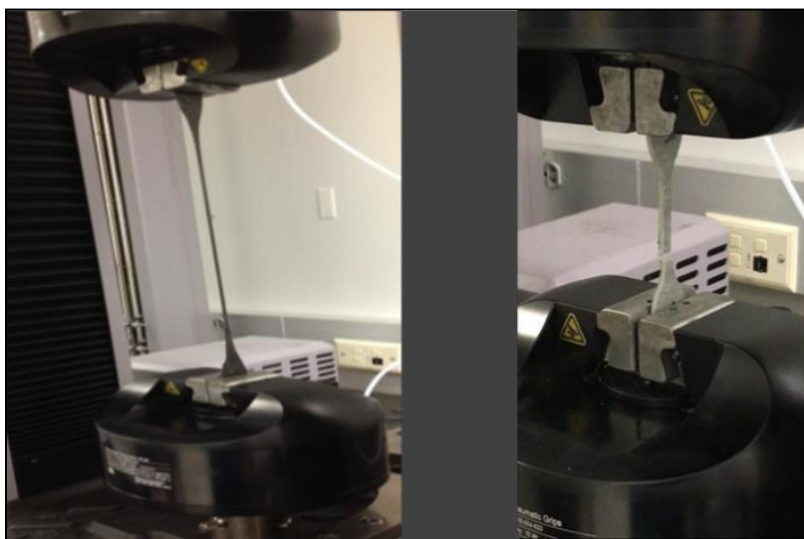

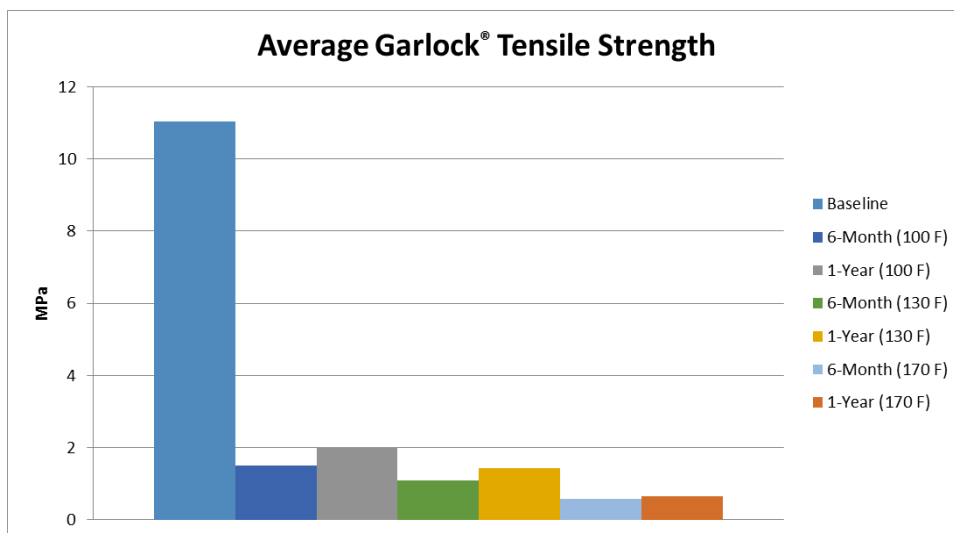**Figure 91. Tensile strength testing of EPDM and Garlock® coupons.**

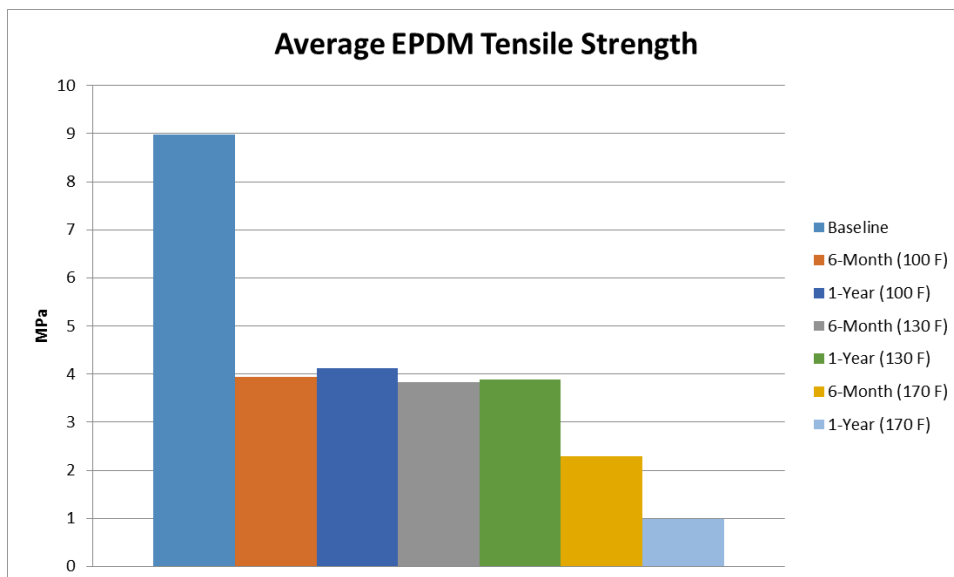**Figure 92. Garlock® coupon tensile strength.**

Figure 93. EPDM coupon tensile strength.

As can be seen from Figure 92 and Figure 93, even though the Garlock® material has a higher initial strength than the EPDM, it loses much of its strength when exposed to the caustic solution. This could be the result of Garlock® being comprised of a paper-type material that loses its strength when it becomes wet. Even when Garlock® material is wet, a trend in strength degradation can be seen as the solution temperature increases. A similar trend is observed with the EPDM material; as the temperature increases, its tensile strength decreases. As can be seen from Table 7 and Table 8, the reduction in the average tensile strength for both the Garlock® and EPDM samples increased as the temperature increased. The 12-month Garlock® results show a reduction of average tensile strength of approximately 91%, 65%, and 63% for the coupons aged at 170ºF, 130ºF and 100ºF, respectively. Meanwhile, the 12-month EPDM results show a reduction of average tensile strength of approximately 89%, 57%, and 54% for the coupons aged at 170ºF, 130ºF and 100ºF, respectively.

Table 7. Garlock material tensile testing results (MPa)

Tank	6-Month	% Change	12-Month	% Change
1 (170°F)	2.113	80.880	0.985	91.085
2 (100°F)	3.656	66.920	4.124	62.686
3 (130°F)	3.592	67.495	3.883	64.865

Table 8. EPDM material tensile testing results (MPa)

Tank	6-Month	% Change	12-Month	% Change
1 (170°F)	2.113	76.478	0.985	89.033
2 (100°F)	3.656	59.303	4.124	54.095
3 (130°F)	3.592	60.011	3.883	56.776

Hose-In-Hose

After the aging process, three HIHTL specimens from each loop (100°F, 130°F, and 170°F) were pressurized until rupture. Their pressure profiles as well as initial and final lengths were measured. The rupture pressures of the specimens were compared with the unaged samples (baseline) which raptured at 2827 psi. Figure. **94** shows the rupture test apparatus and a ruptured hose section.

Figure. 94. Hose burst testing: burst pressure test apparatus (left) and ruptured hose section (right).

Figure 95 shows the burst pressure results of the hoses aged 12-months. For the hoses aged at 100°F the average burst pressure for the 12-month was slightly greater than the average burst pressure for the 6-month (reported last year): 2789 psi vs 2706 psi. Similar results were also observed with the material coupons which showed that the coupons exposed for 12-month displayed higher average strength than those exposed for 6-months (2706.32 psi for 6-month vs 2789.10 psi for 1 year exposure). Unlike the results of the hoses aged at 100°F, the average burst pressures of the hoses aged at 130°F showed that samples aged for 12-months had a lower average burst pressure than those aged for only 6-month at the same temperature (2665 psi for 6-month vs 2784 psi for 1 year exposure). The hoses aged at 170° for a duration of 12-months had a significantly lower average burst pressure than those aged for only 6-month at the same temperature (2637.36 psi for 6-month vs 2014.24 psi for 1 year exposure). Table 9 presents the burst pressures of the specimens tested. When compared with the baseline (unexposed sample), all the samples had lower burst pressures. The burst pressure decreased by 28.75% for the sample

aged at 170°F after one year, in comparison to samples aged at 130°F and 100°F which had about 5.70% and 1.34% loss in burst pressure, respectively, after one year of aging.
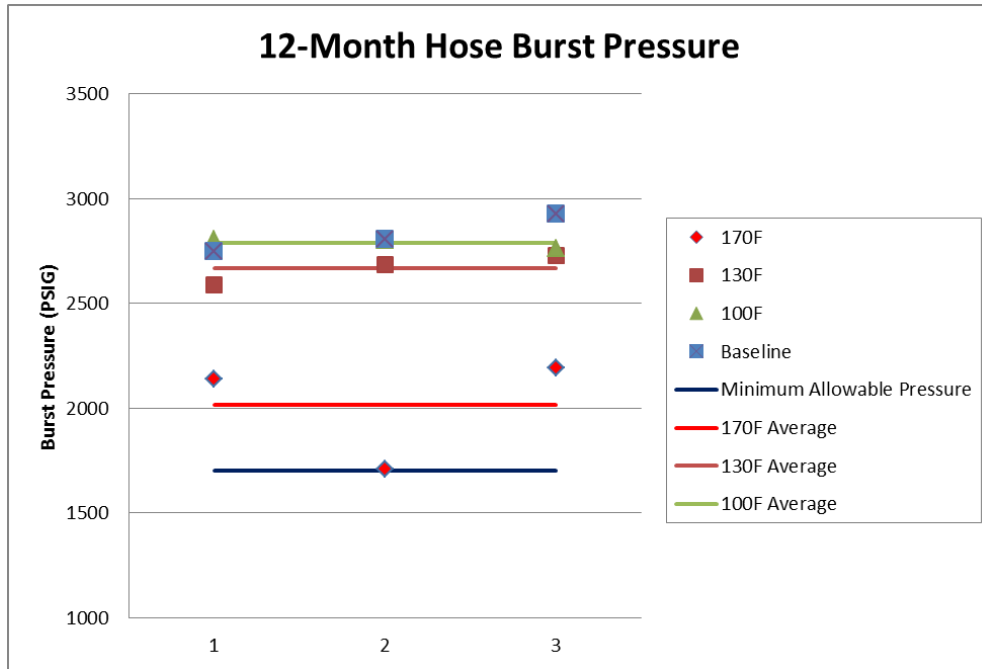

Figure 95. 12-month hose burst pressure results.

Table 9. Comparison of Burst Pressures of the Unaged and Aged EPDM HIHTL Hose Samples

Test condition	Average burst pressure (psi)		Change in burst pressure (%) (compared with baseline)	
	After 6 months	After 12 months	After 6 months	After 12 months
Baseline	2827.03	2827.03	NA	NA
100°F	2706.32	2789.10	-4.27	-1.34
130°F	2784.10	2665.86	-1.52	-5.70
170°F	2637.34	2014.24	-6.71	-28.75

Figure 96. Hose rupture test apparatus (left) and ruptured hose section (right).

Material surface

The surface of the material coupons were examined by a digital microscope to determine the effect of exposure stressors on the material. As can be seen from Figure 97, the amount of surface deterioration increased as the aging fluid temperature increased for the six-month aged coupons. Similar to the six-month results, the twelve-month results also show an increase in the amount of surface deterioration with an increase in temperature. However, the amount of deterioration was greater on the twelve-month aged samples than the six-month aged samples.
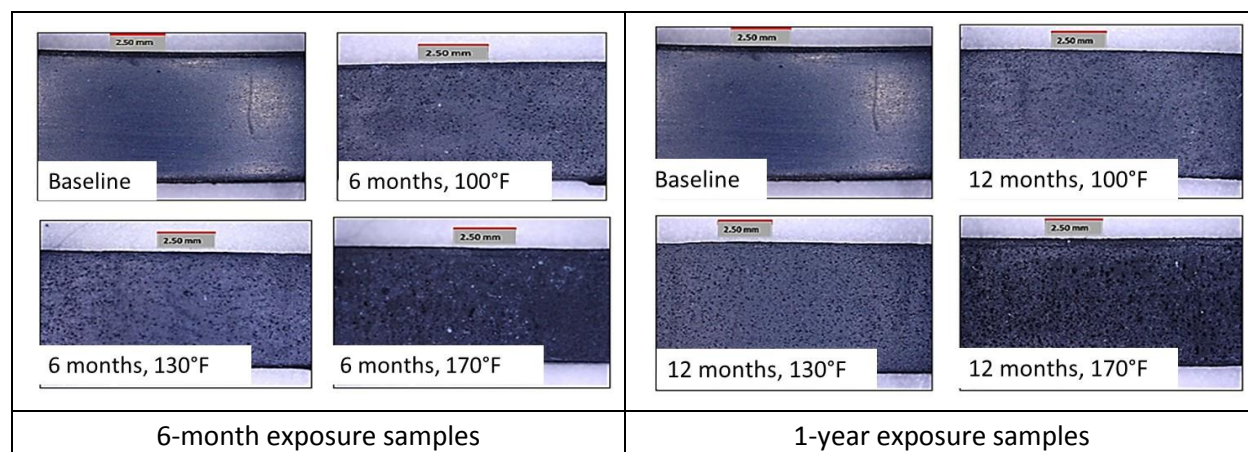

Figure 97. Digital microscope images of material coupon surface.

Scanning electron microscope analysis

Analysis using a scanning electron microscope with energy dispersive X-ray spectroscopy (SEM-EDS) was conducted on the EPDM inner hose samples. The intention was to determine how far the NaOH penetrated into the ethylene propylene diene monomer (EPDM). Figure 98 shows a 40X magnification of a hose section aged at 100°F for 1-year. Figure 99 shows a line scan using SEM-

EDX from the inner surface of the hose. The blue line represents the number of counts obtained of sodium and indicates that some level of sodium hydroxide penetrated into the hose.
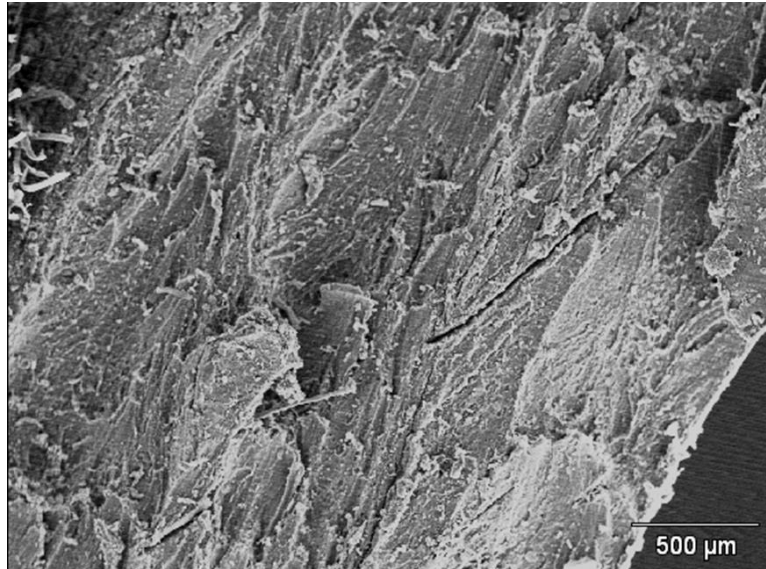

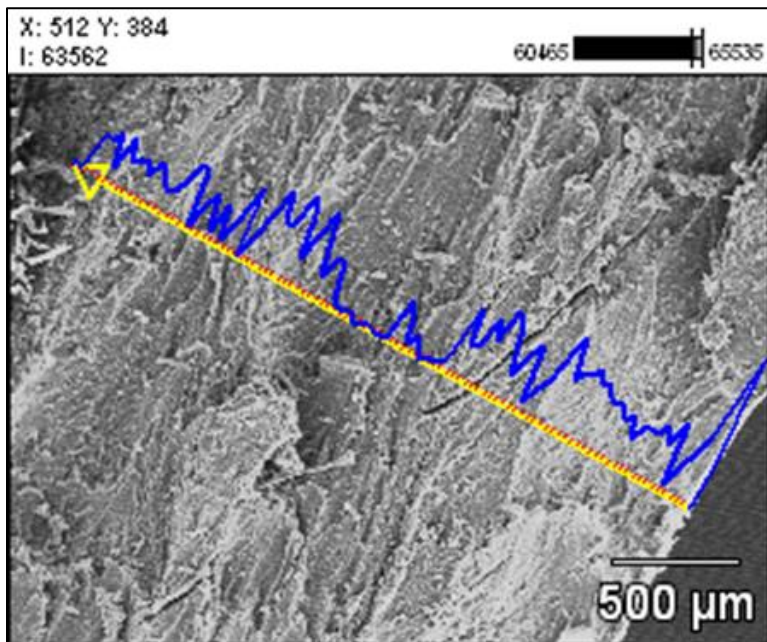**Figure 98. 40X magnification of unaged (baseline) hose sample.**

Figure 99. Cross-section of hose showing sodium penetration.

Current Testing

Currently, FIU is working is conducting aging tests on two HIHTL test specimens using only water at 170°F. This was test was developed after reviewing the data from the tests conducted last year and consultation with site personnel. Previous tests showed the greatest degradation in hose burst pressure as well as the tensile strength of the material coupons occurred at the highest temperatures (170°F). It is also not clear if the degradation to the hoses and material coupons was a result of

being exposed to the high temperature or if it was a result of exposure to the sodium hydroxide. Thus, for this set of experiments, pure water at 170°F was chosen as the stressor in an attempt to determine whether it is the high temperature or the caustic solution that is causing the degradation in the material. Figure 100 shows the current test loop. It consists of two hose test sections connected to a flow loop made of CPVC tubing. The loop has a high temperature pump as well as a turbine flow meter along with a thermocouple and a pressure transducer to provide the flow rate, temperature and pressure of the flow in the loop.

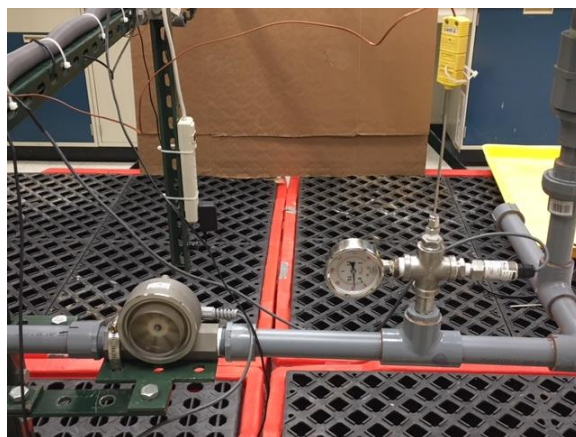**Figure 100. Second phase for testing using only water.**

Figure 101. Flow meter, pressure transducer and thermocouple.

CONCLUSIONS AND FUTURE WORK

After analyzing the experimental data from the samples aged for one year, a significant degradation was observed in the bursting pressure of the hoses. The burst pressure decreased by 28.75% for the sample aged at 170°F, while samples aged at 130°F and 100°F had approximately 5.70% and 1.34% loss in burst pressure, respectively. Similar results were observed when the data was analyzed from the material coupon tensile tests. The Garlock® results showed a reduction of average tensile strength of approximately 91%, 65%, and 63% for the coupons aged at 170°F, 130°F and 100°F, respectively.

The EPDM results showed a reduction of average tensile strength of approximately 89%, 57%, and 54% for the coupons aged at 170°F, 130°F and 100°F respectively. Similarly to the 6-month SEM-EDS results, the 12-month data showed that the sodium hydroxide is penetrating into the hose material. The next phase of testing will include conducting burst pressure tests on the hose specimens aged for one-year with only water at 170°F as well as the tensile tests on the EPDM material coupons samples. In addition, the SEM-EDS analysis of the six-month as well as the one-year hose specimens will be completed. FIU will obtain additional hose sections that will be aged with only water at 100°F and 130°F for a duration of one-year. After each set of hose samples and material coupons are aged for one-year, their burst and tensile strength will be tested.

REFERENCES

1. H Brush, C. O. (2013). Test Plan for the Irradiation of Nonmetallic Materials. Albuquerque, New Mexico: Sandia National Laboratories.

2. Lieberman, P. (2004). Banded (Band-It) and Swaged Hose-In-Hose (HIHTL) Assembly Service Life Verification Program. Santa Clarita, California: National Technical Systems.

3. ASTM D412-16 Standard Test Methods for Vulcanized Rubber and Thermoplastic Elastomers—Tension, ASTM International, West Conshohocken, PA, 2016, https://doi.org/10.1520/D0412-16